

REPUBLIQUE DU CAMEROUN
Paix – Travail – Patrie

UNIVERSITE DE YAOUNDE I

CENTRE DE RECHERCHE ET DE
FORMATION DOCTORALE EN
SCIENCES, TECHNOLOGIE ET
GEOSCIENCES

UNITE DE RECHERCHE ET DE
FORMATION DOCTORALE EN
PHYSIQUES ET APPLICATIONS

B.P. 812 Yaoundé
Email: crfd_stg@uy1.uninet.cm



REPUBLIC OF CAMEROON
Peace – Work – Fatherland

UNIVERSITY OF YAOUNDE I

POSTGRADUATE SCHOOL OF
SCIENCE, TECHNOLOGY AND
GEOSCIENCES

RESEARCH AND POSTGRADUATE
TRAINING UNIT FOR PHYSICS AND
APPLICATIONS

P.O. Box 812 Yaoundé
Email: crfd_stg@uy1.uninet.cm

LABORATOIRE DE MECANIQUE, MATERIAUX ET STRUCTURES
LABORATORY OF MECHANICS, MATERIALS AND STRUCTURES

**DESIGN, MODELING AND DYNAMIC
PERFORMANCE OF OUTRIGGER SYSTEM VIEW
AS STRUCTURAL CONTROL AND SELF-
CONTROL STRUCTURES**

A thesis
submitted to the postgraduate school of sciences, technology and geosciences of the University of
Yaoundé I

by

FANKEM Eliane Raïssa
Registration number: 12W1749
Master's in Physics



in partial fulfillment of the requirements for the degree of Doctorate/PhD in Physics
Option: Fundamental Mechanics and Complex Systems

Supervised by

NANA NBENDJO Blaise Roméo
Professor
University of Yaoundé I

WOAFO Paul
Professor
University of Yaoundé I

©Year 2021

DEPARTMENT OF PHYSICS

**Design, modeling and dynamic performance of Outrigger system
view as structural control and Self-control structures**

Thesis

Submitted and defended for the award of

Doctorat/ PhD in Physics

Specialty: Mechanics, materials and structure

Option: Fundamental mechanics and complex systems

FANKEM Eliane Raïssa

Registration Number: 12W1749

MASTER DEGREE in Physics

supervised by

NANA NBENDJO Blaise Roméo

Professor

WOAFO Paul

Professor

Year 2021

Contents

Dedications	xii
Acknowledgements	xiv
List of abbreviations	xvi
Abstract	xix
Résumé	xxi
General Introduction	1
1 Litterature review	7
1.1 Introduction	8
1.2 The dynamics of structures	8
1.2.1 Models of elastic beams	8
1.2.2 Boundary conditions	12
1.2.3 Models of rigid beams	14
1.2.4 General formalism of vibration control	15
1.3 Structural control systems	17
1.3.1 Structural control system	18

1.3.2	Some structural control for earthquake excitation	18
1.4	The damping by branching	28
1.4.1	A dynamic behavior	29
1.4.2	Damping due to geometrical non-linearities	30
1.5	The Self-vibration control	32
1.5.1	Self-vibration control system	32
1.5.2	A set of pendulum with multi-branched view as mechanical system with self-control of vibration	33
1.6	Importance and reasons of the thesis	33
1.7	Conclusion	34
2	Numerical models of earthquake and wind - Methods and materials	35
2.1	Introduction	36
2.2	Earthquake modelling	36
2.2.1	The earthquake	36
2.2.2	The probabilist ground motions	39
2.2.3	Some examples of excitation Earthquake models	44
2.3	Wind flow models	46
2.3.1	The wind excitation	46
2.3.2	Computational fluid dynamics simulations of wind	48
2.4	Approximate response method - numerical techniques	51
2.4.1	Modal approximation	51
2.4.2	Fourth-order Runge-Kutta method for ordinary differential equations	52

2.4.3	Stochastic Fourth-order Runge-Kutta method for the stochastic differential equations: Kasdin's RK4	55
2.4.4	Lyapunov stability theory	57
2.4.5	Hardware and software	58
2.5	Mathematical modelling	59
2.5.1	Outrigger system applied on a tall building	59
2.5.2	Added branches on a pendulum	62
2.6	Conclusion	66
3	Results and discussion	67
3.1	Introduction	68
3.2	Effect of N-damped outriggers on a high-rise structure subjected to earthquake loads	68
3.2.1	From one outrigger to N-outrigger systems	68
3.2.2	Numerical analysis of the base equations	72
3.3	Reduction of vibration on a cantilever Timoshenko beam subjected to repeated sequence of excitation with magnetorheological outriggers	79
3.3.1	Description of physical system	79
3.3.2	Observation of reduction of vibration	89
3.4	On the mechanical system with self-control of vibration	95
3.4.1	Modelling of the dynamics of self-controlled mechanical system	95
3.4.2	Dynamics explanations	99
3.5	An inverted pendulum with multi-branching view as self-controlled system: modelling and vibration absorber capacity	105

3.5.1	General mathematical formalism of an inverted pendulum with multi-branching	105
3.5.2	Effects of branches on the damping of the central column vibration	108
3.5.3	Energy tranfer leading to damping effect of branches	116
3.6	Conclusion	122
	General conclusion	124
	Bibliography	127
	List of publications	144
	Collection of the published papers	146

List of Figures

1.1	An inverted pendulum	14
1.2	Base Isolation [47]	20
1.3	Hyde system [51]	22
1.4	Principle of Tendon System [52]	23
1.5	Tendon-Spring System Model [52]	24
1.6	Damped outrigger concept [58]	25
1.7	Conceptual detail at outrigger level [58]	26
1.8	Pagoda structures [56]	27
1.9	Adaptation of the pagoda’s “shimbashira” principle to the needs of the Sky Tree project [56]	28
1.10	Linear model of the dynamic of a three proposed by James et al. [77]	29
1.11	Branched geometries, (a) The walnut tree architecture analyzed by Ro- driguez et al [78], (b) and (c) Y-shaped spring-mass model of an elementary branched tree-like structure by Theckes et al [33].	31

1.12	Typical evolution of the total energy, $E(\text{---})$, and modal energies, $E_{\Theta}(\text{- - -})$ and $E_{\Phi}(\text{\cdots\cdots})$, with the respective evolution of the trunk angle, $\Theta(\text{- - -})$, and branch angle, $\Phi(\text{\cdots\cdots})$, of the spring-mass model of a Y-shape, as a function of time over three periods of the trunk mode. The design parameters are set to $\phi_b = \frac{\pi}{2}$, $\xi_b = 0.2$, $\Omega = 2$ and $\Gamma = 0.2$. [33]	31
2.1	Seismology [82, 83]	37
2.2	Ground motion	37
2.3	Earthquake effects in Ecuador	38
2.4	Kanai-Tajimi model	40
2.5	Clough-Penzel model	42
2.6	Envelope function of Shinozuka and Sato model	43
2.7	Envelope function of Amin and Ang model	43
2.8	Envelope function of Boore model	44
2.9	Generated earthquake	45
2.10	Sample simulated acceleration sequences	46
2.11	Cherry tree moving with wind blowing [97]	47
2.12	Collapse due to Wind load [102, 103]	47
2.13	(a) Cup-type anemometer with vertical axis, a sensor on a remote meteorological station, (b) An occluded mesocyclone tornado (Oklahoma, May 1999) [97]	48
2.14	Schematic diagram of the computational setup with a dune as structure. x and z are axis, H the height and L the width of the dune [101].	50
2.15	Time histories of aerodynamic forces on a towers and tension leg platforms (TLP) [104].	51

2.16	Cantilever beam with one level of symmetric attached outriggers	59
2.17	The damper	60
2.18	An inverted pendulum with one level of symmetrical masses	62
2.19	Position and distance measurement	63
3.1	Cantilever beam with N damped outriggers	69
3.2	Dimensionless ground acceleration earthquake.	73
3.3	Optimal position of the damped outrigger	74
3.4	Comparison between one outrigger at the 0.9 position and five outriggers at positions 0.277, 0.379, 0.477, 0.567 and 0.65	76
3.5	Comparison between five outriggers at equidistance and at non-equidistance positions	78
3.6	Cantilever beam with magnetorheological (MR) outriggers	80
3.7	Cross-section of the core tube	80
3.8	Optimal position of damped outriggers, $\zeta_a = 0.762$ and MF= 1.0	91
3.9	Optimal position of damped outriggers, $\zeta_a = 0.095$ and MF= 1.0	91
3.10	Optimal scale coefficient MF	93
3.11	Time histories at the first vibration mode	93
3.12	Time histories at the second vibration mode	94
3.13	Time histories at the third vibration mode	94
3.14	System without any branch and with one branch	96
3.15	System with two branches	96
3.16	System with three branches	97
3.17	Time-histories response of the structure without and with one branch.	101

3.18	Time-histories response of the structure without and with one branch and two branches	102
3.19	Time-histories response of the structure without and with one branch, two branches and three branches	102
3.20	Time-histories response of the structure without and with one branch, two branches and three branches	103
3.21	Effect of length l_1	104
3.22	Effect of length l_3	105
3.23	(a) Physical model of pendulum with multi-branched at rest, (b) Disturbed system.	106
3.24	Angular displacement (a) θ for the central column, (b) ϕ_1 for the first level branches	109
3.25	Angular displacement of Central column with (a)One-Two, (b)Two-Three, (c)Three-Four, (d)Four-Five levels of attached branches	110
3.26	The model of a set of pendulums under earthquake loads	111
3.27	Dimensionless ground acceleration	112
3.28	Angular displacement of (a)Central column θ , (b)First floor ϕ_1 , (c)Second floor ϕ_2 , (d)Third floor ϕ_3 , (e)Fourth floor ϕ_4 , (f)Fifth floor ϕ_5	114
3.29	Angular displacement of Central Column according to the number of floors (a)1 and 2, (b)2 and 3, (c)3 and 4, (d)4 and 5	115
3.30	Energy of the system for (a)One and (b)Two levels branches	119
3.31	Energy of the system for (a)One-Two, (b)Two-Three, (c)Three-Four, (d)Four-Five levels branches	120
3.32	Effects of the design parameters on the energy of the system : (a)mass of central rod, (b)length of central rod, (c)level masses, (d)level length	121

3.33 Model of a building view as a set of pendulum with multi-branched 122

List of Tables

1.1	Four beam theories	9
2.1	Parameters of the filter soil of Clough-Penzien [91]	41
2.2	Coefficients of the SRK4 method . [109]	57
3.1	Properties of the beam	72
3.2	Fourth Order, Time Varying Stochastic Runge-Kutta Coefficients. [109] . .	73
3.3	Parameters of the structural system	90
3.4	Model parameters of the magnetorheological damper	90

Dedications

I dedicate this work:

To **Almighty God** and I also thank Him who with his strong hand and extended arm has renewed in me the breath of life every day of my life and graciously offered me health, strength and ability to carry out this work. May all the glory, the honor and the magnificence be given to Him.

To my Lovely parents **MIBÉ KAMSU Lisette** and **MIBÉ Samuel**

To **William Brice, Benjamin Joël, Merline Huguette, Grâce Divine, Jean**

To my late Grandparents **MBOUNSI Emmanuel** and **DJILE Marthe, NZALI Abraham** and **KEMCHE Marthaline**

"Better is the end of a thing than the beginning thereof: and the patient in spirit is better than the proud in spirit". Ecclesiastes 7: 8

Acknowledgements

This thesis is the fruit of several supports of special persons, and I will take this occasion to give them this few words. I would like to address my very king gratitude:

- To **Pr NANA NBENDJO Blaise Roméo**, Director of this thesis, whose vigor in work, know-how and cordiality have inspired me throughout this work, for his multiform support scientifically, materially and morally. Dear Prof receive the expression of my deep and sincere gratitude and proof that your efforts have not been in vain since the Master degree up to now.
- To **Pr WOAFU Paul** for his urging follow-up during my research studies with this other work as fruit that adds to the Master degree of few years ago.
- To **Prof. Dr.-Ing Uwe Dorka** of University of Kassel, in Germany for his collaboration, fruitful discussions and useful suggestions during all this thesis study and for his warm hospitality, constant availability during my stay in Germany.
- To **Pr NDJAKA Jean-Marie Bienvenu**, the Head of Department of Physics, for the teachings, advices and encouragements that He gave to me during the academic cycles of Master and Doctorate/PhD.
- To All the jury members for the time that they give to evaluate this work and for all their remarks to render it.
- To **Pr KOFANE Timoléon Crépin** whose the wide advices during courses in nonlinear physics and in the research has been very beneficial for me in my work.
- To **Pr TCHAWOUA Clément** for his courses in vibration and elasticity and the large number of advices during the Master's courses and my Master's defence.
- To All the teaching staff and personnel of the Department of Physics, Faculty of

Science, University of Yaoundé I, for their teachings and help since my Master degree in this institution.

- To **Steel and composite structures team of University of Kassel, Kassel, Germany**, For the opportunity that they give me to follow part of this research study in their laboratory through DAAD STIBET PhD Programme for Foreign PhD Student, Scholarship Partner Universities.
- To **Pr LENOUE André**, for being one of that person I can count on during all my university course both scientifically and for advice. Thank you Dear Professor.
- To **Pr DJUIDJE KENMOE** epse **ALOYEM KAZE Germaine**, for being one of the pillar of sustain that I had during all this work. Thank you Madam.
- To All the teaching staff and personnel of the Department of Physics, Faculty of Science, University of Douala, for their teachings and help during my Bachelor degree in that institution.
- To Late **Dr MBOUSSI Aïssatou**, for have being a teacher, an elder sister and a model to follow. Only God knows why you are not here to rejoice with me according to the achievement of this study as you did for my Master degree.
- To **Dr NANA Bonaventure, Dr WOULACHE Rosalie, Dr TALLA Mbe, Dr TAKOUGANG Sifeu, Dr ABOBDA Lejuste, Dr NDOUKOUO Ahoudou, Dr NANHA Armand, Dr TOGUEU MOTCHEYO, Dr TALLA Francis, Dr CHAMGOUE André, Dr GOUNE Geraud, Dr NWAGOUM Péguy, Dr TSAPLA Rolande, Dr TOKOUE Dianorré, Dr NDJOMATCHOUA Frank, Dr DONGMO Eric, Dr TCHAKUI Murielle, Dr OUMBE Gabin,**

Dr NOTUE KADJIE, Dr TCHINANG TCHAMEU, Miss KOUAMI Nandine and Mr KEMAJOU. Receive my gratitude for your inspiring life experiences.

- To my elders in the lab, Dr NDEMANOU Peggy, Dr METSEBO Jules, Dr ANAGUE Merveil, Dr MBA Cloriant, Dr SONFACK Hervé for your fruitful exchanges during my stay; One more time thank you .
- To my pairs and labmates Dr SIMO Ulrich, Dr THEPI Raoul, YANKAM Gaëlle, ASHU Vanessa, DJUITCHOU Thomas, PIEDJOU Alex, YOUTHIA Octave, FEULEFACK Ashley, NGOUNOU Armel, MOKOLA Dalahäï, POUOKAM Paola and all the others, thank for your trust.
- To Maman NZADI NGOUNOU Pauline, Maman MEDJO Désiré, Uncle TEDOM Samuel, families Sop FEKOU, GUÈH BÈH LOH, Té NDEFO DJILO, MANDENG for their full love.
- To that particular group of special persons on which I am extremely happy to be a member of. I think of **Leading Entrepreneurial Researchers (LER: PIEPI Dorian, EMAKOUA Herman, NTOMB Edouard, PIEDJOU Alex, TATOU Yvan, KENTSA Steven, LEPATIO Alain), JEF-Cameroun, CMCI-Maison Blanche, YMCA-Biyem Assi Club Sport** thank for the supports.
- To all my parents, uncles, aunts, brothers, sisters, nephews, nieces, friends those whose names have not been mentioned here, those reading this work for their active support.

Please, receive all of you moreover, my gratefulness for this achievement, your achievement for you guide me unconditionally with love and I will respond also with unconditional and pure love.

List of abbreviations

DOF: Degree Of Freedom

ECT: ECuador Time

HYDE: HYsteretic-DEvice

IRGM: Institut de Recherches Géologiques et Minières

km: kilometer

MDOF: Multi-Degree Of Freedom

MF: Modification Factor

mi: Miles

MR: Magneto-Rheological

ODE(s): Ordinary Differential Equation(s)

PDE(s): Partial Differential Equation(s)

RC building: Reinforced Concrete building

RK4: Fourth-Order Runge-Kutta

SDE(s): Stochastic Differential Equation(s)

CRTV: Cameroon Radio Television

TLP: towers and tension leg platforms

TMD: Tuned Mass Damper

TPMD: Tuned Pendulum Mass Damper

Abstract

One of the best way nowadays of protecting and assure the safety of a building subjected to stochastic external excitations (Earthquake, strong wind, large waves, etc) is to use structural control strategy. This technic was really improved during the time and is without any doubt reliable and efficient. Unfortunately it is almost used without a high knowledge or any specific parametrizing because a deep and solid background work was not really done. So in this thesis, we have built some self control systems in order to quench vibration in specific physical systems particularly mechanical structures. It is done firstly by using outrigger systems (a structural control system) attached on cantilever beam and secondly by the association of pendulums. The excitations responsible of vibration in the system are from two main natures: earthquake and wind loads. And it results that for outriggers and added branches, a damping effect is observed and the damping ratio is increased with the number of added devices. While for a set of pendulums, the design system behaves like trees and vibration is controlled due to the exchange of energy between the main trunk and the branches.

Keywords: Mechanical structure, Cantilever beam, Pendulums, Trees vibration, Outrigger system, Vibration control, Structural control, Self-control, Earthquake loads, Wind load.

Résumé

Une des techniques les plus prisées de nos jours concernant la protection et la sécurité des structures soumises à des excitations aléatoires (séisme, vent violent, raz de marée etc) est l'utilisation des systèmes de contrôle structurels. Cette technique a fait ses preuves pendant déjà quelques années et sans aucun doute, elle est fiable et efficace. Malheureusement des études analytiques poussées n'ont presque pas encore été faites la concernant. C'est pourquoi, dans cette thèse, nous avons conçu quelques stratégies d'auto-contrôle ayant pour but de réduire les vibrations pour certains types de systèmes physiques en particulier les structures mécaniques. Ceci a été fait premièrement en utilisant les systèmes de balancier (qui est un système de contrôle structurel) attachés à une poutre cantilever et deuxièmement par l'association des pendules. Les facteurs responsables des vibrations dans le système sont de deux ordres: le séisme et le vent. Nous établissons que pour le dispositif de balancier attaché et les branches ajoutées, le phénomène d'amortissement est observé et le coefficient d'amortissement croît avec le nombre de niveaux ajoutés. Tandis que pour l'assemblage de pendules, le système se comportant comme les arbres voit ses vibrations réduire grâce à un échange d'énergie entre le tronc principal et les branches.

Mots-clés: Structure mécanique, Poutre Cantilever, Pendules, Vibrations des arbres, Système de balancier, Contrôle des vibrations, Contrôle structurel, Auto-contrôle, Séisme, Mouvement des vents.

General introduction

The development of the countries nowadays passes by an industrial revolution marked by the construction of significant infrastructures. Thus civil and mechanical engineering are main disciplines which should be well mastered in order to achieve this goal. So one can see in order to show their growing, highest buildings in the most of powerful nations and even developing countries. But after they have been built, tall and slender structures require permanent monitoring of the deformations that take place with the time. The causes of the deformations include external factors such as strong winds, earthquakes and floods, accompanied by the natural process of ageing [1–3]. Let us mention that Cameroon is not aside of that phenomena because it is till in mind what happened in December 2019. The 19th December 2019, the regions of Centre and South Cameroon were subjected to a brief earthquake in the beginning of the afternoon. In a communiqué read during the 1PM News of the CRTV Radio, the Monday 23 December 2019, the Minister of scientific research and Innovation of Cameroon Madeleine TCHUINTE declares that “according to the result from the recording of the sismologic station of IRGM of Édea, a local earthquake took place and primary waves were obtained at 4.26 PM and secondary waves at 4.27 PM”. It was a 5.7 magnitude (M_w) earthquake on the Richter scale and the epicenter is located in a radius of 240 km from Édea [4]. Fortunately, no damage was recorded.

Two main consequences of the monitoring are the reparation of the damages suffered by the material structures and the use of control methodes [5, 6], some of which require external devices and energy [7–11]. Considerable efforts have been devoted to the study of nonlinear vibrating structures firstly to predict the behavior of structures facing an external excitation and determine the conditions of appearance of chaos or unwanted phenomena [2] and secondly to propose adapted control. This is generally achieved with passive techniques, such as the classical addition of dampers [12], tuned mass-damper systems [13] or with active or semi-active means such as piezoelectric materials [14], mag-

netorheological device [10], shape memory alloys [15] or even simple hydraulic actuators in feedback or feedforward systems [16]. A new method catches our eyes because since 1980s when it was proposed for the first time, it is recognized as one of the best of semi-active control for high-rise buildings : Outrigger system.

Outrigger system is a revolutionary method to increase the intrinsic damping of the building for giving its the way to reduce more vibrations when it is subjected to different disturbances. The intrinsic damping here refers to the capability of the structure to dissipate the mechanical energy, whatever the physical mechanism involved (viscoelasticity, friction ...). Outrigger system is constituted by a stiff beam that connects the shear walls to exterior columns. This system is quite efficient and more used because the outrigger and the columns resist the rotation of the core [17] and thus significantly reduce the lateral deflection and base moment when the structure is subjected to lateral forces [18]. Compared to a cantilever beam without a controller, a tall building structure which incorporates an outrigger system can face a reduction in core overturning moment up to 40%. To develop a controllable outrigger damping system, the semi-active control devices, magnetorheological (MR) dampers are adopted by Wang [19].

Many works in this domain have been done by engineers and some aspects as the influence of the cantilever beam geometrical non linearity have not been taken into account even the damping modes effects. It is why, our first main goal in this thesis is **firstly to propose a simplify model of an Euler Bernouilli cantilever beam where we locate outrigger system and observe the effect of the location and the number of outriggers on the central column; and secondly by adding a controllable Magneto-rheologic damper on a model of Timochensko beam and pointing out its perfomance.**

Conventional Structures can be earthquake safe, but they are not configured for earth-

quakes and therefore, too many are lost. A multitude of small details in columns, corners or connections decide whether a building will survive or not. Quality control is overwhelmed by this requirement. It is like a game of chance, even for the same type of building in the same location

* Therefore, we need new structural concepts adapted to earthquakes

* A feasible approach is “Structural Control” to control the response of a structure to dynamic loading by introducing special mechanisms into the structural system with suitable control devices. So recently, number of structural concepts [20] which allow rigid body control have been identified and four concepts (Base Isolation, Hysteretic Device System, Tendon system and Pagoda system) have been suggested for seismic control [21,22]. Our second major aim is **to construct a structure design which incorporate a set of pendulums and bring out their abilities to resist to earthquakes and strong winds.**

Pagoda system, inspired by high seismic performance of old built Pagoda structures, is one of the most powerful design structure which react positively when they face earthquakes [23–26]. With many experiments, some assumptions were proposed to explain the resistance of five story pagoda [27]; it was indicated that the good resistance is due to the combined actions of different mechanisms: base isolation, slip joint, friction damper, snake dance, Shin-bashira and tuned mass damper, which makes that structures so resistant to earthquakes. Omori [28] proposed that the compound pendulum system, the center column and the main structure, gives tuned mass damper effect after investigations on pagodas in Senso-ji Temple and Nikko-ji Temple. And the friction damping effect of the wooden joints (pieces of wood are assembled using tenons, mortises) was an important factor in making them earthquake resistant [29]. According to the analyses conducted by Tanabashi [30], the factors increasing the resistance of the structure were the scale effect

of the five-story structure, a characteristic of flexible structure and the wood joint capacity for allowing plastic deformations through slipping or gaps in them. Some years after, it was proposed that, the center column acts as a bolt fastening the whole structure and adding a restraint effect of shearing deformations among individual stories [31]. Ueda [26] considered that each structurally independent stories mounted on top of the other was able to allow each one to act like a balancing toy, cancelling the inertia force of each story out among them.

Because more investigations and theoretical analysis are still required to clarify the five story pagoda behavior [32], an attention was carried on the damping mechanism by branching (to take into account aspects of base isolation, slip joint, snake dance and Shinbashira) studied by Theckes *et al.* [33] where they found that significant levels of damping achieved via branching with typically 30% of the energy being dissipated in one oscillation for two bioinspired architectures.

In order to propose the best modelling that fit the behavior of pagoda's dynamic, to mechanical and to civil engineering, we attempt to solve in this thesis the following problem :

- The modelling of an elastic structure where outriggers systems are located along its length.
- The modelling of a rigid body structure where masses are attached at different levels.
- The dynamic of such structures, the effect of outriggers and masses on the vibration of that structure in the autonomous case (an impulsion move the structure from its initial position) and also when they are subjected to earthquakes or wind flows.

So, the thesis is structured as follow :

- In the first chapter, a summary of the state of the art, on structural control systems

leading to self-vibration control of structures; the dynamics of elastic beam and rigid beam are presented.

- The second chapter consists on the presentation of some technics used to analysis and solve the problematic of the thesis.

- It follows with the third chapter. The presentation of the results which are helpful for mechanical and civil engineering for making stronger structure is done. Discussions and stretching to applications of the work are presented here.

- It ends by a general conclusion which gives the main results obtained and perspectives for future investigations.

CHAPTER I

LITERATURE REVIEW

1.1 Introduction

Vibrations in man-made structures are a central problem in mechanical engineering [13]; this results from external or internal excitations that they face during their live. Since many years, scientists have been proposing a number of methods to reduce the effects of vibrations due to external excitations. Considerable efforts have been devoted to the study of nonlinear vibrating structures [2]. This is generally achieved with many techniques and methods of which some will be presented in this part of the work.

The chapter is organized as follows: Section 1.2 presents the generalities on the dynamics of structures (elastic and rigid), while Section 1.3 is devoted to the definition of structural control systems with some examples. Section 1.4 presents the concept of damping by branching. Section 1.5 will give an overview on the concept of Self vibration control applied in the case of structure. Section 1.6 deals with the presentation of the problems to be solved in the thesis. Finally in Section 1.7, a brief conclusion will mark the end of this chapter.

1.2 The dynamics of structures

According to the modelling of buildings, in particular tall buildings in the litterature, there are two majors ways to model: as Cantilever elastic beams or rigid body beams. This part of work is devoted to the generalities on dynamics of beams.

1.2.1 Models of elastic beams

The used of materials of high resistance for modern buildings and in particular for bridges, ships/boats, planes and tall buildings/skycrapers make their analysis more interesting according to their great capacities. They are four main theories about beams modelling

[34], in the Table 1.1, we present these different beam theories:

Table 1.1: Four beam theories

Beam models	Bending moment	Lateral displacement	Shear deformation	Rotary inertia
Euler - Bernoulli	✓	✓	×	×
Rayleigh	✓	✓	×	✓
Shear	✓	✓	✓	×
Timoshenko	✓	✓	✓	✓

To summarize that table, the Timoshenko model is an extension of the Euler-Bernoulli model taking into account rotary inertia and shear deformation of the beam [35, 36].

1.2.1.1 Euler-Bernoulli beam model

The study of beam vibration is a well known subject [37, 38]. The energetic approach refers to the Hamilton principle which is based on the knowledge of the elastic potential and the kinetic energy of the system under consideration. Thus for a beam of section S , with the density ρ and a Young modulus E submitted to a transversal charge q , we have to write first for this method [39] the kinetic and potential energy of the system written as follows,

$$T = \frac{\rho S}{2} \int \left(\frac{\partial y}{\partial t} \right)^2 dx \quad (1.1)$$

$$U = \int \frac{EI}{2} \left(\frac{\partial^2 y}{\partial x^2} \right) dx - 2 \int qy dx \quad (1.2)$$

where y and I refer respectively to the transversal displacement and the moment of inertia.

The density of the Lagrange function obtained is written as :

$$\Lambda = \frac{\rho A}{2} \left(\frac{\partial y}{\partial t} \right)^2 - \frac{EI}{2} \left(\frac{\partial^2 y}{\partial x^2} \right)^2 + qy \quad (1.3)$$

This leads to obtain according to the variational principle to the following Euler-Ostrograsky equation :

$$\frac{\partial \Lambda}{\partial y} - \frac{\partial}{\partial t} \left(\frac{\partial \Lambda}{\partial y'_t} \right) + \frac{\partial^2}{\partial x^2} \left(\frac{\partial \Lambda}{\partial y''_{xx}} \right) = 0 \quad (1.4)$$

where ' , " represent respectively the first and second derivatives with respect to the variable put in indication.

Thus we can derive the dynamic equation of the defined system.

$$\rho S \frac{\partial^2 y}{\partial t^2} + EI \frac{\partial^4 y}{\partial x^4} = q \quad (1.5)$$

And by taking $m = \rho S$ the mass per unit of length, the mathematical formulation of motion of beam describing the classical Euler-Bernoulli model without a charge is given by:

$$m \frac{\partial^2 y(x, t)}{\partial t^2} + EI \frac{\partial^4 y(x, t)}{\partial x^4} = 0 \quad (1.6)$$

The transverse displacement of the beam $y = y(x, t)$ is described by two variables: x the axial coordinate along the length of the beam and t the time.

1.2.1.2 Rayleigh beam model

The presence of rotary inertia effects adds another term to the Euler-Bernoulli coming from the kinetic energy due to the rotation of the cross-section. The motion of beam is:

$$m \frac{\partial^2 y(x, t)}{\partial t^2} + EI \frac{\partial^4 y(x, t)}{\partial x^4} - \rho I \frac{\partial^4 y(x, t)}{\partial x^2 \partial t^2} = 0 \quad (1.7)$$

with ρ the mass density of the beam material.

1.2.1.3 Shear beam model

Here the tranverse vibration considers the effect of shear distortion (but not rotary inertia).

We introduce new variables α , the angle of rotation of the cross-section due to the bending moment, and β , the angle of distortion due to shear. The total angle of rotation is the sum of α and β and is approximately the first derivative of the defection,

$$\alpha(x, t) + \beta(x, t) = \frac{\partial y(x, t)}{\partial x} \quad (1.8)$$

The equations of motion, using Hamilton's principle, are given by:

$$m \frac{\partial^2 y(x, t)}{\partial t^2} - k_s GA \left(\frac{\partial^2 y(x, t)}{\partial x^2} - \frac{\partial \alpha(x, t)}{\partial x} \right) = 0 \quad (1.9a)$$

$$EI \frac{\partial^2 \alpha(x, t)}{\partial x^2} + k_s GA \left(\frac{\partial y(x, t)}{\partial x} - \alpha(x, t) \right) = 0 \quad (1.9b)$$

where G is the shear modulus of elasticity and $G = \frac{E}{2(1+\nu)}$, k_s is the shape factor depends on the geometric of the cross section of the beam (for exemple, for circular cross section $k_s = \frac{6(1+\nu)}{7+6\nu}$) and S is the cross-section area of the beam.

1.2.1.4 Timoshenko beam model

Timoshenko proposed a beam theory which adds the effects of shear distortion and rotary inertia to the Euler-Bernoulli model. Therefore, the Lagrangian includes the effects of bending moment, lateral displacement, rotary inertia and shear distortion. We assume that there is no rotational kinetic energy associated with shear distortion, but only with

the rotation due to bending. Therefore, the kinetic energy term used in the Rayleigh beam is modified to include only the angle of rotation due to bending by replacing $\partial y/\partial x$ with α . This beam model is suitable for the two following cases:

- The beam is short in length relative to its thickness,
- The long beam vibrating in a higher mode so that the nodal points are close together.

The following set of coupled differential equations in terms of the beam displacement $y(x, t)$ and rotation $\alpha(x, t)$ of the cross-section is thus expressed as follows

$$m \frac{\partial^2 y(x, t)}{\partial t^2} = k_s G A \left(\frac{\partial^2 y(x, t)}{\partial x^2} - \frac{\partial \alpha(x, t)}{\partial x} \right) \quad (1.10a)$$

$$\rho I \frac{\partial^2 \alpha(x, t)}{\partial t^2} = k_s G A \left(\frac{\partial y(x, t)}{\partial x} - \alpha(x, t) \right) + EI \frac{\partial^2 \alpha(x, t)}{\partial x^2} \quad (1.10b)$$

Eliminating α , we obtain the uncoupled equations of motion given by

$$EI \frac{\partial^4 y(x, t)}{\partial x^4} + m \frac{\partial^2 y(x, t)}{\partial t^2} - \rho I \left(1 + \frac{E}{k_s G} \right) \frac{\partial^4 y(x, t)}{\partial x^2 \partial t^2} + \frac{\rho^2 I}{k_s G} \frac{\partial^4 y(x, t)}{\partial t^4} = 0 \quad (1.11)$$

Firstly, the Euler-Bernoulli beam theory which is the simplest one, is used to have a good assessment on how the structure react when it is excited and the behavior of the outriggers. Secondly, to describ more the real situation, the choice of the Timoshenko beam model is justified in the following work.

1.2.2 Boundary conditions

Many systems with flexible beam are encountered in different branches of science (biology, environmental science, and engineering). Depending on the use for which these systems are designed to, beam ends take diverse configurations which lead to a particular dynamics. Ten cases are identified [34]: free-free, hinged-hinged, clamped-clamped,

clamped-free, sliding-sliding, free-hinged, free-sliding, clamped-hinged, clamped-sliding and hinged-sliding supports. As previously said, as this work concern residential and tall buildings and skycrapers, it is righth to choose the instance of clamped-free ends: at the ground level, the structure is clamped and at the top level it is free.

1.2.2.1 clamped-free ends for Euler-Bernoulli beam model

In this configuration:

– At the clamped end, there is no displacement and the angular coefficient of the tangent to the elastic line is zero. Indeed, if the angular coefficient is not zero, then there is a breaking of the beam. The boundary conditions are thus specified by

$$y(0, t) = 0 \quad \text{and} \quad \frac{\partial y(0, t)}{\partial x} = 0 \quad (1.12)$$

– Let L be the total length of the building. The moment of bending and the shearing force are nulls at the free end. The mathematical formulation is

$$\frac{\partial^2 y(L, t)}{\partial x^2} = 0 \quad \text{and} \quad \frac{\partial^3 y(L, t)}{\partial x^3} = 0 \quad (1.13)$$

1.2.2.2 clamped-free ends for Timoshenko beam model

Here, The mathematical formulation for the clamped end is the same as Euler-Bernoulli one while at the free end, it is

$$\frac{\partial y(L, t)}{\partial x} - \alpha(L, t) = 0 \quad \text{and} \quad \frac{\partial \alpha(L, t)}{\partial x} = 0 \quad (1.14)$$

These previous boundary conditions will be used in the next chapter to carry out the modal analysis.

1.2.3 Models of rigid beams

To model the structure as a rigid body, an inverted pendulum is considered, attached to the soil by a rotary spring and dashpot (viscous damper) as shown in figure 1.1. The forces acting on this system are: the weight and the reaction of the soil. This reaction is related to the mechanical properties of the soil. The coefficients of the reaction (damping and elastic coefficients) of each structure can be deduced from a free vibration test. The inclination of the rod must be less than the critical amplitude, if not the structure will break [40].

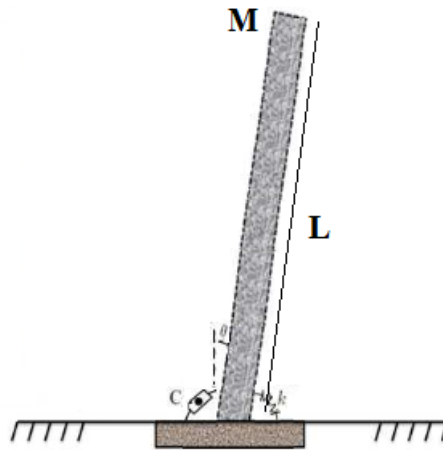


Figure 1.1: An inverted pendulum

This type of structure is in various domains: in civil engineering, one can assimilate tall buildings to its, in biomechanics the prosthetic limb for physically disabled persons can also be described by such a model, in agriculture, it represents rigid plants such as trees.

Under the action of the external excitation, the motion of the inverted pendulum is obtained using the fundamental equation governing the dynamics of the system in rotation and it is given by

$$J \frac{d^2\theta}{dt^2} + C \frac{d\theta}{dt} + k\theta - \frac{1}{2}MgL \sin \theta = M'(t) \quad (1.15)$$

where J is the moment of inertia, M the rod mass and L the height at length of the rod. g , C and k are respectively the gravitational acceleration, the damping coefficient and the spring constant. θ is the angle that the rod makes with the equilibrium position and $M'(t)$ stands for the external forces. $M'(t)$ can be the effects of earthquake, wind, strong waves or the action of machine used to uproot the mechanical structure.

Very often, these forces are stochastic and when the amplitude is small, one can assimilate it to a gaussian white noise. They can also be approximated by periodic functions whose amplitude and frequency are deduced by using averaging procedures (statistics analysis, Fourier analysis, noise analysis, etc...).

1.2.4 General formalism of vibration control

Innovative methods of control became, in recent years, of great relevance, they allow to project structures to resist, without appreciable damage, dynamic actions, for example storms, strong waves, a great seismic action, etc. At the same time, during the construction or after, structures are to be protected by protective systems, by reducing response, effective and at the same time reliable. Between these innovative methods of control, three different approaches can be distinguished: passive, active and semi-active; to these can be added a fourth which is the hybrid control.

1.2.4.1 Passive control

Passive control consists in superposing on the structure a device which modifies the rigidity or the damping of the structural system without requiring an external energy source and without introducing energy for its operation [41]. Some examples of these kind devices

are: tuned mass dampers, base isolator systems, friction dampers, viscous fluid dampers, etc.

1.2.4.2 Active control

The active control aims at imposing a force or a displacement at certain points of the system to be checked, depending in particular on the measured state or the history of the latter [42, 43]. This type of control requires an external power source to operate the actuators which provide the control forces whose magnitudes are determined by using the measurements from the sensors, excitation and/or response of the structure. These forces can be used to add or dissipate the energy of the structure to be controlled. In order to build such a system, there are two approaches that are radically different: the first method is to identify the disturbance that creates the vibrations to cancel it by superposing a reverse excitation; it is feedforward control. The second method is to identify the response of the structure rather than the excitation that makes it vibrate. It therefore requires the modeling of the dynamic behavior of the structure; it is feedback control. As example: active variable stiffness, active bracing systems, active tendon systems, etc.

1.2.4.3 Semi-active control

Semi-active control combines the main features of active and passive systems. These systems require a low power source to alter the mechanical property of the control device. One of particularities of this kind of devices is its capacity to adapt its dynamics related to the effects of environmental or external loadings [44]. It consists in changing, in real time, the characteristics of passive energy dissipation devices and this change induces a low energy requirement. Therefore, as for active control, the system needs sensors, processors, actuators. Semi-active systems represent an evolution of passive systems and thus

preserve fundamental characteristics of reliability, security and simplicity, in addition to that adjustment to increase performances. There is a strong conceptual link between semi-active systems and passive systems; indeed the various terminologies used in literature to identify the semi-active control are: Variable passive control, Variable structure system (VSS), Parametric control to say that we play on one of the system parameters to provide dynamic control over the structure. As Semi-active control, we can cite: Continuous variable stiffness, electrorheological dampers, magnetorheological dampers, etc.

1.2.4.4 Hybrid control

A control system is hybrid if it uses a combination of passive and active control system. Here, the control system is both passive and active; and each of its parts contribute to increase the performance of the controller. It comes with the need for reliable and robust control systems, such as passive, efficient and controllable control such as active control. The hybrid active-passive control system therefore uses viscoelastic (passive) and piezoelectric (active) materials. The first ensures the reliability and robustness of the system since in case of malfunction of the active control, the system remains damped. The second improves the performance of the system for very low frequencies. The both passive and active controls therefore act in complementarity [45]. As some hybrid control systems, we can have: hybrid damper actuator bracing control, hybrid mass damper, etc.

1.3 Structural control systems

For several years, always with the aim of improving the performance of controllers and having stronger structures, Structural control system has emerged and is now more and more widespread in the world. It can be passive, active, semi-active or hybrid; it depends

on how it is modeled.

1.3.1 Structural control system

Structural control is the control of selected response variable of a structure subjected to dynamics loading [46].

- Such variables may be displacements or their time derivatives (velocities, accelerations) and/or forces

- Full controllability can be achieved in mode control and the control of rigid body mechanism

- For mode control, a structural system is needed that has clearly defined modes

- For rigid body control, a structural system must consist of an assemblage of rigid bodies

Therefore, Structural Control is **NOT**:

- Added damping

- Added damping and stiffness

- Or any conventional structural system with additional devices: **No system variable is controlled in such structures!**

The first step in structural control is to select a structural concept that is controllable! [47]

1.3.2 Some structural control for earthquake excitation

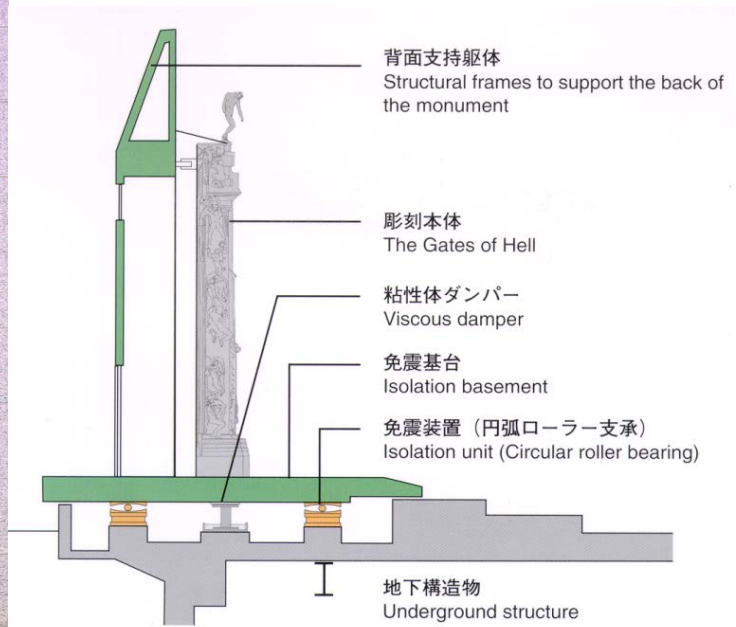
On the way of structural control systems, one can have as Rigid body mechanisms:

1.3.2.1 Base isolator systems or seismic base isolation

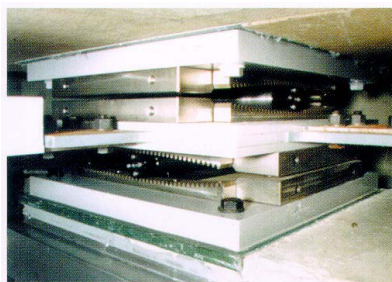
These systems consist of placing, between the foundations and the superstructure, devices that have a very high horizontal deformability and a very high vertical stiffness. These devices make the decouple of the movement of the ground from the structure possible in order to reduce the forces transmitted to it. The isolator captures deformations (inelastic) and filters the accelerations (high frequencies) so that the isolated superstructure moves essentially in a rigid mode undergoing low accelerations and almost no deformation. As a result, the inertial forces transmitted to the foundation elements are limited and remain below the elastic capacity of such elements. Base isolation is based on the principle that if the vibration period is increased sufficiently to move away from the predominant earthquake excitation period, the accelerations transmitted to the structure (and consequently the inertial forces) are considerably reduced. On the other hand, the increase of the period generates larger displacements concentrated at the level of the isolator [48] (Figure 1.2).



(a) The Gates of Hell Auguste Rodin

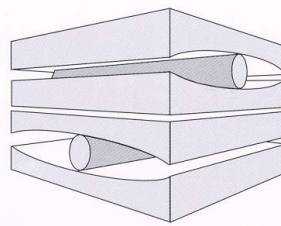


(b) Base isolated Structure



免震装置 (円弧ローラー支承)
Isolation unit (Circular roller bearing)

(c)



免震装置の設置された基礎
Isolation units

(d)

Figure 1.2: Base Isolation [47]

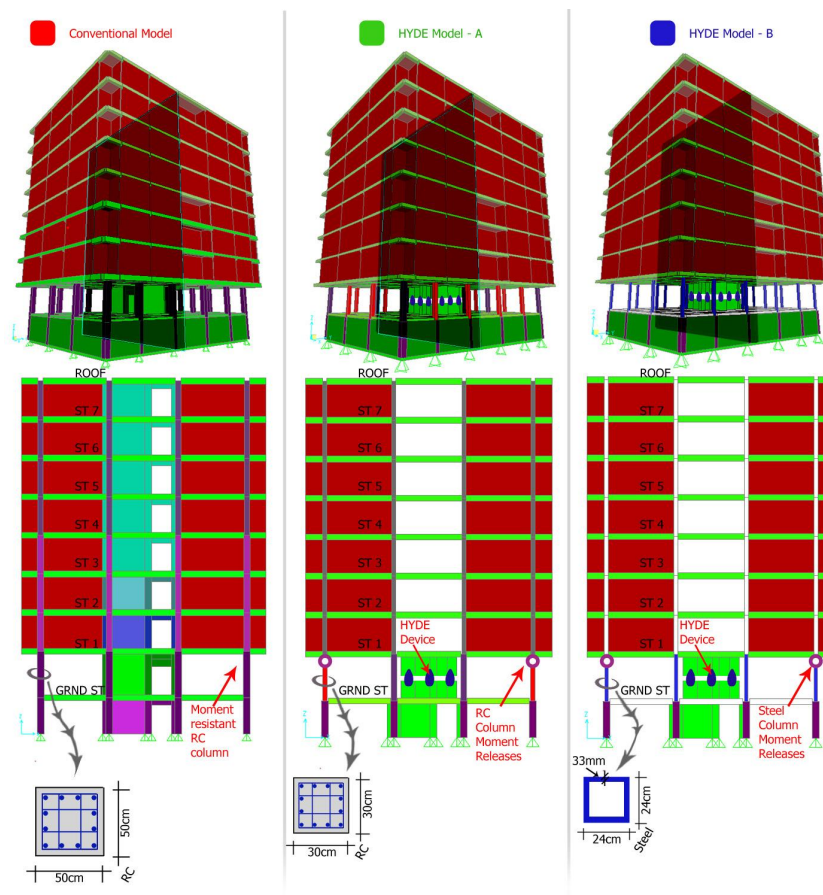
1.3.2.2 Hysteretic device (Hyde) system

HYsteretic-DEvice- or HYDE-systems are a kind of structural control system that introduces a stiff-ductile mechanism into the structure [49, 50]. By doing so, the structure becomes an assembly of rigid bodies moving in a defined pattern with internal forces limited by the yield level of the devices that are placed in the joints between the rigid bodies. Such an assembly dissipates almost all the input energy due to an earthquake in these devices through plastic yielding or friction. This characteristic leads to very small stresses in the structure and at the same time limits the motion of the mechanism. It is a system that can be applied to new structures but is most suitable for retrofitting, especially when it comes to the so-called soft storey structures. Such structures are abundant in modern cities due to the presence of open spaces in the ground floor and apartment floors above stiffened by “non-structural” partition walls usually made of bricks. The upper storeys thus form a rigid block on top of a horizontal seismic joint: The natural place for stiff-ductile devices to make it a HYDE-system (as seen in Figure 1.3).

The beneficial performance of HYDE-systems has been shown in many studies and an early application has been the 7 storey constructed building in Shkup, Macedonia [51]. Here, simple shear panels have been used as HYDEs and the retrofit was 60% cheaper than any conventional approach.



(a) 7 storey constructed building in Shkup, Macedonia, 2009



(b) 3D mathematical models representative for the 7 storey building constructed in Shkup, Macedonia

Figure 1.3: Hyde system [51]

1.3.2.3 Tendon system

Tendon Systems are one of the structural control systems for earthquake protection. In this system, rigid bodies are connected through single cables or through a cable network as shown in Figure 1.4 below [52]. Systems of this type generally consist of a set of prestressed tendons connected to a structure with their tensions being controlled by servomechanisms. One of the reasons for favoring such a control mechanism has to do with the fact that tendons are already existing members of many structures. This is attractive, for example in the case of retrofitting or strengthening an existing structure [22]. The pre-stressing forces of the cables are regulated strategically at given locations. Therefore, a suitable dynamic mechanism can be established (Figure 1.5). Suitable devices are spring-dashpot combinations or shape memory alloy devices like those in the Tendon System for the seismic retrofit of a historic bell tower in Trignano, Italy [53].

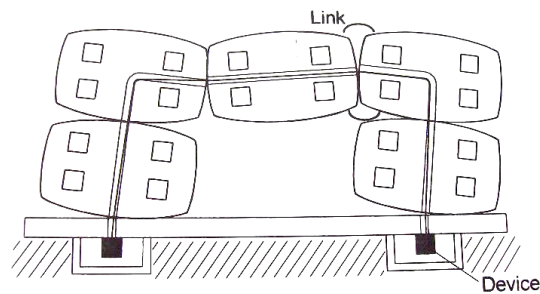
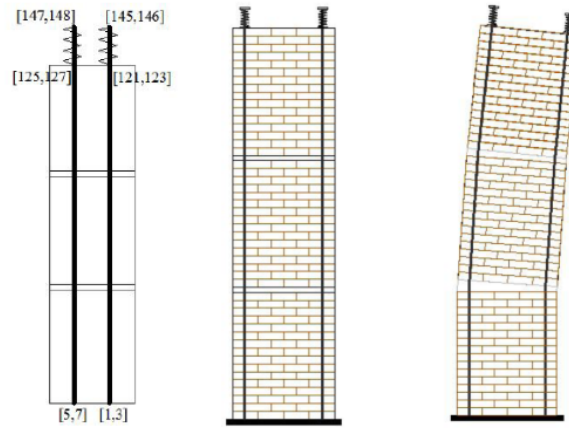
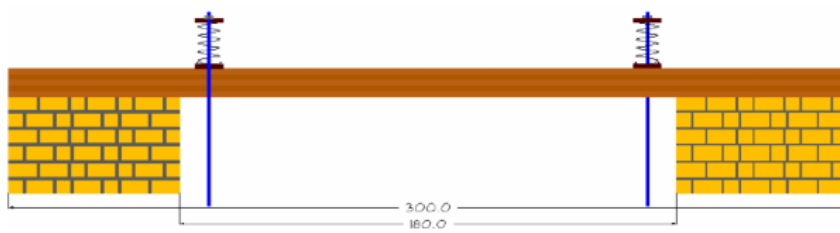
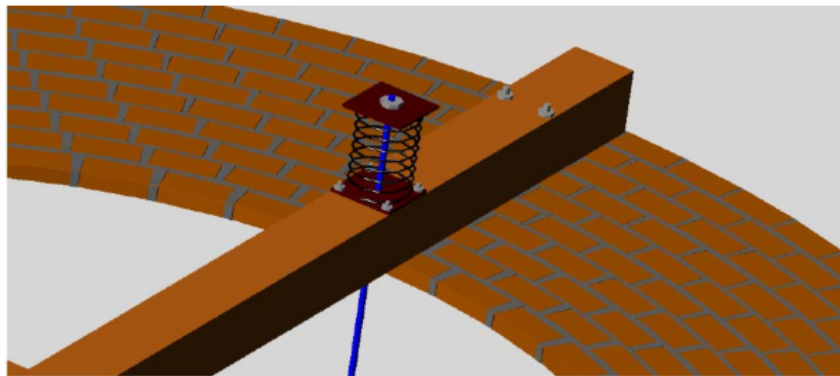


Figure 1.4: Principle of Tendon System [52]



(a)



(b) Preliminary proposal for Position of Tendon System

Figure 1.5: Tendon-Spring System Model [52]

1.3.2.4 Outrigger system

Outrigger system is a revolutionary method to increase the intrinsic damping of the building for giving its the way to reduce more vibrations when it is subjected to different disturbances (Figure 1.6). The intrinsic damping here refers to the capability of the structure to dissipate the mechanical energy, whatever the physical mechanism involved (viscoelasticity, friction ...). Outrigger system is constituted by a stiff beam that connects the shear walls to exterior columns (see Figure 1.7). This system is quite efficient and more used because the outrigger and the columns resist the rotation of the core [17] and thus significantly reduce the lateral deflection and base moment when the structure is subjected to lateral forces [18, 57].

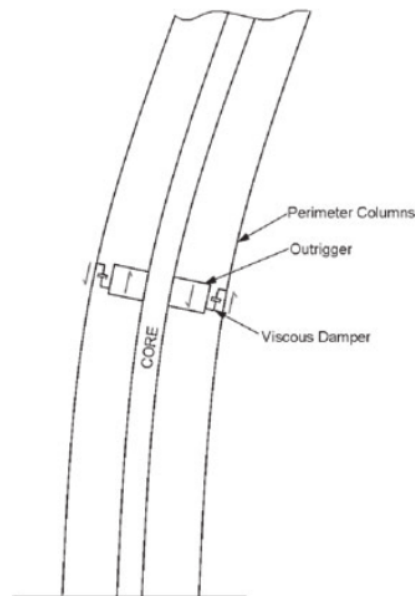


Figure 1.6: Damped outrigger concept [58]

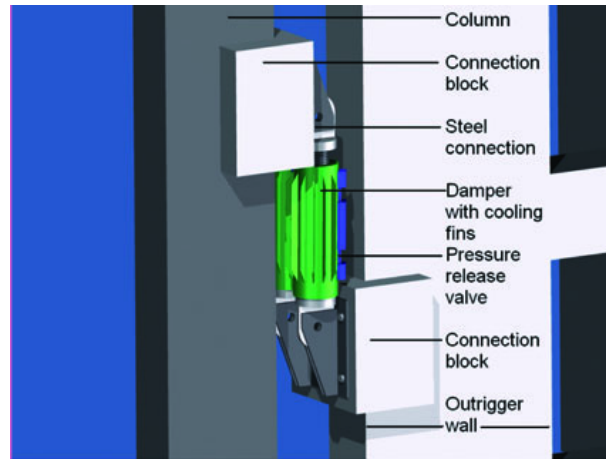


Figure 1.7: Conceptual detail at outrigger level [58]

1.3.2.5 Pagoda system

Pagoda system, inspired by high seismic performance of old built Pagoda structures (Figure 1.8), is one of the most powerful design structure which react positively when they face earthquake [26, 54, 55]. The traditional Pagoda already was built by a highly flexible kit system allowing the building to move and shake in a controlled way thus absorbing the vibrations. The Pagoda performs a so-called “snake dance” during an earthquake, which has protected it from failure for over 1300 years. Therefore, the beams and columns of such a house were only plugged together (interlocking technology) and not joined in a fixed way or nailed. These joints allowed the joined elements to move within a certain scope [56]. Figure 1.9 shows a building with the construction particularly based on pagoda structure. In the literature, according to dear configuration, it is two different kinds of Pagoda structures:

- The first one is most built with wood, we usually see that kind of building in China and all the pieces of wood are assembled without the least nail! All is indeed fitted one in another thanks to sets of tenons, mortises.
- The second one is characterized by his central mast called “**Shimbashira**” which

can be useful for repositioning of one story if it is deviated, we can also notice that Load at different levels can help to stabilize the building after a disturbance.

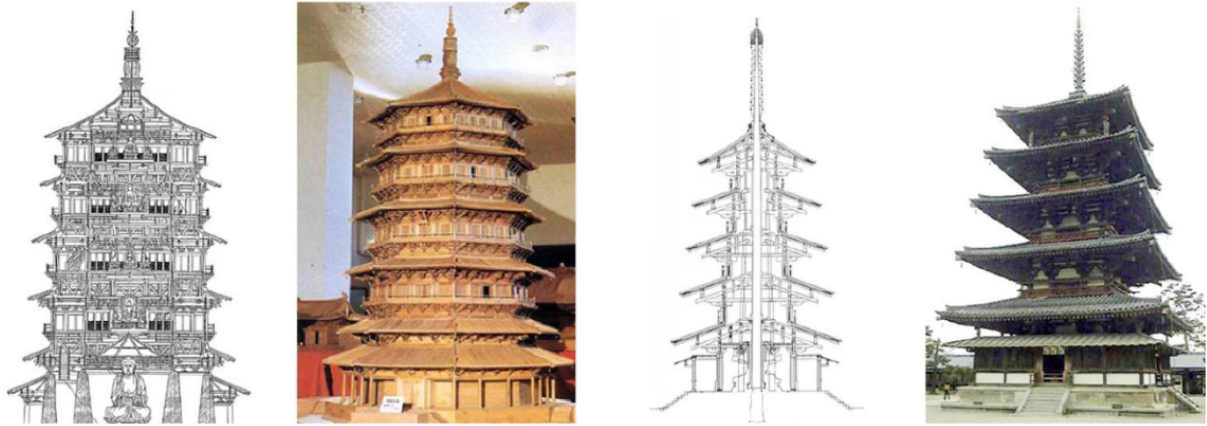
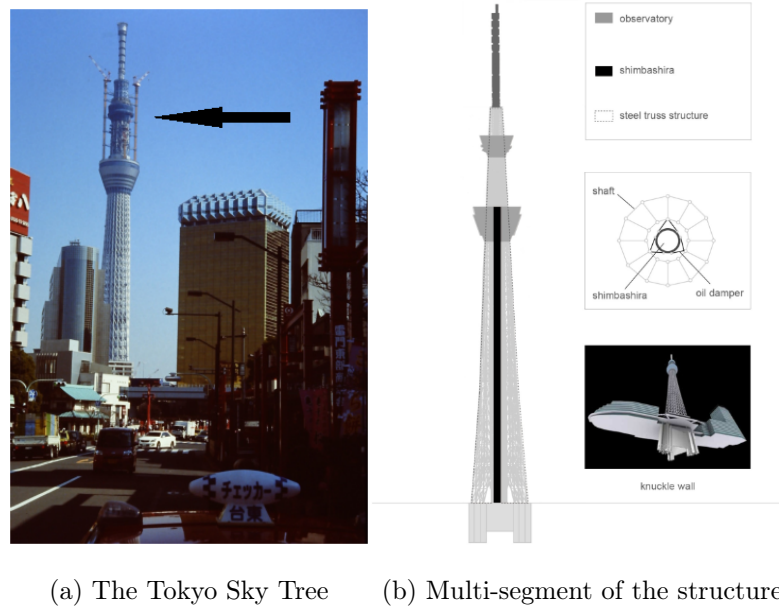


Figure 1.8: Pagoda structures [56]

In this thesis the outrigger system will be investigated. A modeling of single and multi-outrigger will be shown; the way it appears on the structure and reduces the vibrations will be exposed by numerical simulation



(a) The Tokyo Sky Tree (b) Multi-segment of the structure

Figure 1.9: Adaptation of the pagoda’s “shimbashira” principle to the needs of the Sky Tree project [56]

1.4 The damping by branching

For many of engineering problems, the nature can be a source of innovative inspiration, [59–61]. Trees are a source of several bio-inspired applications for example on the creation of autorepairing materials [62], or on the optimisation of mechanical links.

Unfortunately, just few bio-inspired works were done on the damping notion. One can enumerate for example, works of Yoon and Park [63] who recently developed a damped device using electronic microcomponents undergoing shocks, inspired by the green woodpecker. As fruit of evolution, trees, which are regularly suggested to aerodynamic loads, are likely to possess mechanisms for specific defences.

In front of the different time scales of the loadings under the trees, several adaptive mechanisms have recently been discovered. Over long periods, thigmomorphogenesis allows trees, and plants in general, to adapt their growth to better withstand the usual

loadings of their environment [64, 65]. For example, a tree in a windy environment will grow its trunk and branches more in diameter than in length [66]. In short time and from a static point of view, the work of Gosselin et al. [67] showed that the flexibility of the plants, in comparison with the rigid case, allows a reduction of the aerodynamic drag force. This mechanism of reconfiguration thus increase the resistance of plants, especially trees, to aerodynamic loading. [68, 69]

1.4.1 A dynamic behavior

First of all, remember that, there are three sources of damping in the trees, namely: [70–76]

- Wood, known for its viscoelastic properties, which has been the source of bio-inspired materials;
- The interactions between the shaft and the air cause forces in the opposite direction to the local speed in the shaft, bringing a dissipation highly dependent on the amplitude of the movement of the shaft;
- Considering the global motion of the tree by bending the trunk, another mechanism is often described in the literature as “Structural damping”.

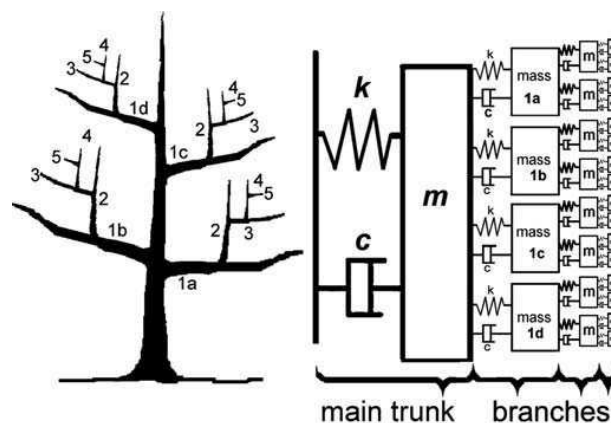


Figure 1.10: Linear model of the dynamic of a tree proposed by James et al. [77]

This third mechanism is interpreted as the possible transfer of mechanical energy of

the trunk to branches; where that energy will be dissipated by the two viscoelastic and aeroelastic mechanisms. James et al. proposed a first model of energy transfer presented in figure 1.10 which model the structure of three branches as multitude of TMD coupled oscillators.

1.4.2 Damping due to geometrical non-linearities

In order to develop strategies for bioinspired designs of slender structures including an efficient damping effect specific to large amplitudes, it is crucial to clarify the nonlinear mechanism involved in the energy transfer that many authors invoke. For this purpose, Theckes et al consider the simplest model of a branched dynamical system in figure 1.11, a spring-mass model of a Y-shape [33]. The model consists of three massless rigid bars linked by rotational springs and supporting three masses. The first bar, representing a trunk of length l_1 , is linked to the ground by a rotational spring k_1 and supports a mass m_1 . The branches are two symmetrical bars of length l_2 , each forming an angle ϕ_b with respect to the trunk axis. Each branch is linked to the tip of the trunk by a rotational spring k_2 and supports a mass m_2 .

The dimensionless equations of motion of the trunk (Θ) and his branches (Φ) are:

$$\begin{cases} \ddot{\Theta} + \Theta = 2\Gamma \left[\dot{\Theta}\dot{\Phi} \sin(\phi_b + \Phi) - \ddot{\Theta}J_\phi(\phi) \right] \\ \ddot{\Phi} + 2\Omega\xi_b\dot{\Phi} + \Omega^2\Phi = -\dot{\Theta}^2 \sin(\phi_b + \Phi) \end{cases} \quad (1.16)$$

And the dimensionless total mechanical energy is given by

$$E(\tau) = \frac{1}{2} \left[(2\Gamma J_\phi(\phi) + 1) \dot{\Theta}^2 + \Theta^2 + \Gamma (\dot{\Phi}^2 + \Omega^2\Phi^2) \right] \quad (1.17)$$

The initial energy is $E_0 = 1$, i.e $\Theta_0 = \pi/2$, in the trunk mode only. The total energy decreases as a consequence of the energy nonlinearly transferred to the damped branch

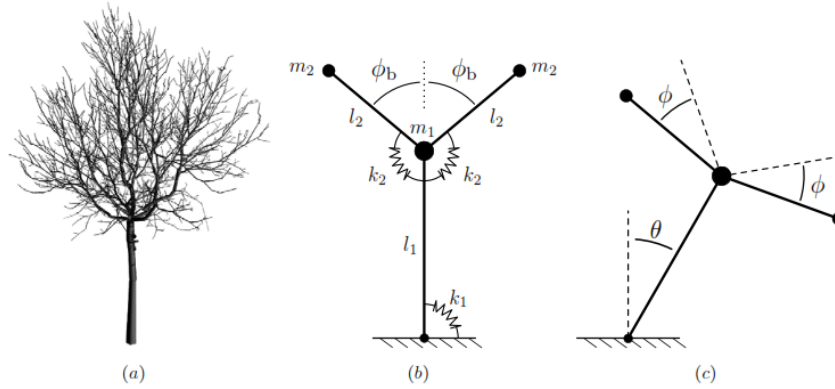


Figure 1.11: Branched geometries, (a) The walnut tree architecture analyzed by Rodriguez et al [78], (b) and (c) Y-shaped spring-mass model of an elementary branched tree-like structure by Theckes et al [33].

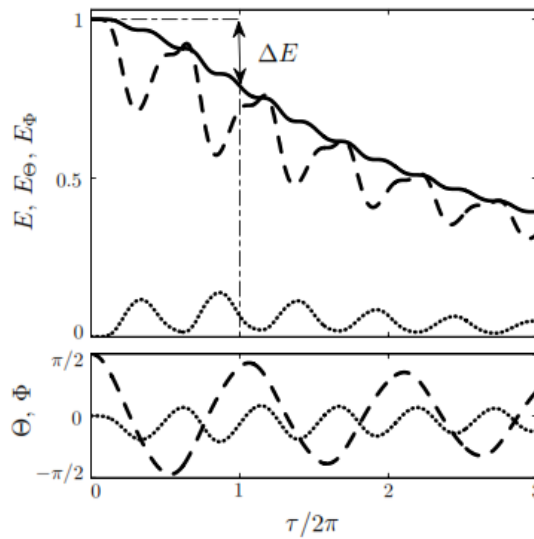


Figure 1.12: Typical evolution of the total energy, E (—), and modal energies, E_{Θ} (- - -) and E_{Φ} (···), with the respective evolution of the trunk angle, Θ (- - -), and branch angle, Φ (···), of the spring-mass model of a Y-shape, as a function of time over three periods of the trunk mode. The design parameters are set to $\phi_b = \frac{\pi}{2}$, $\xi_b = 0.2$, $\Omega = 2$ and $\Gamma = 0.2$. [33]

mode. Since the two modes are coupled by nonlinear terms, energy is exchanged between them. The dissipation in the branch mode damps the energy received from the trunk mode, resulting in an effective damping of the whole structure.

1.5 The Self-vibration control

1.5.1 Self-vibration control system

- A self-controlled system is a system which has the ability to maintain or turn back itself in a suitable stage whatever what disturb it and put it away from that stage
- Self-controlled is also known as maintained self-oscillation, self-excited, self-induced, spontaneous, autonomous.
- These structures do not need any external help (added after the building of structure) or internal system (structural control system, etc) to be controlled
- This new system is suitable for high-rise buildings because there generally have flexible and low damping characteristics

This fact is already scientifically explained, but no modern structure has been built with this robust structural system, which belongs to a class of seismic control concepts. These concepts rely on the control of rigid body motions allowing for a drastic reduction in kinetic and potential energy in the structure, thus leading to a very robust behaviour. In this field, two first models were already proposed and is shown in the following paragraphs.

1.5.2 A set of pendulum with multi-branched view as mechanical system with self-control of vibration

Inspired by both Pagoda system and branch on tree architectures, and called “**Modern pagoda system**”, this new structure consists of an inverted pendulum of finite length and mass as a rigid rod attached to the soil by a rotary spring and dashpot (viscous damper), with massless rigid bars or inextensible cables linked on that central column. Masses are attached at different length of the central column on that bars or cables. Each level is one bar or cable or two symmetrical bars or cables, forming an angle with imaginary horizontale line. These bars or cables are linked to the central column by a rotational spring and viscous damper. That attaches masses here are different floors.

1.6 Importance and reasons of the thesis

Chinese traditional timber structure is one of the oldest structural forms of China and has also been widely adopted in other Southeast Asian countries, such as Japan and Korea. Many great timber palaces, temples and pagodas that were built through history have been preserved and stand as an invaluable legacy to human civilization [32, 56, 79]. In Japan no pagodas have ever suffered serious damage from earthquakes. Even in the Great Hanshin-Awaji Earthquake, there were no reports of serious damage to wooden pagodas in Hyogo, Kyoto and Nara. This fact must be scientifically explained. Since the end of the Meiji era, many researches have studied the earthquake resistance of five-story pagodas. And several factors of earthquake resistance of them has been pointed out, such as friction damping and sliding effect of the wooden joints, base isolation effects, balancing toy effects of deep eaves, bolt fastening effect of the center column and so on [80]. Because more investigations and theoretical analysis are still required to clarify the five story

pagoda behavior, it is imperative to investigate their structural performance, especially their dynamic performance, to provide a fundamental basis for structural appraisal and strengthening. Base isolation effects, balancing toy effects, bolt fastening effect of the center column are the firsts taking into account in this scientific labour which consists of setting up a mathematical model of a mechanical structure mimicking the behavior of pagoda system. Thus the attention of this thesis work is to carry on the damping mechanism of such structures; starting from the mathematical modelling, analytical and numerical study of the behavior of outrigger systems as a high damping performance system to a proposition of a model of self-vibration control and its simulation results while passing by analysis of damping coefficient of N-damped outriggers systems and the effect of the multibranches (damping by branching) on a pendulum.

1.7 Conclusion

In this chapter, we have provided a state of art with as much detail as possible about the four main groups of classification of mechanisms for control of structural response. The structural control systems with some examples, the concept of Self-control of vibration applied in the case of structure and generalities on beam models (elastic, rigid and boundary conditions) are too presented. The detail on the problems solved in this thesis work in chapter III have been settled. Therefore, in the following chapter a general background of the methods used to deal with the problem will be presented.

CHAPTER II

NUMERICAL MODELS OF EARTHQUAKE AND WIND - METHODS
AND MATERIALS

2.1 Introduction

The present chapter is devoted to the presentation of the principles of each methods used along the thesis. Earthquake load and Wind flow are chosen here as the external force/excitation that induce vibrations to structures. They are generated numerically following some principles that will be shown in Sections 2.2 and 2.3. In Section 2.4, the computational techniques used to solve the structure equations under control and plot the results are briefly presented. To end this chapter, a conclusion is given in section 2.5.

2.2 Earthquake modelling

2.2.1 The earthquake

An earthquake is the shaking of the surface of the earth. It result of a sudden release of energy in the earth's crust that creates seismic waves. It is also defined as a natural phenomenon that usually starts at a depth of less than $100km$ below the ground [81]. The main cause is when tectonic plates ride one over the other, causing orogeny (mountain building), and severe earthquakes. Mainly cause by slip along faults, the energy from an earthquake propagate as body waves and surface waves.

- Seismic waves generated by an earthquake travel through Earth.
- Ground moves forward and backward (horizontal Earth motion), up and down (vertical Earth motion), and shifts from side to side.
- Ground ripples like waves do in water.

Magnitude of earthquake measures the energy of an earthquake. So, each earthquake is characterized by a unique release of strain energy. This is calculated from Richter scale. Intensity of earthquake is based on observation of damaged engineering structures

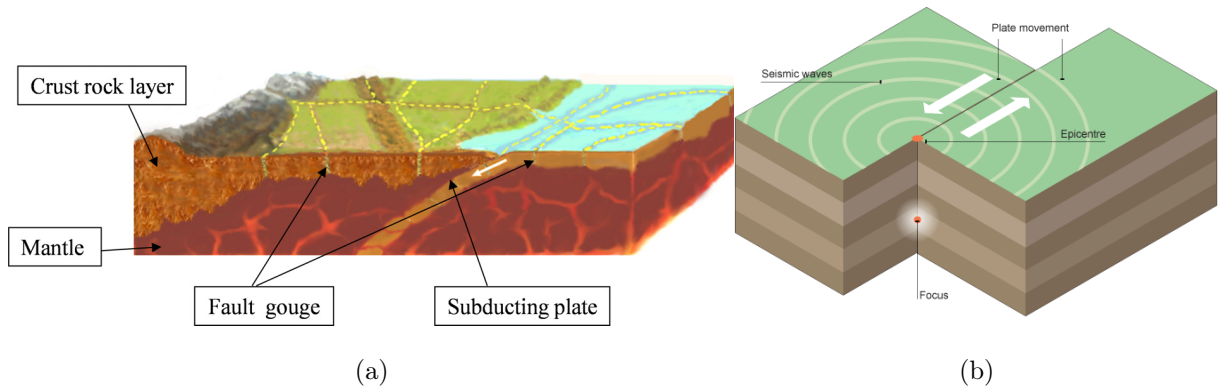


Figure 2.1: Seismology [82, 83]

as well as reactions of people. The point of origin or the point where an earthquake or underground explosion originates, called the seismic focus or hypocenter, is located with the help of seismograph. The point on Earth's surface directly above the hypocenter is called the epicentre [84] (as seen in Figure 2.1(b)). The epicentral distance is the distance from the epicenter or epicentre to the point of interest on the surface of the earth.

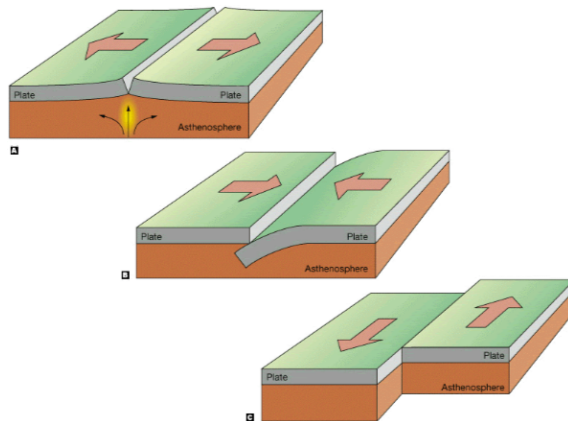


Figure 2.2: Ground motion

Thus, to have other information from earthquake, such as

- peak ground acceleration (PGA) is the maximum amplitude of ground acceleration.
- peak ground velocity (PGV) is the maximum amplitude of velocity.
- peak ground displacement (PGD) is the maximum respective amplitude of displace-

ment.

The recording of seismic waves cause by that earth-shaking phenomenon is assured by a seismograph. It is an instrument that records the shaking of the earth's surface caused by seismic waves, and is to accurately record the motion of the ground during a quake.

At 18:58 ECT on April 16, 2016 a 7.8 magnitude (M_w) earthquake struck the coast of Ecuador approximately 27km (17mi) south-souteast of Muisne, in the province of Esmeraldas, at a depth of 20.6km (12.8mi). This catastrophic caused heavy destruction as shown in the following Figure 2.3, as balance 668 killed, 8 missing and 6274 severely injured, An estimaed 35000 houses were destroyed or badly damaged leaving more than 100000 people in need of shelter [85].



(a)

(b)

Figure 2.3: Earthquake effects in Ecuador

By seeing the impacts of earthquake on Lifes, Man-made structures etc, studies were focus on the recording of earthquake signals, prediction of that disaster and the ways to avoid the maximum of damage. According to that last idea, recent earthquakes have demonstrated the vulnerability of buildings. And researchers and engineers direct their researchs on the way of having stronger buildings for earthquake by testing that resistance on generated ground motion.

There are two methods used to estimate ground motion in engineering practice [86].

- Deterministic seismic hazard analysis defined as the first method
- probabilistic seismic hazard analysis, referred to as the second method.

2.2.2 The probabilist ground motions

Various mathematical models in the literature for estimating the acceleration ground motion, include the soil characteristics at a site. The modelling of the earthquake excitation require to take into account many aspects such as the peak ground acceleration, magnitude, intensity, epicentre distance and frequency content [87]. Advantage with the mathematical approach is that, we can generate many forms of recorded ground motion at different sites by adjusting on the intensity and frequency content varies with time. Since the nonstationary earthquakes are focused on these two mentioned parameters.

The following flow diagram presents different steps to generate of the numerical way a nonstationary earthquake.

$$\text{White noise} \rightarrow \begin{cases} \text{-Kanai-Tajimi} \\ \text{-Clough-Penzel} \end{cases} \rightarrow \text{Envelope function} \rightarrow \text{Nonstationary earthquake}$$

2.2.2.1 White-noise

Let $\xi(t)$ be defined as white noise. It is a random process and described as Gaussian whether checked the following properties: a zero mean value and has an auto-correlation function

$$\langle \xi(t) \rangle = 0, \quad \text{and} \quad \langle \xi(t) \xi(t') \rangle = \delta(t - t') \quad (2.1)$$

where $\delta()$ is the Dirac delta function.

2.2.2.2 Kanai-Tajimi

The analyse of recorded data from strong ground motion demonstrates that earthquake power spectra are not independent of frequency [88]. The KanaiTajimi (Kanai 1957; Tajimi 1960) model is well-known and used very widely in the analysis of engineering structures under earthquake excitation [89]. Thus, the power spectral intensity of the ground acceleration is given by

$$S_{\ddot{w}}(\omega) = s_0 \frac{\omega_g^4 + (2\zeta_g \omega_g \omega)^2}{(\omega_g^2 - \omega^2)^2 + (2\zeta_g \omega_g \omega)^2} \quad (2.2)$$

where S_0 is the intensity of the white noise process at the rock level, ω_g is the dominant frequency of the soil site and ζ_g is the associated damping ratio of the soil strata.

Figure 2.4 illustrates different forms of Kanai-Tajimi model for $\zeta_g = 0.4$, $\omega_g = 3\pi \text{rad/s}$ (a) $S_0 = 0.02 \text{m}^2/\text{s}^3$, (b) $S_0 = 0.015 \text{m}^2/\text{s}^3$.

The site soil is considered as the place where a white noise disturbance is applied at bedrock and the motion is transmitted to the ground surface through a soil layer.

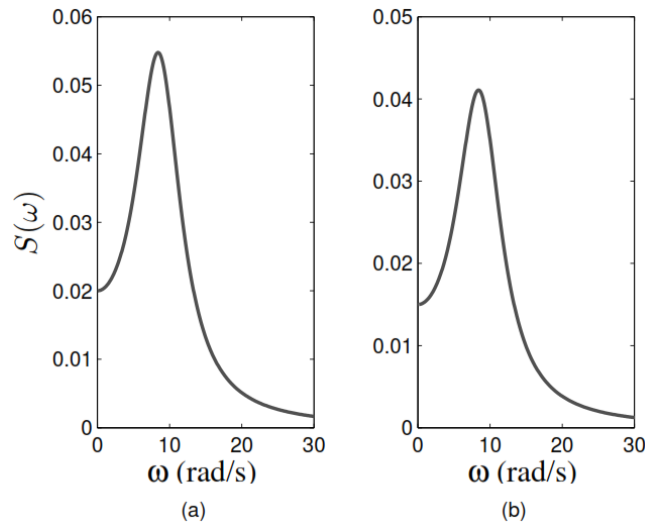


Figure 2.4: Kanai-Tajimi model

This Kanai-Tajimi model has the attractive feature because it is the ability to simulate

Table 2.1: Parameters of the filter soil of Clough-Penzien [91]

Soil	$\omega_g(\text{rad/s})$	ζ_g	$\omega_f(\text{rad/s})$	ζ_f
Hard	15.0	0.6	1.5	0.6
Medium	10.0	0.4	1.0	0.6
Soft	5.0	0.2	0.5	0.6

ground acceleration in a very simple way. The most serious shortcoming of the original Kanai-Tajimi model is its treatment of earthquakes as stationary random processes [90].

2.2.2.3 Clough-Penzien

Despite of the fact that the Kanai-tajimi shows advantage of the simple way for the simulation of the stationary ground motion but presents a drawback specially, in low frequency in which the variances of ground velocity and ground displacement become infinite ($\omega \rightarrow \infty$). These can be seen from the relationships between power spectra for ground acceleration, velocity and displacement.

To solve this noticed problem therefore the concept consists to remove the singularity at $\omega = 0$, Clough and Penzien modified the Kanai-Tajimi formulation by adding an another term.

Hence, the mathematical expression has been rewritten and given as follows

$$S(\omega) = S_0 \left[\frac{\omega_g^4 + 4\zeta_g^2 \omega_g^2 \omega^2}{(\omega_g^2 - \omega^2)^2 + 4\zeta_g^2 \omega_g^2 \omega^2} \right] \left[\frac{\omega^4}{(\omega_f^2 - \omega^2)^2 + 4\zeta_f^2 \omega_f^2 \omega^2} \right] \quad (2.3)$$

where ω_f and ζ_f are high-pass filter parameters with some examples in the table 2.1.

Figure 2.5 displays the different forms of Clough-Penzei model for $\zeta_g = 0.4$, $\omega_g = 3\pi \text{rad/s}$ $S_0 = 0.02 \text{m}^2/\text{s}^3$.

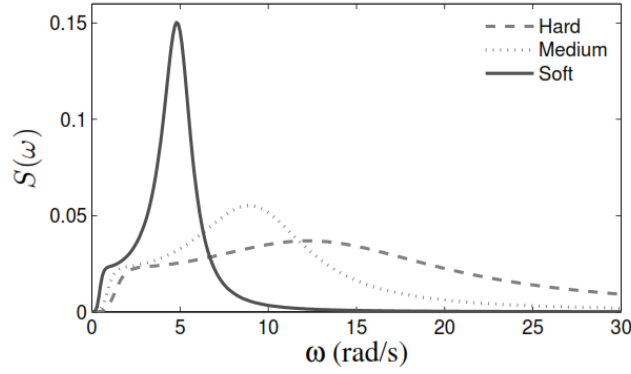


Figure 2.5: Clough-Penzei model

2.2.2.4 Envelope Functions

The envelope function $E_n(t)$ describes the variation of ground motion intensity with time. Various models have extensively been suggested in the literature to illustrate time-varying intensities and among them, three will be given in this work:

- The **Shinozuka and Sato model** is based on the difference between two exponential function given as follows [88] (Figure 2.6)

$$E_n(t) = e_0(e^{-\beta_1 t} - e^{-\beta_2 t}) \quad (2.4)$$

$$\text{with } e_0 = \frac{1}{\left(\frac{\alpha}{\beta}\right)^{\beta-\alpha} - \left(\frac{\alpha}{\beta}\right)^{\alpha-\beta}}$$

The time duration depends on the choice of parameters α and β ; the time at which the envelope function reaches the maximum value, $E_n(t) = 1$ is :

$$t_{\max} = \frac{\ln\left(\frac{\beta}{\alpha}\right)}{\beta - \alpha} \quad (2.5)$$

So by changing the values of these ones we have of different time-modulating functions.

Figure 2.6 shows the envelope function of Shinozuka and Sato model, the short duration ($\alpha = 0.10$, $\beta = 0.20$), and the long duration ($\alpha = 0.25$, $\beta = 0.75$).

- The mathematical expression of **Amin and Ang model** is generalised by Jennings

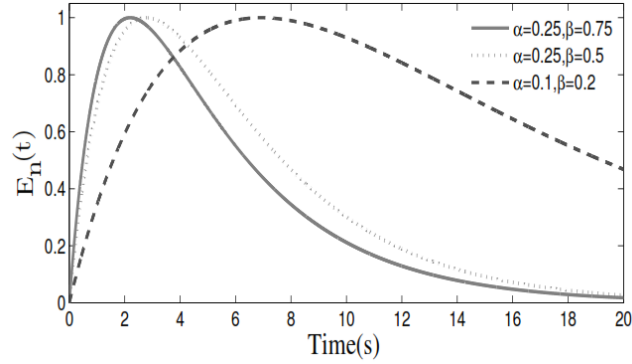


Figure 2.6: Envelope function of Shinozuka and Sato model

et al. [92], therefore the equation is

$$E_n(t) = \begin{cases} t^2/4, & 0 \leq t \leq 2 \\ 1.0, & 2 \leq t \leq 4 \\ \exp(-0.268(t-4)), & 4 \leq t \leq 12 \end{cases} \quad (2.6)$$

This form give in Figure 2.7 the illustration of the envelope function of Amin and Ang.

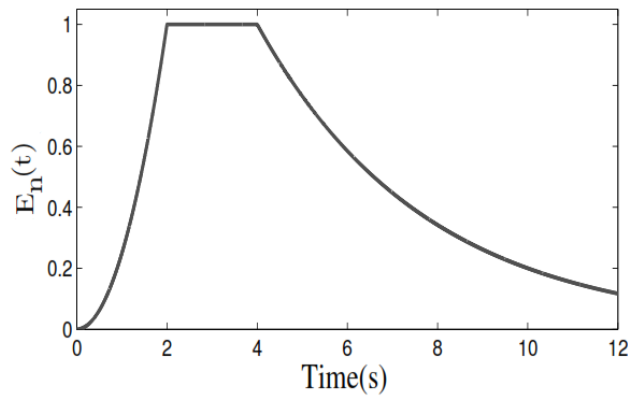


Figure 2.7: Envelope function of Amin and Ang model

– The mathematical model described by **Boore** [93] is expressed as follows

$$E_n(t) = at^b e^{-ct} H(t) \quad (2.7)$$

where $H(t)$ is the unit-step function. a is the normalizing factor, and b and c are the shape parameters.

The Envelope function of Boore model with the values of parameters $a = 0.117$; $b = 1.825$; $c = 0.277$ obtained by Saragoni and Hart [94] is

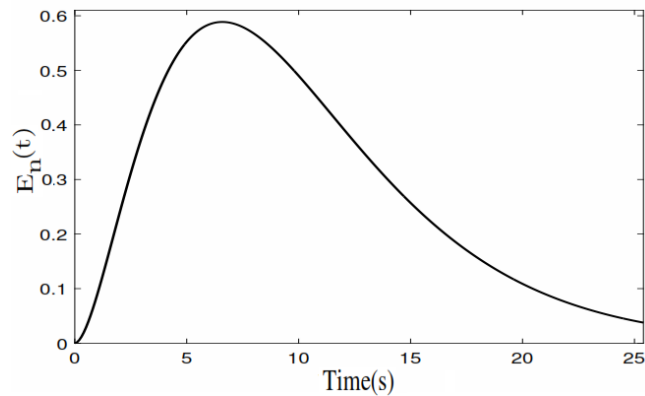


Figure 2.8: Envelope function of Boore model

2.2.3 Some examples of excitation Earthquake models

2.2.3.1 Kanai-Tajimi ground motion model+Envelope function Shinozuka and Sato model

The Kanai-Tajimi model for the earthquake ground motion is based on the observation that the absolute acceleration of the ground may be sought as a white noise process filtered through superimposed soil deposit modelled as a single degree of freedom (DOF) oscillator [95]. By modulating that model of ground motion by the envelope function of Shinozuka and Sato with the parameters $c_e = 0.2445$, $\alpha = 0.0075$ and $\beta = 0.015$, One obtain for a single sequence the figure 2.9:

2.2.3.2 Abbas and Takewaki

The nonstationary ground acceleration \ddot{X}_g of n sequences is presented by Abbas and Takewaki [96]. Authors pointed up, ground acceleration of multiple sequences could result in more damage to the structure than a single ordinary event. Because the structure

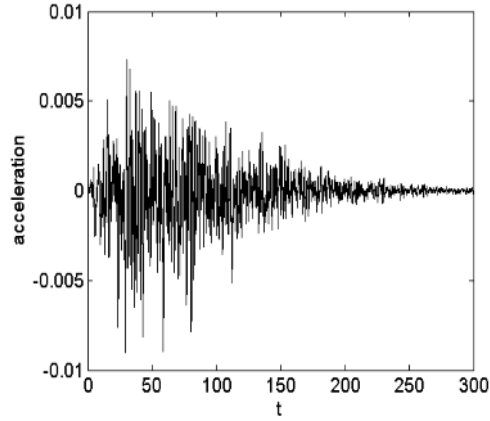


Figure 2.9: Generated earthquake

gets damaged in the first sequence, and additional damage accumulates from secondary sequences before any repair is possible.

The acceleration expression proposed to take the form of a filtered Gaussian stationary white noise modulated by a deterministic envelope function of time, as defined

$$\ddot{X}_g = \begin{cases} e_1(t) \ddot{w}_1(t) & 0 \leq t \leq T_1 \\ 0 & T_1 \leq t \leq \sum_{i=1}^2 T_i \\ e_2\left(t - \sum_{i=1}^2 T_i\right) \ddot{w}_2(t) & \sum_{i=1}^2 T_i \leq t \leq \sum_{i=1}^3 T_i \\ 0 & \sum_{i=1}^3 T_i \leq t \leq \sum_{i=1}^4 T_i \\ \dots & \dots \\ e_n\left(t - \sum_{i=1}^{n+1} T_i\right) \ddot{w}_n(t) & \sum_{i=1}^{n+1} T_i \leq t \leq \sum_{i=1}^{n+2} T_i \end{cases} \quad (2.8)$$

where $e_1(t)$, $e_2(t)$, ..., $e_n(t)$ are the envelope functions associated with the acceleration sequences 1, 2, ..., n ,

$\ddot{w}_1(t)$, $\ddot{w}_2(t)$, ..., $\ddot{w}_n(t)$ are stationary random processes,

$T_1, T_2, T_3, \dots, T_{n+2}$ are the time durations of the acceleration sequences.

The envelope function for the i th sequence is expressed as

$$e_i(t) = e_{0i} \left(t - \sum_{i=1}^n T_i \right) \exp \left[-\alpha_i \left(t - \sum_{i=1}^n T_i \right) \right]; \quad \sum_{i=1}^{n+1} T_i \leq t \leq \sum_{i=1}^{n+2} T_i; \quad (2.9)$$

where e_{0i} and α_i are $2n$ positive constants that control the intensity and the nonstationarity trend of the i th acceleration sequence.

The parameters of envelope function are $\alpha_1 = 0.3$, and $\alpha_2 = 0.35$, $A_1 = 0.8155$, $A_2 = 0.9514$, $\omega_g = 3\pi \text{rad/s}$, $\eta_g = 0.4$, (the time duration of the sequences is about 25 s, and 20 s respectively) and the separating time interval between the sequences is 40 s.

The dimensionless nonstationary ground acceleration for two sequences with the separating time interval both of them, is shown in Figure 2.10.

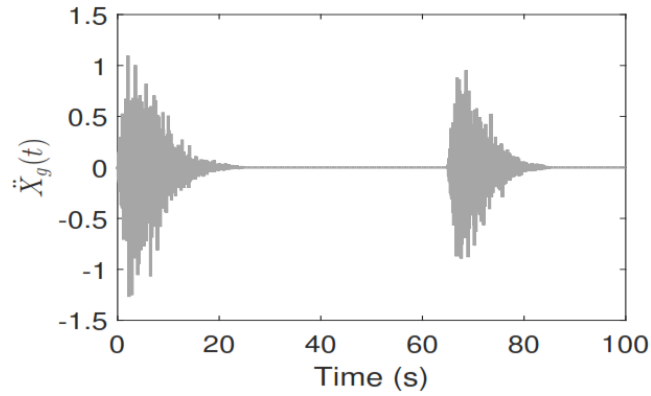


Figure 2.10: Sample simulated acceleration sequences

2.3 Wind flow models

2.3.1 The wind excitation

Wind is the flow of gases on a large scale. On the surface of the Earth, wind consists of the bulk movement of air. It is essentially the large scale horizontal movement of free air. Winds are commonly classified by their spatial scale, their speed, the regions in which they occur, and their effect (See Figures 2.11 and 2.12).

In meteorology, winds are often referred to according to their strength, and the direction from which the wind is blowing. Strong winds of intermediate duration (around one minute) are termed squalls. Long-duration winds have various names associated with their average strength, such as breeze, gale, storm and hurricane.



Figure 2.11: Cherry tree moving with wind blowing [97]

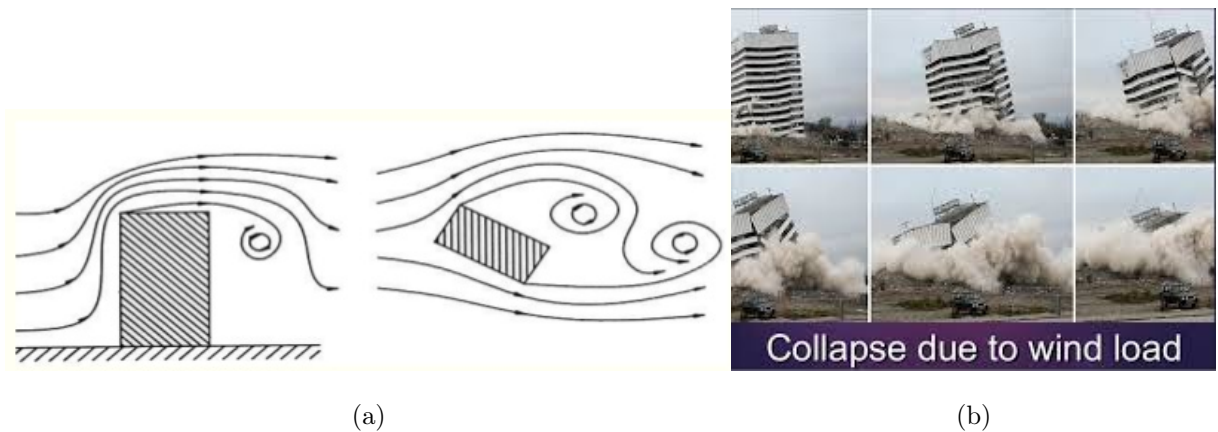


Figure 2.12: Collapse due to Wind load [102, 103]

Wind direction is usually expressed in terms of the direction from which it originates. For example, a northerly wind blows from the north to the south [98]. Weather vanes pivot to indicate the direction of the wind [99]. Wind speed is measured by anemometers,

most commonly using rotating cups or propellers. When a high measurement frequency is needed (such as in research applications), wind can be measured by the propagation speed of ultrasound signals or by the effect of ventilation on the resistance of a heated wire [100].

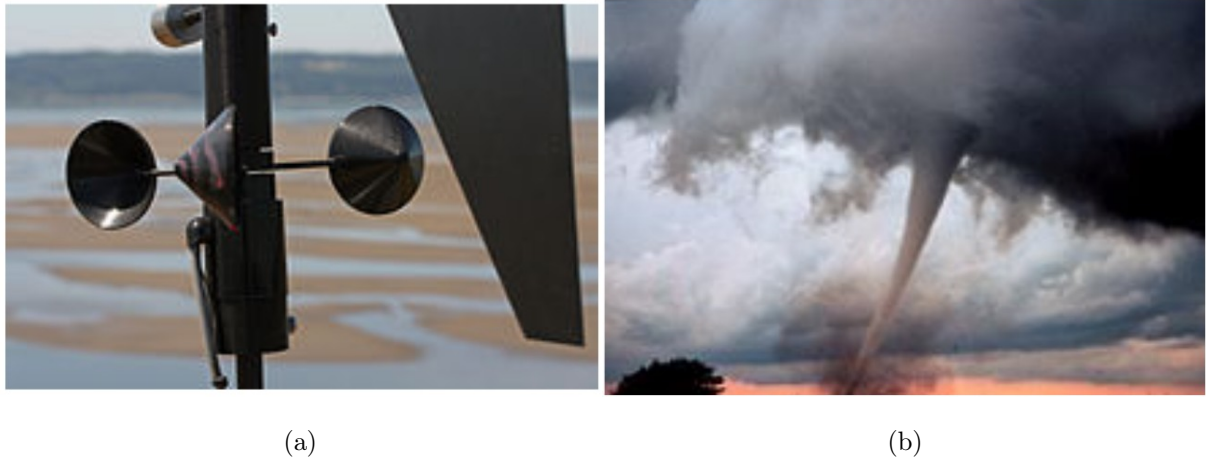


Figure 2.13: (a) Cup-type anemometer with vertical axis, a sensor on a remote meteorological station, (b) An occluded mesocyclone tornado (Oklahoma, May 1999) [97]

2.3.2 Computational fluid dynamics simulations of wind

Wind plays an important role in the designing of tall structures because it exerts loads on building. It is a phenomenon of great complexity because of the many flow situations arising from the interaction of wind with structures.

In order to model the impact of the wind flow on the structure, a numerical description of the average turbulent wind flow is required to express the fluid force which is applied to the structure. A turbulent wind flow can be modelled by a drag wind force and a lift wind force [126].

$$F_{\bar{D}} = \frac{1}{2} \rho b U_{rel}^2 (C_D \cos \theta + C_L \sin \theta) \quad (2.10)$$

$$F_L = -\frac{1}{2}\rho b U_{rel}^2 (C_L \cos \theta + C_D \sin \theta) \quad (2.11)$$

where C_D and C_L are respectively the drift and lift coefficients, ρ is the air mass density and b is the projected area of the structure, and

$$U_{rel}^2 = \left(\bar{U} + u(x, t) - \dot{W} \right)^2 + (\dot{y} + \dot{v})^2, \quad \tan \theta = \frac{\dot{y} + \dot{v}}{\bar{U} + u(x, t) - \dot{W}} \quad (2.12)$$

with W the displacement of the cantilever beam in along wind direction, \bar{U} the steady part of the wind flow, u the unsteady part of the wind flow along W direction and v the unsteady part of the wind flow along y direction.

Since in our topic we are focus on the vibration of the structure in the across wind direction, we will set $W = 0$ and we will consider only the lift wind force, this implies that :

$$\tan \theta = \frac{\dot{y} + \dot{v}}{\bar{U} + u(x, t)} \quad (2.13)$$

We suppose that u is just time dependent, and we set:

$$U(t) = \bar{U} + u(t) \quad (2.14)$$

Equation (2.13) becomes, assuming that the speed of the structure along y direction is greater than the unsteady part of the wind flow in the same direction

$$\tan \theta = \frac{\dot{y}}{U(t)} \quad (2.15)$$

with all the above informations, we can write equation (2.11) as:

$$F_L = \frac{1}{2}\rho b U^2(t) C_y(\theta), \quad (2.16)$$

with $C_y(\theta) = -[C_D(\theta)\tan(\theta) + C_L(\theta)]\sec(\theta)$,

It is showed that $C_y(\theta)$ can be expressed as polynomials of $\tan(\theta)$ and F_L can be expressed by:

$$F_L = \frac{1}{2}\rho b U^2(t) \sum_i D_i \tan^i \theta \quad (2.17)$$

The wind force (lift wind force) which blows orthogonally to the structure with time-depending velocity $U(t)$. The general form of the most used fluid force is, taking into account the direction [127]:

$$\vec{F} = \frac{1}{2} b C_y \rho |U| \vec{U} \quad (2.18)$$

Where, C_y is the aerodynamic coefficients relevant to square sections and can be written as $C_y = [D_0 + D_1 \left(\frac{\dot{y}}{U}\right) + D_2 \left(\frac{\dot{y}}{U}\right)^2 + D_3 \left(\frac{\dot{y}}{U}\right)^3]$, y is the longitudinal velocity fluctuations. And it can be rewritten according to it intensity as

$$F = \frac{1}{2} \rho U^2 b \left[D_0 + D_1 \left(\frac{\dot{y}}{U}\right) + D_2 \left(\frac{\dot{y}}{U}\right)^2 + D_3 \left(\frac{\dot{y}}{U}\right)^3 \right] \quad (2.19)$$

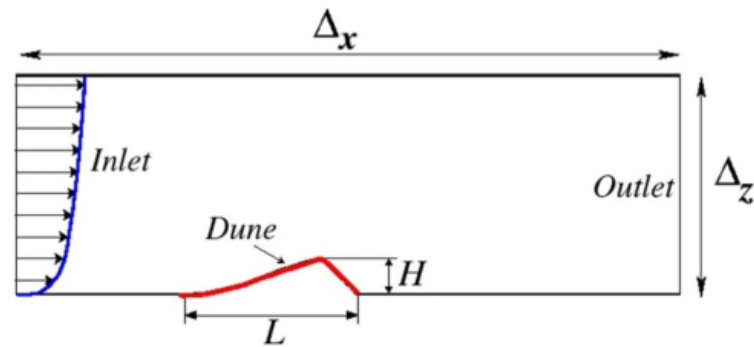


Figure 2.14: Schematic diagram of the computational setup with a dune as structure in x and z are axis, H the height and L the width of the dune [101].

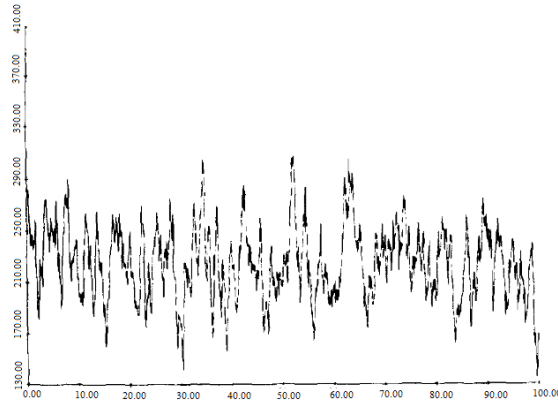


Figure 2.15: Time histories of aerodynamic forces on a towers and tension leg platforms (TLP) [104].

2.4 Approximate response method - numerical techniques

For all the differential equations obtained in the second part of this chapter, analysis of ordinary differential equations (ODEs), partial differential equations (PDEs) and Stochastic differential equations (SDEs) of a physical system will be done by using modal approximation and Runge-Kutta methods in this work.

2.4.1 Modal approximation

Galerkin modal method is used for modal approximation to reduce the system of PDEs to the system of ODEs [105]. In this procedure, the solution of the partial derivative equations is assumed to be separable into amplitude and mode shapes (the mode shapes must satisfy the geometry and natural boundary conditions). The transverse displacement and the flexibility of the beam can thus be written as

$$Y(X, \tau) = \sum_{n=1}^N U_n(X) Q_n(\tau) \quad (2.20)$$

where N represent the number of modes retained in the solution along x .

Substituting Equation (2.20) into the equation governing the dynamics of the system, multiplying by $U_n(X)$ and integrating over the length of the beam, we obtain the modal equation (nonlinear ODE).

2.4.2 Fourth-order Runge-Kutta method for ordinary differential equations

Runge-Kutta methods are among the most popular ODEs solver. It has been elaborated for the first time in 1894 by Carle Runge and has been improved by Martin W. Kutta in 1901. Their modern developments are mostly due to John Butcher in the 1960s, it is widely used since it is most stable [106]. Generally, we distinguish 04 important families of Runge-Kutta methods: Second-order, Fourth-order, Five-order and Six-order Runge-Kutta Methods. But the most used method is the Fourth-order one since that it is easy to use and no equations need to be solved at each stage, highly accurate for moderate values of the normalization integration time step and easy to code. Let us consider the ordinary first order differential equation:

$$\frac{dX(t)}{dt} = F(t, X(t)) \quad (2.21)$$

With $X(t_0) = X_0$; this equation can also be under a vectorial form (X and F being vectors). One define h as the time step size and $t_i = t_0 + ih$. The aim of the RK4 method is to find solutions after each time step, the next solution as a function of the previous one. The classical RK4 flow for this problem is given by:

$$\begin{aligned}
x_{0,j} &= X_0 \\
L_{1,j} &= hf_j(t_i, x_{i,j}) \\
L_{2,j} &= hf_j\left(t_i + \frac{h}{2}, x_{i,j} + \frac{L_{1,j}}{2}\right) \\
L_{3,j} &= hf_j\left(t_i + \frac{h}{2}, x_{i,j} + \frac{L_{2,j}}{2}\right) \\
L_{4,j} &= hf_j(t_i + h, x_{i,j} + L_{3,j}) \\
x_{i+1,j} &= x_{i,j} + \frac{1}{6}(L_{1,j} + 2L_{2,j} + 2L_{3,j} + L_{4,j})
\end{aligned} \tag{2.22}$$

where i runs for time incrementation and j labels the variables related to x_j . $L_{1,j}$, $L_{2,j}$, $L_{3,j}$ and $L_{4,j}$ are intermediate coefficients. This procedure needs in its iteration only the initial value X_0 , to calculate all the other values taken by the function X at other times separated by the time step h .

In the case m-order differential equation

$$\begin{cases} \frac{d^m X}{dt^m} = F_m\left(t, y, \frac{dX}{dt}, \frac{d^2 X}{dt^2}, \dots, \frac{d^{m-1} X}{dt^{m-1}}\right) \\ \frac{d^k X(t_0)}{dt^k} = X_0^{(k)} \end{cases} \tag{2.23}$$

with successive variables change, the equation (2.23) can be written under the form

$$\left\{ \begin{array}{l}
 \frac{d^0 X}{dt^0} = B_0 = X = F_0(t, B_0, B_1, \dots, B_{m-1}) \\
 \frac{dX}{dt} = \frac{dB_0}{dt} = B_1 = F_1(t, B_0, B_1, \dots, B_{m-1}) \\
 \frac{d^2 X}{dt^2} = \frac{dB_1}{dt} = B_2 = F_2(t, B_0, B_1, \dots, B_{m-1}) \\
 \cdot \\
 \cdot \\
 \cdot \\
 \frac{d^{m-1} X}{dt^{m-1}} = \frac{dB_{m-2}}{dt} = B_{m-1} = F_{m-1}(t, B_0, B_1, \dots, B_{m-1}) \\
 \frac{d^m X}{dt^m} = \frac{dB_{m-1}}{dt} = F_m(t, B_0, B_1, \dots, B_{m-1}) \\
 \frac{d^k X(t_0)}{dt^k} = B_k(t_0) = X_0^{(k)} \\
 k \in \{1; 2; \dots; m-1\}
 \end{array} \right. \quad (2.24)$$

With this general vectorial and form, iterations can be performed to determine all the values of X and its derivative at different time separated by the time step h using:

$$B_k(t+h) = B_k(t) + \frac{1}{6} (L_1^k + 2L_2^k + 2L_3^k + L_4^k) \quad (2.25)$$

where

$$\begin{aligned}
 L_1^k &= hF_k(t, B_0(t), B_1(t), \dots, B_{m-1}(t)); \\
 L_2^k &= hF_k\left(t + \frac{h}{2}, B_0(t) + \frac{L_1^0}{2}, B_1(t) + \frac{L_1^1}{2}, \dots, B_{m-1}(t) + \frac{L_1^{m-1}}{2}\right); \\
 L_3^k &= hF_k\left(t + \frac{h}{2}, B_0(t) + \frac{L_2^0}{2}, B_1(t) + \frac{L_2^1}{2}, \dots, B_{m-1}(t) + \frac{L_2^{m-1}}{2}\right); \\
 L_4^k &= hF_k(t+h, B_0(t) + L_3^0, B_1(t) + L_3^1, \dots, B_{m-1}(t) + L_3^{m-1})
 \end{aligned}$$

This generalized form will serve to solve numerically first-order coupled ODEs.

2.4.3 Stochastic Fourth-order Runge-Kutta method for the stochastic differential equations: Kasdin's RK4

SDEs are the differential equations which contain a stochastic process. These type of equations play an important role in physics but existing numerical methods for solving it are of low accuracy and poor stability. The efficient SRK4 scheme [107] developed by Jeremy N. Kasdin is used in this thesis to numerically treat the random process of the systems models.

Consider for simulation the following Itô stochastic differential equation:

$$\begin{cases} \frac{dX(t)}{dt} = F(t, X(t)) + G(t, X(t)) \xi(t) \\ X(t_0) = X_0 \end{cases} \quad (2.26)$$

where $X(t) = (x_1(t), x_2(t), \dots, x_n(t))$ is a vectorial variable with n -dimensional, $F = (f_1, f_2, \dots, f_n)$ and $G = (g_1, g_2, \dots, g_n)$ the vectorial flows. $\xi(t)$ is a random (stochastic) processes. This excitation is parametric (multiplicative) if its accompanying coefficient $G(t, X(t))$ is a function of X . Otherwise, it is external (additive). $\xi(t)$ can be:

– a white noise defines as [108]:

$$\langle \xi(t) \rangle = 0, \quad \text{and} \quad \langle \xi(t) \xi(t') \rangle = \delta(t - t') \quad (2.27)$$

– a colored (Ornstein-Uhlenbeck) noise defines as [108]:

$$\langle \xi(t) \rangle = 0, \quad \text{and} \quad \langle \xi(t) \xi(t') \rangle = \frac{1}{2\tau} e^{-\frac{|t-t'|}{\tau}} \quad (2.28)$$

– a bounded noise which is a harmonic function with constant amplitude and random phase defines as [108]:

$$\begin{aligned} \langle \xi(t) \rangle &= 0, & \langle \xi(t) \xi(t') \rangle &= \frac{\sigma^2}{2} \exp\left(-\frac{\gamma^2 |t-t'|}{2}\right) \cos \Omega(t-t'), \\ \xi(t) &= \sigma \cos(\Omega t + \gamma B(t) + \Gamma) \end{aligned} \quad (2.29)$$

where σ and γ are positive constants, $B(t)$ is a standard Wiener process, Γ is a random variable uniformly distribution in $[0, 2\pi]$. The brackets $\langle \dots \rangle$ denote the time average.

Let us consider the SDE gives by Equation (2.26) and assuming that $\xi(t)$ is a Gaussian white noise (since that it is the type of noise used in our work) defined as shown in (2.27).

Thus, the Kasdin's scheme is described as follows

$$x_{i+1,j} = x_{i,j} + \frac{1}{6} (L_{1,j} + 2L_{2,j} + 2L_{3,j} + L_{4,j}) \quad (2.30)$$

in which

$$K_{1,j} = hf_j(t_i, x_{i,j}) + hg_j(t_i, x_{i,j}) \xi_1$$

$$K_{2,j} = hf_j(t_i + c_2h, x_{i,j} + a_{21}K_1) + hg_j(t_i + c_2h, x_{i,j} + a_{21}K_1) \xi_2$$

$$K_{3,j} = hf_j(t_i + c_3h, x_{i,j} + a_{31}K_1 + a_{32}K_2) + hg_j(t_i + c_3h, x_{i,j} + a_{31}K_1 + a_{32}K_2) \xi_3$$

$$K_{4,j} = hf_j(t_i + c_4h, x_{i,j} + a_{41}K_1 + a_{42}K_2 + a_{43}K_3) + hg_j(t_i + c_4h, x_{i,j} + a_{41}K_1 + a_{42}K_2 + a_{43}K_3) \xi_4$$

c is a constant that can be obtained by

$$c_2 = a_{21} \quad (2.31)$$

$$c_3 = a_{31} + a_{32} \quad (2.32)$$

$$c_4 = a_{41} + a_{42} + a_{43} \quad (2.33)$$

The Mean is given

Table 2.2: Coefficients of the SRK4 method . [109]

Coefficients	Value	Coefficients	Value
a21	0.66667754298442	a52	0.67428574806272
a31	0.63493935027993	a53	-0.00831795169360
a32	0.00342761715422	a54	0.08401868181222
a41	-2.32428921184321	q1	3.99956364361748
a42	2.69723745129487	q2	1.64524970733585
a43	0.29093673271592	q3	1.59330355118722
a51	0.25001351164789	q4	0.26330006501868

$$\bar{X} = \frac{1}{n} \sum_{m=1}^n x_m(t) \quad (2.34)$$

2.4.4 Lyapunov stability theory

With a view to obtain the optimal input voltage corresponding to the desired damper force of the MR damper controller use in the system to control vibration; and to assess the performance of control system, the control algorithm as an effective mean used in semiactive control based on the Lyapunov stability theory [110] is employed. Thus, the Lyapunov function denoted $L_y(\mathbf{W})$ must be a positive function of the state of the system, \mathbf{W} . According to the Lyapunov stability theory, if the rate of change of lyapunov function, $\dot{L}_y(\mathbf{W})$, is negative semidefinite, the origin is stable.

Lyapunov function is chosen of the form

$$L_Y = \frac{1}{2} \|W\|_p^2, \quad (2.35)$$

where $\|\Sigma\|$ =P-norm of the states defined by

$$\|\Sigma\|_p = |\Sigma' P_L \Sigma|^{1/2}, \quad (2.36)$$

where \mathbf{P}_L is real, symmetric, positive definite matrix. \mathbf{P}_L is found using Lyapunov equation.

$$\Sigma' P_L + P_L \Sigma = -Q_p \quad (2.37)$$

\mathbf{Q}_p is a positive definite matrix. The derivative of the Lyapunov function for a solution of the state-space equation is

$$\dot{L}_Y = -\frac{1}{2} W' Q_p W + W' P_L B_1 F_d + W' P_L B \ddot{y}_g. \quad (2.38)$$

The above parameters are defined as follows:

$$W = \begin{bmatrix} \chi_j \\ \dot{\chi}_j \end{bmatrix}, \Sigma = \begin{bmatrix} 0 & 1 \\ -\zeta_j & -\zeta_j \end{bmatrix}, B = \begin{bmatrix} 0 \\ -\sigma_j \end{bmatrix}, B_1 = \begin{bmatrix} 0 \\ -\zeta_a \eta_j \end{bmatrix}.$$

The control law which will minimize L_y

$$V_C = V_{\max} H(-W' P_L B_1 F_d), \quad (2.39)$$

where V_{\max} is the maximum voltage and $H(\cdot)$ is Heaviside step function. When this function is greater than zero, the voltage (V_c) applied to the damper should be maximum (V_{\max}), otherwise, the command voltage is set to zero.

2.4.5 Hardware and software

As machine support during this thesis work, we used a Laptop computer running Windows 10 Pro operating system and three major software's: Fortran for differential equations,

Matlab for data analysis and Maple for integral calculus.

2.5 Mathematical modelling

This section is devoted to the details of all the modelling used during this work.

2.5.1 Outrigger system applied on a tall building

The dynamics of the Cantilever beam is described by the Euler-Bernoulli theory as presented in subsection 1.2.1. When the beam has an internal damping coefficient, taking into account the moment generated by the damped outrigger $M(x, t)$, the general equation describing the structure of Figure 2.16 is:

$$m \frac{\partial^2 y(x, t)}{\partial t^2} + \lambda \frac{\partial y(x, t)}{\partial t} + EI \frac{\partial^4 y(x, t)}{\partial x^4} = - \frac{\partial M(x, t)}{\partial x} \quad (2.40)$$

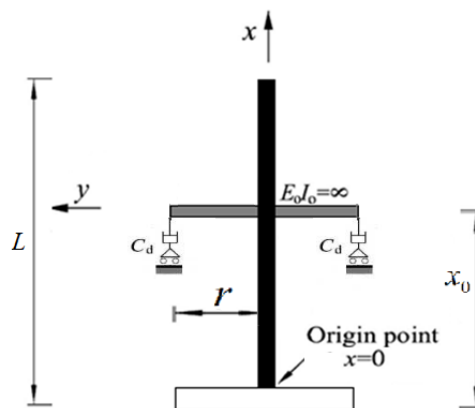


Figure 2.16: Cantilever beam with one level of symmetric attached outriggers

- Derivation of the expression of $M(x, t)$

Let us consider Figure 2.17 which shows the behavior of the damper of each side of outrigger.

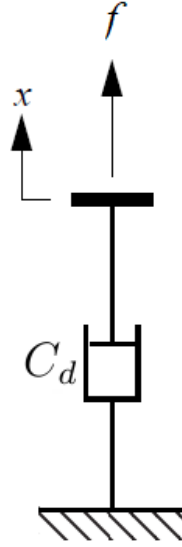


Figure 2.17: The damper

When the system of the cantilever beam is subjected to an external excitation, the damped outrigger moves following x -direction. The distributed moment incited by the damper is given by:

$$M(x, t) = 2fr \quad (2.41)$$

where f is the viscous force brought by the damped outrigger. It can be expressed by:

$$f = -C_d \frac{dx}{dt} \quad (2.42)$$

with C_d the damping coefficient, $\frac{dx}{dt}$ the speed of displacement of the cantilever beam.

According the damper lateral displacement, an angle is defined θ and $\sin\theta \simeq \theta = \frac{dx}{r}$, which implies that equation (2.42) can also be written as follows

$$f = -C_d r \frac{d\theta}{dt} \quad (2.43)$$

For small displacements, $\tan\theta \simeq \theta = \frac{\partial y}{\partial x}$, so equation (2.43) become:

$$f = -C_d r \frac{\partial^2 y}{\partial x \partial t} \quad (2.44)$$

Then the moment distributed is equal to

$$M = -2C_d r^2 \frac{\partial^2 y(x, t)}{\partial x \partial t} \quad (2.45)$$

► Dynamic equation with the explicit expression of $M(x, t)$

Since the distributed moment is localized at position $x = x_0$ from the ground (the fixed end of the beam), as figure 2.16 shows, it is written as:

$$M = -2C_d r^2 \frac{\partial^2 y(x, t)}{\partial x \partial t} \delta(x - x_0) \quad (2.46)$$

where $\delta(x - x_0)$ represents the Dirac delta function define as follows:

$$\delta(x - x_0) = \begin{cases} 1 & \text{if } x = x_0 \\ 0 & \text{Otherwise,} \end{cases} \quad (2.47)$$

Inserting equation (2.46) into equation (2.40), the equation of the dynamics of cantilever beam with Damper outriggers becomes:

$$m \frac{\partial^2 y(x, t)}{\partial t^2} + \lambda \frac{\partial y(x, t)}{\partial t} + EI \frac{\partial^4 y(x, t)}{\partial x^4} = 2C_d r^2 \left[\frac{\partial^3 y(x, t)}{\partial x^2 \partial t} \delta(x - a) + \frac{\partial^2 y(x, t)}{\partial x \partial t} \frac{\partial \delta(x - x_0)}{\partial x} \right] \quad (2.48)$$

In the case of continuous differentiable function $\psi(x)$, the Dirac distribution satisfies the equation [111]:

$$\psi(x) \frac{d}{dx} \delta(x - x_0) = \psi(x_0) \frac{d}{dx} \delta(x - x_0) - \delta(x - x_0) \frac{d}{dx} \psi(x) \quad (2.49)$$

Using relation (2.49), we can write equation (2.48) as follows:

$$m \frac{\partial^2 y(x, t)}{\partial t^2} + \lambda \frac{\partial y(x, t)}{\partial t} + EI \frac{\partial^4 y(x, t)}{\partial x^4} = 2C_d r^2 \frac{\partial^2 y(x, t)}{\partial x \partial t} \Big|_{x=x_0} \frac{\partial \delta(x - x_0)}{\partial x} \quad (2.50)$$

And for many attached level of outriggers, one obtains:

$$m \frac{\partial^2 y(x, t)}{\partial t^2} + \lambda \frac{\partial y(x, t)}{\partial t} + EI \frac{\partial^4 y(x, t)}{\partial x^4} - ES \left[\frac{1}{2L} \int_0^L \left(\frac{\partial y}{\partial x} \right)^2 dx \right] \frac{\partial^2 y(x, t)}{\partial x^2} \quad (2.51)$$

$$-2C_d r^2 \sum_{i=1}^N \frac{\partial^2 y(x, t)}{\partial x \partial t} \Big|_{x=x_i} \frac{\partial \delta(x - x_i)}{\partial x} = -m \ddot{x}_e$$

with x_i the distance between the fixed end of the beam on the ground and the point where the outrigger is hanged on the centre core.

2.5.2 Added branches on a pendulum

The inverted pendulum is considered as a rigid rod on which a level of symmetrical branches is fixed (see Figure 2.18). Those branches are made of massless rigid bars with masses at their free end linked on that central column.

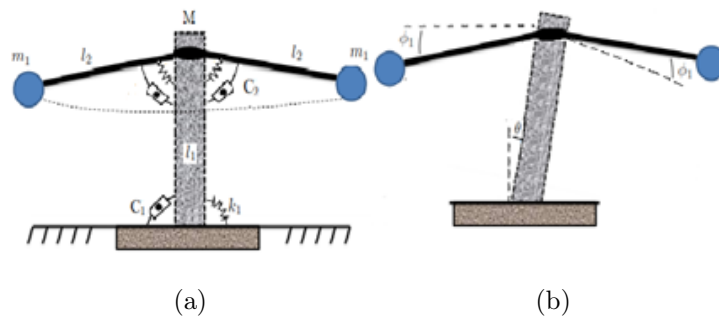


Figure 2.18: An inverted pendulum with one level of symmetrical masses

Equation (1.15) gives the dynamic of the central column only, modelled as an inverted pendulum. With attached masses, the new model is given by Figure 2.19.

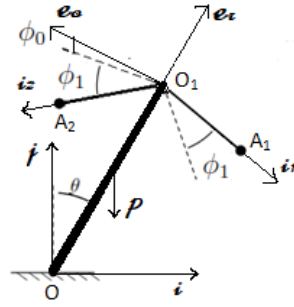


Figure 2.19: Position and distance measurement

O is the origin of the principal system with (i, j) the axes; it is also the fixed end (the base) of the central column of the structure. O_1 is the origin of the moving system with (e_r, e_θ) the axes of polar system and the free end (the top) of the structure where masses are joined for one level of attached branches. A_1 and A_2 are positions at any time of the right and the left masses respectively; while i_1 and i_2 are unit vectors of lines (O_1A_1) and (O_1A_2) respectively. The angle ϕ_0 is the one make by the bar of length l_2 with imaginary horizontale line at rest.

► Determination of potential and kinetic energies of the system

The system is divided in three: the main rigid rod, the left mass and the right mass. Potential and kinetic energies are:

$$E_{p_f} = E_p(M) + E_p(m_1) + E'_P(m_1) \quad (2.52)$$

and

$$E_{c_f} = E_c(M) + E_c(m_1) + E'_c(m_1) \quad (2.53)$$

with

$$E_p(M) = \frac{1}{2}k_1\theta^2 + \frac{1}{2}MgL \cos \theta; \quad E_p(m_1) = -m_1gz_1 + \frac{1}{2}k_2\phi_1^2; \quad E'_P(m_1) = -m_1gz_2 + \frac{1}{2}k_2\phi_1^2 \quad (2.54)$$

and

$$E_c(M) = \frac{1}{8}ML^2\dot{\theta}^2; \quad E_c(m_1) = \frac{1}{2}m_1 \left(\frac{d\overrightarrow{OA_1}}{dt} \right)^2; \quad E'_c(m_1) = \frac{1}{2}m_1 \left(\frac{d\overrightarrow{OA_2}}{dt} \right)^2 \quad (2.55)$$

z_1 and z_2 are vertical components of positions of A_1 and A_2 . Let us determine $\left(\frac{d\overrightarrow{OA_1}}{dt} \right)^2$ and $\left(\frac{d\overrightarrow{OA_2}}{dt} \right)^2$.

$$\overrightarrow{OA_1} = \overrightarrow{OO_1} + \overrightarrow{O_1A_1} = l_1\vec{e}_r + l_2\vec{i}_1 \quad (2.56)$$

and

$$\overrightarrow{OA_2} = \overrightarrow{OO_1} + \overrightarrow{O_1A_2} = l_1\vec{e}_r + l_2\vec{i}_2 \quad (2.57)$$

while

$$\left\{ \begin{array}{l} \vec{e}_r = \sin \theta \vec{i} + \cos \theta \vec{j} \\ \vec{e}_\theta = -\cos \theta \vec{i} + \sin \theta \vec{j} \end{array} \right. \quad \text{and} \quad \left\{ \begin{array}{l} \vec{i}_1 = -\cos(\phi_0 + \phi_1)\vec{e}_\theta - \sin(\phi_0 + \phi_1)\vec{e}_r \\ \vec{i}_2 = \cos(\phi_0 - \phi_1)\vec{e}_\theta - \sin(\phi_0 - \phi_1)\vec{e}_r \end{array} \right. \quad (2.58)$$

so

$$\left\{ \begin{array}{l} \left(\frac{d\overrightarrow{OA_1}}{dt} \right)^2 = l_1^2\dot{\theta}^2 - 2l_1l_2\dot{\theta}(\dot{\theta} + \dot{\phi}_1)\sin(\phi_0 + \phi_1) + l_2^2(\dot{\theta} + \dot{\phi}_1)^2 \\ \left(\frac{d\overrightarrow{OA_2}}{dt} \right)^2 = l_1^2\dot{\theta}^2 - 2l_1l_2\dot{\theta}(\dot{\theta} + \dot{\phi}_1)\sin(\phi_0 - \phi_1) + l_2^2(\dot{\theta} + \dot{\phi}_1)^2 \end{array} \right. \quad (2.59)$$

Potential and kinetic energies become:

$$E_{c_f} = \frac{1}{8}ML^2\dot{\theta}^2 + m_1 \left[l_1^2\dot{\theta}^2 + l_2^2(\dot{\theta} + \dot{\phi}_1)^2 - 2l_1l_2\dot{\theta}^2 \sin \phi_0 \cos \phi_1 - 2l_1l_2\dot{\theta}\dot{\phi}_1 \sin \phi_0 \cos \phi_1 \right] \quad (2.60)$$

and

$$E_{p_f} = \frac{1}{2}k_1\theta^2 + \frac{1}{2}MgL \cos \theta + 2m_1g [l_2 \sin \phi_0 \cos (\theta + \phi_1) - l_1 \cos \theta] + k_2\phi_1^2 \quad (2.61)$$

► Lagrangian and equations of the system

The Lagrangian of the system is given by:

$$L_a = \frac{1}{8}ML^2\dot{\theta}^2 + m_1 \left[l_1^2\dot{\theta}^2 + l_2^2(\dot{\theta} + \dot{\phi}_1)^2 - 2l_1l_2\dot{\theta}^2 \sin \phi_0 \cos \phi_1 - 2l_1l_2\dot{\theta}\dot{\phi}_1 \sin \phi_0 \cos \phi_1 \right] - \frac{1}{2}k_1\theta^2 - \frac{1}{2}MgL \cos \theta - 2m_1g [l_2 \sin \phi_0 \cos (\theta + \phi_1) - l_1 \cos \theta] - k_2\phi_1^2 \quad (2.62)$$

And the system of equations which describe the motion of the central column and his branches is:

$$\left\{ \begin{array}{l} \left(\frac{1}{4}ML_1^2 + 2m_1l_1^2 - 2m_1l_1^2 \cos^2 \phi_0 \sin^2 \phi_1 \right) \ddot{\theta} + \left(C_1 - 4m_1l_1l_2\dot{\phi}_1 \cos \phi_0 \cos \phi_1 \right) \dot{\theta} \\ + (2m_1l_1^2 \cos^2 \phi_0 \cos \phi_1 \sin \phi_1 - 2m_1l_1l_2 \cos \phi_0 \cos \phi_1) \dot{\theta}^2 + k_1\theta + \left(2m_1 - \frac{1}{2}M \right) gl_1 \sin \theta \\ + \left(\frac{l_1}{l_2} \cos \phi_0 \sin \phi_1 - 1 \right) C_2\dot{\phi}_1 + 2 \left(\frac{l_1}{l_2} \cos \phi_0 \sin \phi_1 - 1 \right) k_2\phi_1 - 2m_1l_1l_2\dot{\phi}_1^2 \cos \phi_0 \cos \phi_1 \\ - m_1gl_1 \sin (2\phi_0) \sin \phi_1 \sin (\theta + \phi_1) = 0 \\ 2m_1l_2^2\ddot{\phi}_1 + C_2\dot{\phi}_1 + 2k_2\phi_1 - 2m_1gl_2 \sin \phi_0 \sin (\theta + \phi_1) + 2m_1l_1l_2\dot{\theta}^2 \cos \phi_0 \cos \phi_1 = \\ (2m_1l_1l_2 \cos \phi_0 \sin \phi_1 - 2m_1l_2^2) \ddot{\theta} \end{array} \right. \quad (2.63)$$

2.6 Conclusion

The present chapter consists of the modelling of earthquake load; mathematical and numerical techniques used for the analysis of the problem of this thesis and the support materials used in this work.

Using all these methods and materials, we are now able to follow this study and obtain different results that give us informations about the different states of the studied systems.

The results are presented in Chapter 3.

CHAPTER III

RESULTS AND DISCUSSION

3.1 Introduction

This third chapter is devoted to the results and discussions on the work carried out in this thesis. In the second and the third sections of this chapter, the effect of N-damped outriggers on a high-rise structure subjected to earthquake loads is described, modelled and its dynamical study performed and an application of one outrigger MR damped on a Timoshenko beam is studied. The fourth and fifth sections focus on an inverted pendulum with multi-branching view as self-controlled system: Modelling and vibration absorber capacity for single attached mass and symmetrical attached masses. The behavior of self-control vibration system and the performance prediction of an inverted pendulum are also highlighted. The last section concludes the chapter.

3.2 Effect of N-damped outriggers on a high-rise structure subjected to earthquake loads

3.2.1 From one outrigger to N-outrigger systems

3.2.1.1 Mathematical model

The system is constituted by a uniform cantilever beam equipped N symmetrical damped outriggers (See figure 3.1). The length of the beam is L the mass per unit length $m = \rho S$ where S is the cross-sectional area and ρ the density ; δ is the internal damping of the beam. By ignoring the axial deformations of the perimeter columns, the dampers between the ends of the outriggers and the perimeter columns are regarded as external dampers. Outriggers, which are located at x_i with $i = 0 \dots 5$ from the fixed end of the beam, behave as a rigid body and the exterior columns have commonly a high stiffness, which are assumed to be infinitely rigid and written $E_0 I_0$ [112]. The bending stiffness of the beam is

characterized by EI , where E is the Young's modulus and I , the area moment of inertia of the cross section about the neutral axis. The distance from the central core to the damper is written r , and for this system the damper is a viscous damper with the damping coefficient C_d . All the device is under the earthquake loads modeled, in this work, as a nonstationary ground acceleration with a random function which take the form of a filtered Gaussian stationary white noise modulated by a deterministic envelope function.

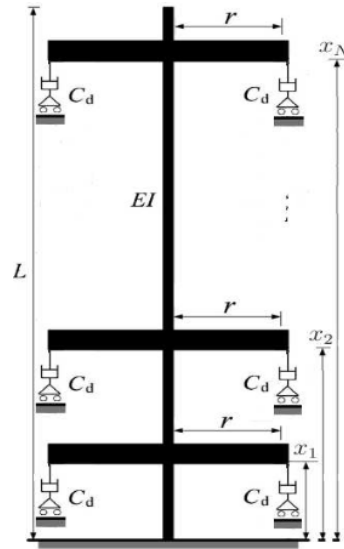


Figure 3.1: Cantilever beam with N damped outriggers

$$m \frac{\partial^2 w(x,t)}{\partial t^2} + \delta \frac{\partial w(x,t)}{\partial t} + EI \frac{\partial^4 w(x,t)}{\partial x^4} - ES \left[\frac{1}{2L} \int_0^L \left(\frac{\partial w}{\partial x} \right)^2 dx \right] \frac{\partial^2 w(x,t)}{\partial x^2} \quad (3.1)$$

$$-2C_d r^2 \sum_{i=1}^N \left. \frac{\partial^2 w(x,t)}{\partial x \partial t} \right|_{x=x_i} \frac{\partial \delta(x-x_i)}{\partial x} = -m \ddot{x}_e$$

Where $w(x, t)$ is the transversal displacement of the beam and \ddot{x}_e the excitation force. To reduce the number of compatible equations, the Dirac function is introduced into the differential function by locating the coordinate at the outrigger position [113] : $\delta(x - x_i)$. Thus x_i is the distance between the fixed end of the beam on the ground and the point where the outrigger is hanged on the centre core.

With Σ to take into account each of the N levels of outriggers and x_i their locations.

By having a regard on the Eq. (3.1), the first three terms are those of the classical Euler-Bernoulli beam model ; but the fourth and the fifth ones are respectively the geometrical non linearity term and the outriggers impact on the centre core. That cubic term represents the restoring force due to stretching of the neutral axis. In fact, that geometrical non linearity comes from high displacements and the deformation of the average line. The axial deformations in the beam are due to the movements of traction/compression and flexion of the core tube [37, 114].

By using the Kanai Tajimi model, the ground acceleration \ddot{x}_e is assumed to be represented by

$$\ddot{x}_e = e_0(e^{-\beta_1 t} - e^{-\beta_2 t})\ddot{w}(t) \quad (3.2)$$

with the spectral density given by :

$$S_{\ddot{w}}(\omega) = s_0 \frac{\omega_g^4 + (2\zeta_g \omega_g \omega)^2}{(\omega_g^2 - \omega^2)^2 + (2\zeta_g \omega_g \omega)^2} \quad (3.3)$$

where S_0 is the intensity of the white noise process at the rock level, ω_g is the dominant frequency of the soil site and ζ_g is the associated damping ratio of the soil strata.

Boundary conditions corresponding to the beam, are:

$$w(x, t)|_{x=0} = 0, \quad \frac{\partial w}{\partial x}|_{x=0} = 0 \text{ for the fixed end} \quad (3.4)$$

$$\text{And } \frac{\partial^2 w(x, t)}{\partial x^2}|_{x=L} = 0, \quad \frac{\partial^3 w(x, t)}{\partial x^3}|_{x=L} = 0 \text{ for the free end}$$

These conditons means that for the fixed end, the part of the structure which is clamped into the ground, there is no displacement and the angular coefficient of the tangent to the elastic line is null; and for the free end, the top of the structure, the flexion moment and the sharp effort are constantly nulls.

The initial conditions are supposed to be zero when the external force appears on beam:

$$w(x, t)|_{t=0} = 0, \quad \left. \frac{\partial w(x, t)}{\partial t} \right|_{t=0} = 0 \quad (3.5)$$

3.2.1.2 Modal equations

For the analytical purpose, the equation of a single mode dynamic leads us to express w in the form:

$$w(x, t) = X_n(x) \cdot Q_n(t) \quad (3.6)$$

where $Q_n(t)$ is the amplitude of the n^{th} mode, and $X_n(x)$ is the solution of the eigenvalue problem which depends on the boundary conditions of the free oscillations of the beam :

$$X_n(x) = -\frac{\sin(\lambda_n) + \sinh(\lambda_n)}{\cos(\lambda_n) + \cosh(\lambda_n)} [\cos(\lambda_n \frac{x}{L}) - \cosh(\lambda_n \frac{x}{L})] + [\sin(\lambda_n \frac{x}{L}) - \sinh(\lambda_n \frac{x}{L})] \quad (3.7)$$

After substituting Eq.(3.7) into Eq.(3.1), multiplying both sides of the resultant equation by the spatial part X_n , then integrating with respect to the beam axis x over the length L , and considering the dimensionless variables

$$\theta_n = \frac{q_n}{L}, \quad \tau = w_0 t \quad (3.8)$$

The dimensionless modal equation, for the each modes (with $n = 1, 2, \dots, \infty$), is given by :

$$\frac{d^2 \theta_n}{d\tau^2} + [\gamma + H(C_d, x_N)] \frac{d\theta_n}{d\tau} + \theta_n - \beta \theta_n^3 = -V \ddot{x}_e \quad (3.9)$$

With the coefficients :

$$\gamma = \frac{\delta L^2}{\lambda_n^2 \sqrt{mEI}}, \quad H(C_d, x_N) = 2C_d r^2 \sum_{N=1}^5 \left[\left. \frac{\partial X_n}{\partial x} \right|_{x=x_N} \right]^2, \quad k = \frac{SL^5}{2I\lambda_n^4},$$

$$\beta = k \cdot \left[\int_0^L \left(\frac{\partial X_n}{\partial x} \right)^2 dx \right] \cdot \int_0^L X_n \cdot \frac{\partial^2 X_n}{\partial x^2} dx, \quad z = \frac{mL^3}{EI\lambda_n^4}, \quad V = z \cdot \left[\int_0^L X_n dx \right]$$

In the following, the analysis will be done until the fifth modes of vibration jointly because of the cubic term, the modes cannot be independently studied.

Table 3.1: Properties of the beam

Item	Notation	Value
Length	L	20.78 m
Mass	m	760 Kg
Young modulus (steel)	E	12 MPa
Cross-sectional area	S	2.9 m^2
Mass density	ρ	262.06897 Kg/m^2
Moment of inertia	I	0.667 m^4
Stiffness	δ	180.723 N/m^2

3.2.2 Numerical analysis of the base equations

For numerical purpose, the physical and geometrical properties of the beam, which is here the central column, are for a wooden structure. And the length, the mass, the mass density in the following Table 3.1 are those of Fujita [115].

Thus, except $\gamma = 0.009$, the dimensionless parameters of Eq.(3.9): $H(c, x_N) = f(\lambda_n, x_i)$, $\beta = g(\lambda_n)$ et $V = h(\lambda_n)$ take into account either the position or the mode, or the both. $g(\lambda_n)$ and $h(\lambda_n)$ are two functions with the only variable parameter λ which pointed out the mode of vibration. And $f(\lambda_n, x_i)$ is a function of λ due to the mode of vibration and x_i the location of the outrigger: for one outrigger $i = 1$ and for N outriggers $i = 1, \dots, N$.

Because earthquake is a stochastic force, it was generated by a Gaussian white noise which is essentially made from random numbers. To obtain our following results, we used stochastic four-order Runge-Kutta algorithm with the coefficients of Table 3.2:

For one outrigger located on the cantilever beam, we find the right position by observing the response of the structure to an earthquake generate numerically with the taken

Table 3.2: Fourth Order, Time Varying Stochastic Runge-Kutta Coefficients. [109]

Coefficients	Value	Coefficients	Value
a21	0.66667754298442	a52	0.67428574806272
a31	0.63493935027993	a53	-0.00831795169360
a32	0.00342761715422	a54	0.08401868181222
a41	-2.32428921184321	q1	3.99956364361748
a42	2.69723745129487	q2	1.64524970733585
a43	0.29093673271592	q3	1.59330355118722
a51	0.25001351164789	q4	0.26330006501868

spectral density defined by the Kanai Tajimi model, because it is one of the best model which fitted most the earthquake [116, 117]. The dimensionless ground acceleration earthquake is shown on the following Fig. 3.2:

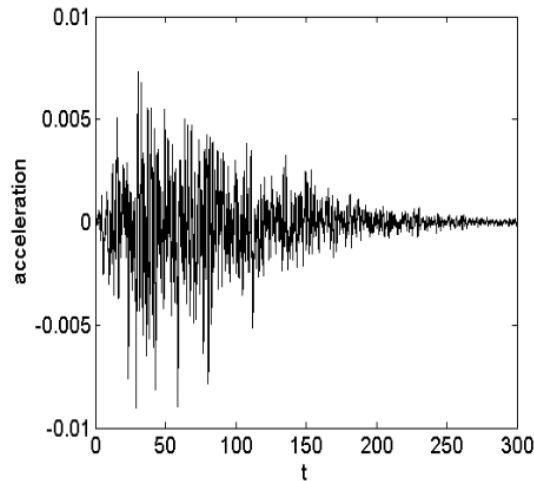
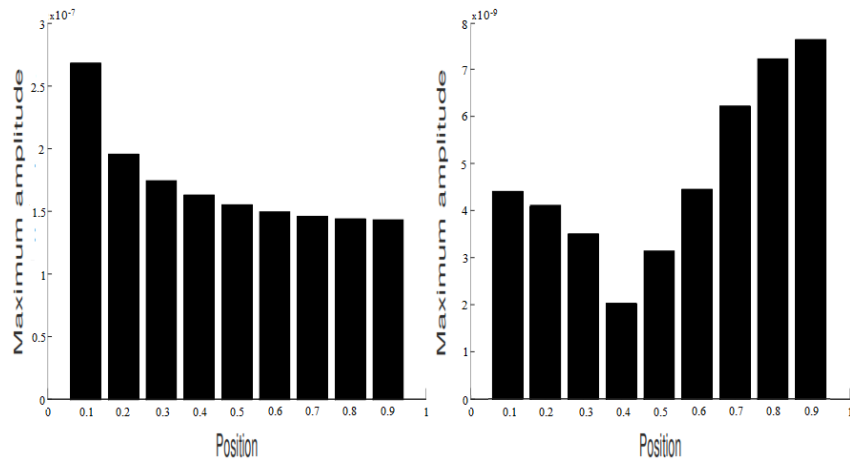


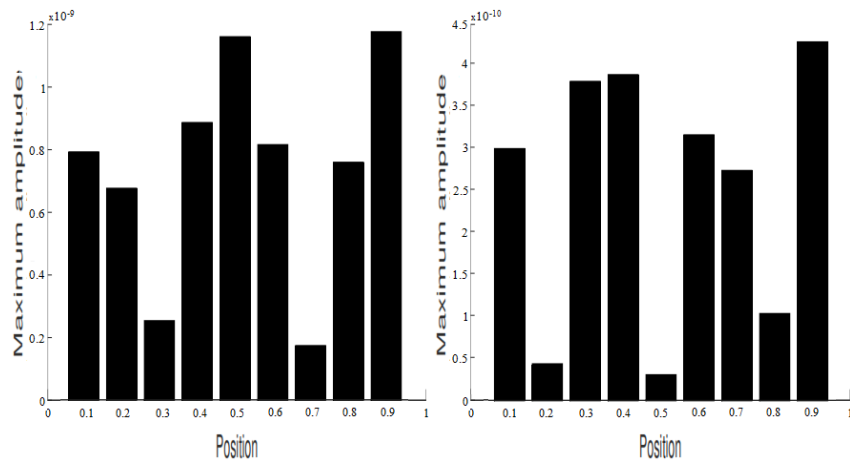
Figure 3.2: Dimensionless ground acceleration earthquake.

By applying that earthquake on our structure of outrigger system, for the first five modes of vibrations, the following histograms of the mean's peak of values of displacement responses is obtained (Fig. 3.3):



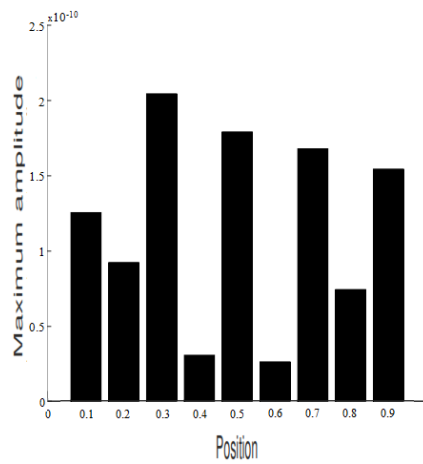
(a) First mode

(b) Second mode



(c) Third mode

(d) Fourth mode



(e) Fifth mode

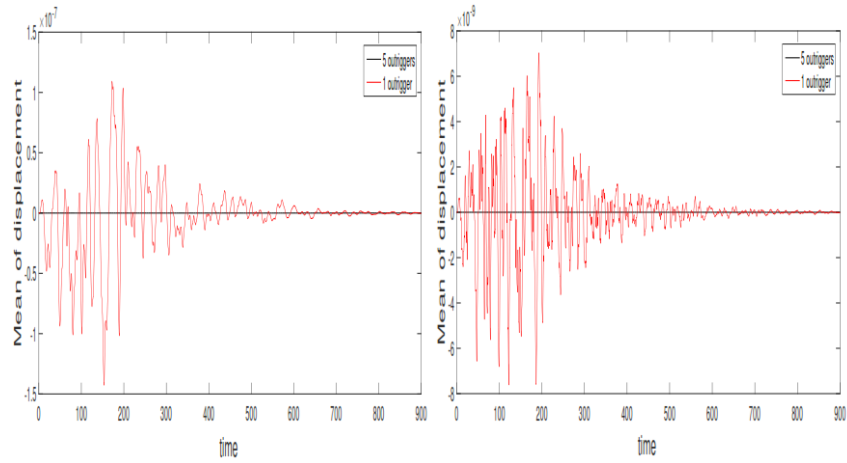
Figure 3.3: Optimal position of the damped outrigger

Figure 3.3 presents at the first mode, after the position 0.1, a tiny variation between the amplitude at the different positions of outriggers on the core tube. From that histogram, we can notice that 0.8 and 0.9 are the most suitable positions to locate an outrigger because the displacement of the structural system is lower than others positions. The second mode shows only one best position of outriggers on the core tube which is 0.4. The third mode exhibits two positions where the displacement is more reduced, which are 0.3 and 0.7. For the fourth mode, we can easily see that the right locations of outriggers on the core tube are 0.2 and 0.5. It is sure that at these points the amplitude of vibration is reduced considerably. As to the fifth mode, the optimal position is 0.6 and 0.4 is the next. At these points the peak amplitude of vibration of the structure are lower than other positions. At the end of these observations, it is not possible to make a global analysis of different results of Figure 3.3 by giving one optimal attachment point of outriggers benefits for the five modes of vibration as it is the case in the article of Ndemanou [8]. And this could be explained by the consideration of the geometrical non linearity in the modelling of the system.

To do more analysis as mentioned in the introduction, the modelling of five outriggers systems give us the motion of the building. And a comparison of displacements of the structure under earthquake, between the 0.9 position of one outrigger and a five outriggers system with same parameters, has been done and the result is without question.

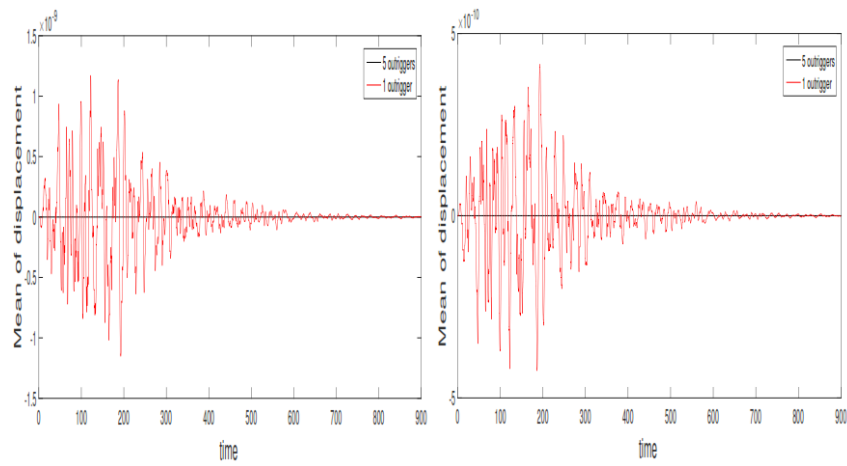
As regards the figure 3.4, one can realize that for each of the first five modes of vibrations, five outriggers drastically reduce the amplitude of vibrations and comparing to one outrigger, it is like there is no vibration of our structure when the earthquake appears because the amplitude is extremely tiny.

To know the best configuration of a five outrigger system, firstly we dispose the different levels of outriggers at same distance one to another (0.166, 0.333, 0.5, 0.667 and 0.833)



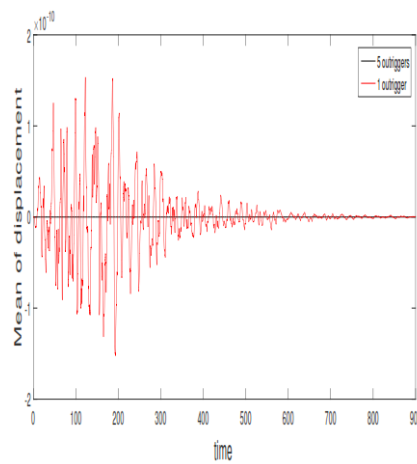
(a) First mode

(b) Second mode



(c) Third mode

(d) Fourth mode

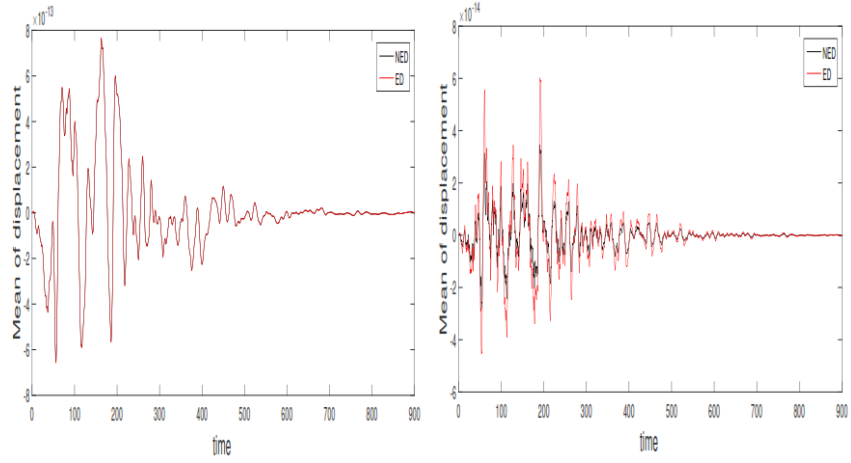


(e) Fifth mode

Figure 3.4: Comparison between one outrigger at the 0.9 position and five outriggers at positions 0.277, 0.379, 0.477, 0.567 and 0.65

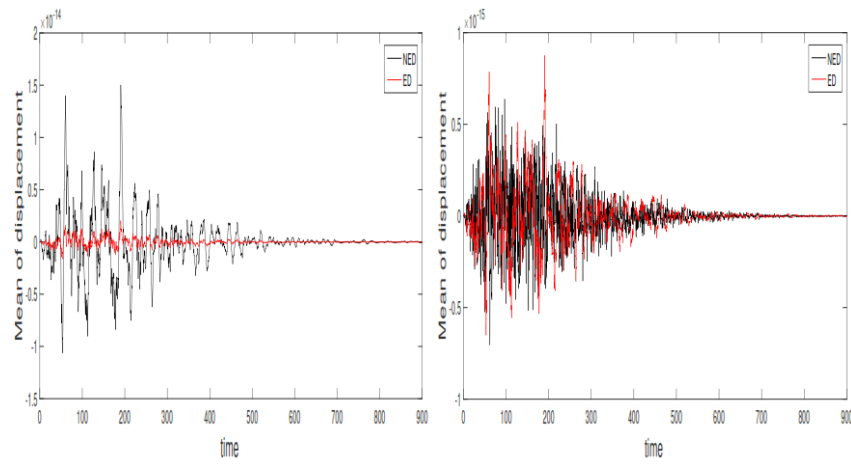
and we obtain an equidistance five outriggers ; and for the five first modes we collect the simulated displacement. And secondly, the five outriggers were randomly disposed on the structure (0.277, 0.379, 0.477, 0.567 and 0.65), here outriggers are mainly located near the base and the mid length of the structure and the comparison is giving in figure 3.5.

Unlike the figure 3.4 which has the same results for all the first five modes of vibration, the figure 3.5 has some particularities. The first mode show exactly the same motion of the two configurations of five outriggers systems. But after that for the next modes, we observe some differences. At the second, the fourth and the fifth mode, the highest peak of the amplitude of vibration of the building is more observed for the equidistance positions of outriggers, the third mode is the only one that stands out because here we see a better reduction of amplitude of the equidistance configuration than the non-equidistance configuration of five outriggers.



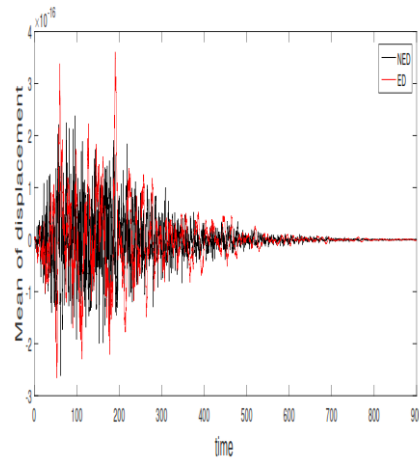
(a) First mode

(b) Second mode



(c) Third mode

(d) Fourth mode



(e) Fifth mode

Figure 3.5: Comparison between five outriggers at equidistance and at non-equidistance positions

3.3 Reduction of vibration on a cantilever Timoshenko beam subjected to repeated sequence of excitation with magnetorheological outriggers

This section presents an outrigger system on a cantilever Timoshenko beam under seismic excitation. The central column is the frame-core tube linked at a point of its length by two vertical magneto-rheological (MR) damped outriggers.

3.3.1 Description of physical system

The physical model represented in Figure 3.6 is a structural system that is constituted of an uniform cantilever beam and one outrigger truss. The set of the system is subjected to the same environmental dynamic force in the horizontal direction denoted ground excitation, which is considered to simulate a seismic motion. The outriggers and the exterior columns have commonly a high stiffness. In this context, they are assumed to be infinitely rigid. As a result, the outrigger behaves as a rigid body and is located at a point a from the end of the core tube. In view of increasing the capacity of the dynamic response of the structural system to resist of the better way against the nonstationary excitation, two semiactive devices dubbed MR dampers (D) are installed vertically and symmetrically; therefore, the generated forces are applied to the core tube through the outriggers.

3.3.1.1 Dynamic model formulation

The mass per unit length is m_1 ; I is the moment of inertia of the cross-section about the neutral axis, E is the Young's modulus; G is the shear modulus of elasticity; r_a is

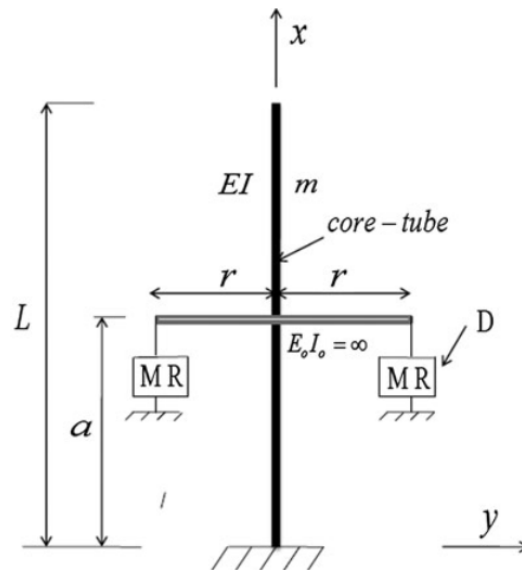


Figure 3.6: Cantilever beam with magnetorheological (MR) outriggers

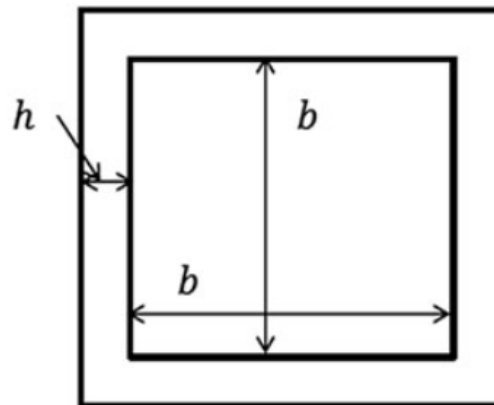


Figure 3.7: Cross-section of the core tube

the radius of gyration. These geometrical characteristics are assumed constant. Thus, the lateral displacement is defined by $y(x, t) = y$, which varies with the coordinate along the beam x and with time t . The control device f_d is generated by a MR damper. The influence of the perimeter columns on the dynamics of the core is not taken into consideration. As a result, the governing equations describing the dynamics of the cantilever Timoshenko beam with one damped outrigger under the earthquake loadings can be written as

$$m_1 \frac{\partial^2 y}{\partial t^2} + EI \frac{\partial^4 y}{\partial x^4} - m_1 r_a^2 \left(1 + \frac{E}{k_s G} \right) \frac{\partial^4 y}{\partial x^2 \partial t^2} = -m_1 \ddot{x}_g(t) + \frac{\partial M_a}{\partial x} \quad (3.10)$$

where the distributed moment generated by the MR dampers is

$$M_a = 2\delta(x - a) r f_d(t). \quad (3.11)$$

in which $\delta(x - a)$ denotes the Dirac function. This one indicates that the point a is the place where the damped outriggers is installed. The distance from the control devices to the centre of the core is denoted r . The dimensionless quantity k_s is the shear coefficient depending on the geometric of the cross section of the beam and depend on as well as of the Poisson's ratio. It is assumed in this paper that the dimensional ratio of the width on the area to the thickness is very small, reason why the core tube is considered like a beam being the cross section at the small thickness. This analysis leads us to adopt that, the expression of this mentioned coefficient associated with the cross-section of the core tube is given by Cowper [118]:

$$k_s = \frac{20(1 + \nu)}{48 + 39\nu}. \quad (3.12)$$

ν is the Poisson's ratio coefficient, it is clearly seen that k_s is connected with that coefficient, which its value depends solely on the material property.

In what follows, the moment of inertia and area of the cross-section can be formulated as (Figure 3.7)

$$A = (b + 2h)^2 - b^2; \quad I = \frac{(b + 2h)^4}{12} - \frac{b^4}{12}.$$

In this formulation in Equation 3.10, the first two terms correspond to the classical Bernoulli-Euler beam model. The third term represents the correction for rotary inertia, and the fourth term represents the shear deformation effect [119]. For convenience in the present study, the joint action of rotary inertia and shear deformation effects is neglected. Thereafter, the bending stiffness for the outriggers is assumed to be infinite [113].

The mathematical model of the nonstationary ground acceleration $\ddot{x}_g(t)$ of n sequences proposed by Abbas and Takewakib [96] is adopted in this paper. According to the authors, ground acceleration of multiplied sequences could result in more damage to the structure than a single ordinary event. This is because the structure gets damaged in the first sequence, and additional damage accumulates from secondary sequence before any repair is possible. As a result, this random function is assumed to take the form of a filtered Gaussian stationary white noise modulated by a deterministic envelope function under the sequence form. Expression of this term is defined in Equation 3.13 as follows:

$$\ddot{u}_g = \begin{cases} e_1(t) \ddot{w}_1(t) & 0 \leq t \leq T_1 \\ 0 & T_1 \leq t \leq \sum_{i=1}^2 T_i \\ e_2\left(t - \sum_{i=1}^2 T_i\right) \ddot{w}_2(t) & \sum_{i=1}^2 T_i \leq t \leq \sum_{i=1}^3 T_i \\ 0 & \sum_{i=1}^3 T_i \leq t \leq \sum_{i=1}^4 T_i \\ \dots & \dots \\ e_n\left(t - \sum_{i=1}^{n+1} T_i\right) \ddot{w}_n(t) & \sum_{i=1}^{n+1} T_i \leq t \leq \sum_{i=1}^{n+2} T_i \end{cases} \quad (3.13)$$

where $e_1(t)$, $e_2(t)$, ..., $e_n(t)$ are the envelope functions associated with the acceleration

sequences $1, 2, \dots, n$, $\ddot{w}_1(t), \ddot{w}_2(t), \dots, \ddot{w}_n(t)$ are stationary random processes, T_1, T_3, \dots, T_{n+2} are the time durations of the acceleration sequences, and T_2, T_4, \dots, T_{n+1} are the time intervals separating these sequences. Thus, the envelope function for the i th sequence is expressed as

$$e_i(t) = e_{0i} \left(t - \sum_{i=1}^n T_i \right) \exp \left[-\alpha_i \left(t - \sum_{i=1}^n T_i \right) \right]; \quad \sum_{i=1}^{n+1} T_i \leq t \leq \sum_{i=1}^{n+2} T_i; \quad (3.14)$$

where e_{0i} and α_i are $2n$ positive constants that control the intensity and the nonstationarity trend of the i th acceleration sequence.

The phenomenological model, which is based on Bouc-Wen modified version, proposed by Spencer et al. [120] is adopted here to describe the dynamic of the control device in order to predict its response. This model can exhibit a wide variety of hysteretic behaviours. To valid their mathematical model, authors have done a comparative approach between these analytical data and those obtained experimental results. The analysis of that study on the basis of their results have pointed out the approach numerically tractable and effectively portrays the behaviour of the MR damper. In other words, the proposed mathematical model describes the dynamic behaviour of the MR damper very well. As a result, the equation governing force f_d generated by the control device:

$$f_d(t) = c_1 \dot{y}_1 + k_1 (y(a, t) - y_0). \quad (3.15)$$

The internal displacement y_1 is illustrated:

$$\dot{y}_1 = \frac{1}{(c_0 + c_1)} (\alpha z + c_0 \dot{y}(a, t) + k_0 (y(a, t) - y_1)), \quad (3.16)$$

and z is an evolutionary variable given by

$$\dot{z} = -\gamma|\dot{y}(a, t) - \dot{y}_1|z|z|^{n+1} + (\delta_1 - \beta|z|^n)(\dot{y}(a, t) - \dot{y}_1), \quad (3.17)$$

where c_0 and c_1 are the viscous damping at larger and low velocities, respectively; k_1 is the accumulator stiffness; k_0 represents the stiffness at large velocity; γ , δ_1 and β are the shape parameters of the hysteresis loops. Moreover some of these parameters depend on the command voltage u_1 , which are given by

$$c_0 = c_{0a} + c_{0b}u_1, \quad c_1 = c_{1a} + c_{1b}u_1, \quad \alpha = \alpha_a + \alpha_b u_1, \quad (3.18)$$

where the command voltage u_1 is accounted for through the first order filter:

$$\dot{u}_1 = \eta_p (u_1 - v_c). \quad (3.19)$$

v_c is the maximum applied voltage that is associated with the saturation of the magnetic field in the MR damper, and η_p is a positive number that reflects the delay time of the MR damper.

Introducing the new parameters, one has the expressions defined as follows:

$$Y = \frac{y}{L}, \quad \tau = \frac{t}{T}, \quad \delta_a = \delta_1 L, \quad \gamma_L = \gamma L, \quad \ddot{y}_g(\tau) = \frac{T^2}{L} \ddot{x}_g(t); \quad a_1 = \frac{EIT^2}{mL^4}, \quad a_2 = \frac{r_a^2}{L^2} \left(1 + \frac{E}{k_s G}\right),$$

$$C_0 = \frac{c_0}{c_0 + c_1}, \quad K_0 = \frac{k_0 T}{c_0 + c_1}, \quad \alpha_b = \frac{\alpha T}{(c_0 + c_1)L}, \quad C_1 = \frac{c_1 T}{mL}, \quad T = L \sqrt{\frac{\rho}{k_s G}}, \quad Y_0 = \frac{y_0}{L}.$$

The relationship between the parameters leads to new reformulation, which is described by the below equation:

$$\frac{\partial^2 Y}{\partial \tau^2} + a_1 \frac{\partial^4 Y}{\partial X^4} + a_2 \frac{\partial^4 Y}{\partial X^2 \partial \tau^2} = -\ddot{y}_g(\tau) + \zeta_a F_d(\tau) \frac{\partial}{\partial X} \delta(X - X_0). \quad (3.20)$$

The dimensionless equation of the MR damper force is rewritten as

$$F_d(\tau) = C_1 \dot{Y}_1 + K_1 (Y(X_0, \tau) - Y_0). \quad (3.21)$$

Y_1 and Z are governed by the below equations:

$$\dot{Y}_1 = \alpha_b Z + C_0 \dot{Y}(X_0, \tau) + K_0 (Y(X_0, \tau) - Y_1), \quad (3.22)$$

$$\dot{z} = -\gamma_1 \left| \dot{Y}(X_0, \tau) - \dot{Y}_1 \right| |Z| |Z|^{n-1} + (\delta_l - \beta_l |Z|^n) (\dot{Y}(X_0, \tau) - \dot{Y}_1), \quad (3.23)$$

where X_0 is the location of the damped outriggers. By observing closely the Equations 3.21, 3.22, and 3.23, one can notice that these depend on the quoted location point. This shows that the outrigger position is an important issue in terms of ensuring the efficiency of lateral displacement control [121]. For the sake of simplicity, it is necessary to assess the dynamic responses of the structural system through the modal properties.

3.3.1.2 Modal equations

To reduce the partial differential equations to a set of ordinary differential equations, in order to assess the dynamic behaviour response of the structural system. Thus, the general solution of the Equation 3.20 can be written as separation variables of $\chi(\tau)$, which is the time dependent function and the shape function $\Phi(\chi)$:

$$Y = \sum_{j=1}^{n_m} \Phi_j(X) \chi_j(\tau). \quad (3.24)$$

n_m is the total of modes with

$$\Phi(X) = (d_1^j \sin(\delta_1^j X) + \cos(\delta_1^j X) - d_3^j \sinh(\epsilon_1^j X) - \cosh(\epsilon_1^j X)). \quad (3.25)$$

The spatial function is obtained from Equation 3.20 without the right member. The superscript j represents the j th mode.

The coefficients d_1^j and d_3^j are obtained by using the boundary conditions of the cantilever Timoshenko beam [19, 20]:

$$d_1^j = \frac{\cos(\delta_1^j) + \frac{(\epsilon_1^{j2} + \mu_1 \delta_1^{j2})}{(\delta_1^{j2} + \mu_1 \epsilon_1^{j2})} \cosh(\epsilon_1^j)}{-\left(\sin(\delta_1^j) + \frac{\epsilon_1^j}{\delta_1^j} \sinh(\epsilon_1^j)\right)}, \quad d_3^j = -\left(\frac{\delta_1^j + \mu_1 \frac{\epsilon_1^{j2}}{\delta_1^j}}{\epsilon_1^j + \mu_1 \frac{\delta_1^{j2}}{\epsilon_1^j}}\right) d_1^j.$$

In which δ_1^j and ϵ_1^j are eigenvalues defined at the j^{th} mode of the vibration. Impossible to adopt an analytical consideration, these quoted eigenvalues are obtained from Equation 3.26, by using an numerical appropriate algorithm:

$$\left\{ \begin{array}{l} \left[(\delta_1^{j2} + \Gamma_1 \epsilon_1^{j2})^2 + (\epsilon_1^{j2} + \Gamma_1 \delta_1^{j2})^2 \right] \cos(\delta_1^j) \cosh(\epsilon_1^j) - (\delta_1^{j2} + \Gamma_1 \epsilon_1^{j2}) (\epsilon_1^{j2} + \Gamma_1 \delta_1^{j2}) \times \\ \quad \left(-2 + \frac{(\delta_1^{j2} - \epsilon_1^{j2})}{\delta_1^j \epsilon_1^j} \sin(\delta_1^j) \sinh(\epsilon_1^j) \right) = 0 \\ (\delta_1^{j2} - \epsilon_1^{j2}) \Gamma_2^2 - \left(1 + \frac{1}{\Gamma_1} \right) \delta_1^{j2} \epsilon_1^{j2} = 0 \end{array} \right. \quad (3.26)$$

$$\text{with } \Gamma_1 = \frac{E}{k_s G}, \quad \Gamma_2 = L \frac{k_s G A}{EI}.$$

In what follows, by using the mode decomposition of the illustrated expression in Equation 3.24 and substituting them into Equation 3.20, multiplying by the different spatial expression and performing the integration from 0 to 1, by adding the damping coefficient. One gets the modal forms of above equations that can be expressed as follows:

$$\ddot{\chi}_j(\tau) + \zeta_j \dot{\chi}_j(\tau) + \varsigma_j \chi_j(\tau) = -\sigma_j \ddot{Y}_g(\tau) - \zeta_a \eta_j F_d(\tau). \quad (3.27)$$

The dimensionless equation of the force generated by the MR device is satisfied by the illustrated expressions as follows:

$$F_d(\tau) = C_1 \dot{Y}_1 + K_1 (\chi_j(\tau) \Phi_j(X_0) - Y_0), \quad (3.28)$$

where Y_1 and Z can be rewritten as

$$\dot{Y}_1 = \alpha_b Z + C_0 \dot{\chi}_j(\tau) \Phi_j(X_0) + K_0 (\chi_j(\tau) \Phi_j(X_0) - Y_1), \quad (3.29)$$

$$\dot{Z} = -\gamma_L \left| \dot{\chi}_j(\tau) \Phi_j(X_0) - \dot{Y}_1 \right| |Z| |Z|^{n-1} + (\delta_L - \beta_L |Z|^n) \left(\dot{\chi}_j(\tau) \Phi_j(X_0) - \dot{Y}_1 \right). \quad (3.30)$$

The applied voltage to the control device is defined by the dimensionless expression which is given by

$$U = \eta_T (U - V_C), \quad (3.31)$$

with

$$\varsigma_j = \frac{a_1 b_3}{b_1 + a_2 b_2}, \quad \eta_j = \frac{\Phi_j'(X_0)}{b_1 + a_2 b_2}, \quad \sigma_j = \frac{b_4}{b_1 + a_2 b_2},$$

in which

$$b_1 = \int_0^1 \Phi_j(X)^2 dX, \quad b_2 = \int_0^1 \Phi_j''(X) \Phi_j(X) dX, \quad b_3 = \int_0^1 \Phi_j''''(X) \Phi_j(X) dX, \quad b_4 = \int_0^1 \Phi_j(X) dX.$$

Equations 3.27-3.31 describe the time evolution of the concrete core tube which is fixed at the point X_0 by the damped outriggers. It is useful to observe that the parameter of the Equation 3.27 varied at each vibration mode and that the force generated by MR device depends on the attachment point of the damped outriggers on core tube. All these results indicate that outrigger locations could modify the structural response at the different vibration mode and can provide a better understanding of the outrigger design.

3.3.1.3 Semiactive controller

With a view to obtain the optimal input voltage corresponding to the desired damper force and to assess the performance of control system, the control algorithm as an ef-

fective mean used in semiactive control based on the Lyapunov stability theory [110] is employed. Because the control device is not directly controllable and that only applied voltage can be adjusted. Also the mentioned control algorithm is developed for characterizing adequately the damper's intrinsic nonlinear behaviour [120]. Thus, the Lyapunov function denoted $L_y(\mathbf{W})$ must be a positive function of the state of the system, \mathbf{W} . According to the Lyapunov stability theory, if the rate of change of lyapunov function, $\dot{L}_y(\mathbf{W})$, is negative semidefinite, the origin is stable.

Lyapunov function is chosen of the form

$$L_Y = \frac{1}{2} \|W\|_p^2, \quad (3.32)$$

where $\|\Sigma\| = P$ -norm of the states defined by

$$\|\Sigma\|_p = |\Sigma' P_L \Sigma|^{1/2}, \quad (3.33)$$

where \mathbf{P}_L is real, symmetric, positive definite matrix. \mathbf{P}_L is found using Lyapunov equation.

$$\Sigma' P_L + P_L \Sigma = -Q_p \quad (3.34)$$

\mathbf{Q}_p is a positive definite matrix. The derivative of the Lyapunov function for a solution of the state-space equation is

$$\dot{L}_Y = -\frac{1}{2} W' Q_p W + W' P_L B_1 F_d + W' P_L B \ddot{y}_g. \quad (3.35)$$

The above parameters are defined as follows:

$$W = \begin{bmatrix} \chi_j \\ \dot{\chi}_j \end{bmatrix}, \Sigma = \begin{bmatrix} 0 & 1 \\ -\varsigma_j & -\varsigma_j \end{bmatrix}, B = \begin{bmatrix} 0 \\ -\sigma_j \end{bmatrix}, B_1 = \begin{bmatrix} 0 \\ -\zeta_a \eta_j \end{bmatrix}.$$

The control law which will minimize L_y

$$V_C = V_{\max} H(-W' P_L B_1 F_d), \quad (3.36)$$

where V_{\max} is the maximum voltage and $H(\cdot)$ is Heaviside step function. When this function is greater than zero, the voltage (V_c) applied to the damper should be maximum (V_{\max}), otherwise, the command voltage is set to zero.

3.3.2 Observation of reduction of vibration

To investigate efficiency of the simplified model, the concrete core is assumed to be $12m \times 12m$ with a $0.5m$ thickness, and with the height of $210m$ [112]. The mass per unit length is $m_1 = 62500K_g/m$. The eigenvalues are obtained from Equation 3.26 through the Newton-Raphson numerical. These results obtained through this method are illustrated in Table 3.3.

The listed parameter values in Table 3.4 when $MF = 1.0$ are those obtained from the analysis of experimental data and theoretical results by Jung et al [122]. As it is difficult to have an MR damper with the obtained parameters experimentally that will lead to the optimal minimization of excessive vibration of mechanical structures. To avoid this drawback, it is observed from this Table 3.4 that some parameters depend on MF, named, the modification factor that allows of multiplying the damping; stiffness and hysteretic constants of the model magnify the damper force. In this regard, the objective here is to modify the properties of the damper, in view of having the parameter values for a large scale MR damper, enable to control the mechanical structure [123].

To assess the optimal position of outriggers on the core tube, the passive-on strategy of the controller is employed. Thus,

Table 3.3: Parameters of the structural system

Parameter	First	Second	Third
δ_1^j	1.873	4.649	7.752
ϵ_1^j	1.860	4.465	6.979
d_1^j	-0.743	-1.127	-1.283
d_3^j	-0.731	-1.023	-0.998
ς_1^j	0.039	1.579	13.918

Table 3.4: Model parameters of the magnetorheological damper

Parameter	Value	Parameter	Value
δ_a	1107.2	n_1	2
$\gamma(m^{-2})$	164.0×10^4	$n_p(s^{-1})$	190
$\beta(m^{-2})$	164.0×10^4	$K_1(N/m)$	9.7 MF
$K_0(N/m)$	2 MF	$Y_0(m)$	0.0
$\alpha_a(N/m)$	46.2×10^3 MF	$\alpha_b(N/mV)$	41.2×10^3 MF
$C_{0a}(Ns/m)$	11×10^4 MF	$C_{0b}(Ns/mV)$	114.3×10^3 MF
$C_{1a}(Ns/m)$	8359.2×10^3 MF	$C_{1b}(Ns/mV)$	7482.9×10^3 MF

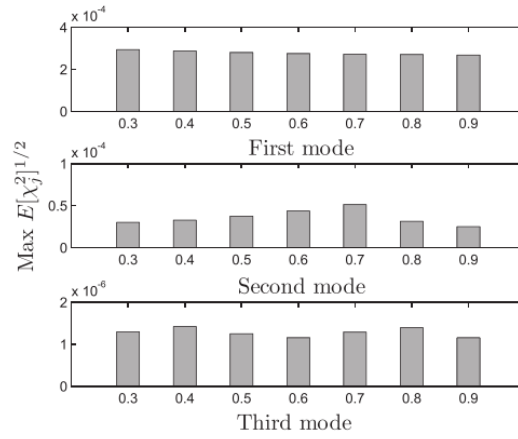


Figure 3.8: Optimal position of damped outriggers, $\zeta_a = 0.762$ and $\text{MF} = 1.0$

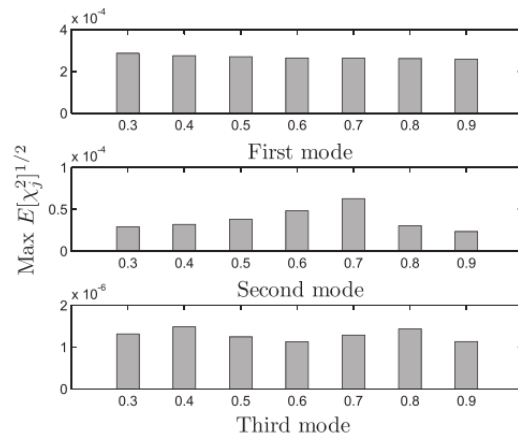


Figure 3.9: Optimal position of damped outriggers, $\zeta_a = 0.095$ and $\text{MF} = 1.0$

Figures 3.8 and 3.9 display the peak RMS versus locations of outriggers on the structure.

Figure 3.8 presents at the first mode, a slight variation between the amplitude at the different position of outriggers on the core tube. For that, one can realize that the positions 0.7, 0.8, and 0.9 at this quoted mode are the location points of damped outriggers where the displacement of the structural system is reduced slightly in relation to other positions. The second mode exhibits only one best position of outriggers on the core tube which is 0.9. It is well-seen that at this point the vibration amplitude is reduced dramatically. As regards the third mode, the optimal positions are 0.6 and 0.9. In these points, the peak amplitude of the structure are reduced than other positions. The global analysis of different observations from Figure 3 leads us to mention that the optimal attachment point of outriggers benefits for the three vibration modes is 0.9.

The same observation from Figure 3.8 is illustrated in Figure 3.9, that is to say that the point 0.9 stays only the best position of outriggers on the frame core tube. Analysing these figures, as can be seen, the point 0.9 is better attachment point of damped outriggers on the frame-core tube favourable for the three first vibration mode. Moreover, the variation of the length of each outrigger does not affect the value of its optimal attachment point on the beam.

As mentioned before, it is difficult to have the best parameters from experimental results of the MR damper, which incorporated into the structure leading to efficient control. For that, Figure 3.10 displays the peak RMS versus the scale coefficient MF at the first three vibration modes. It is observed from this figure that the increasing of this quoted coefficient affects the performance of damped outrigger in reducing the seismic response of the structure. It is important to note that the choice of MF is done such as the control device cannot increase the mechanical energy in the structural system. In other words,

the control device should reinforce the stability of the structure in order to avoid their premature destruction.

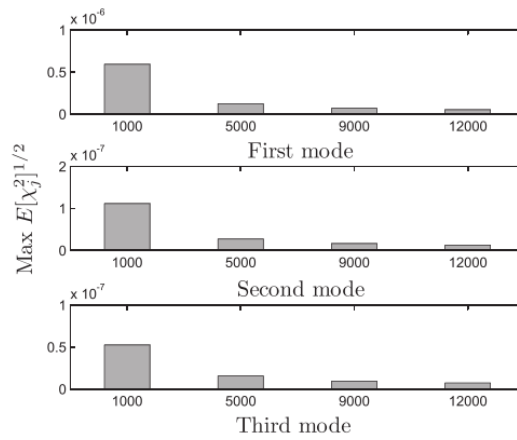
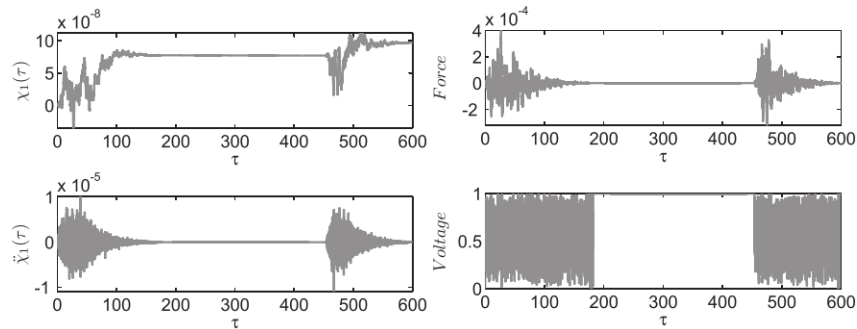


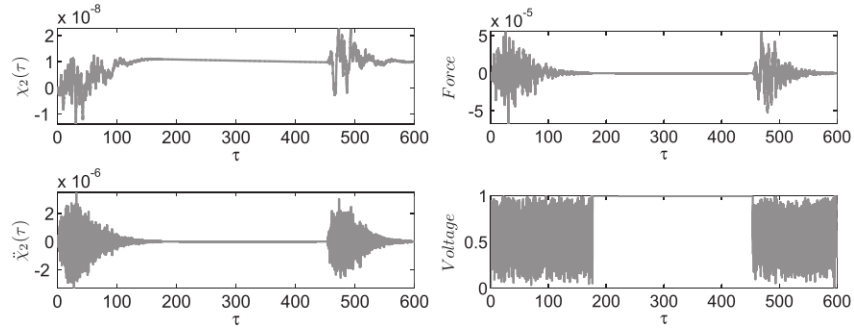
Figure 3.10: Optimal scale coefficient MF



(a) Displacement and acceleration of the outrigger system (b) Control force and applied voltage to MR damper

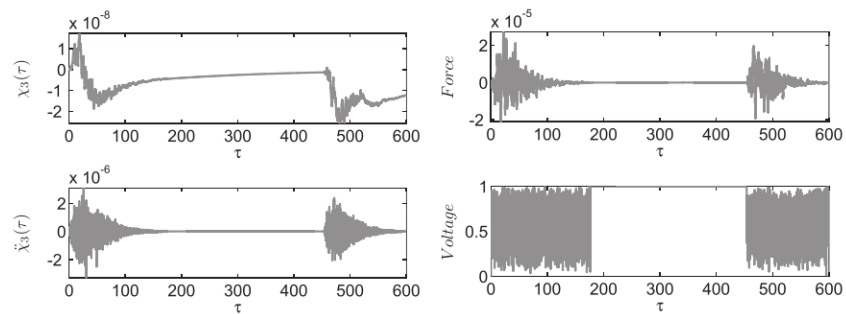
Figure 3.11: Time histories at the first vibration mode

By taking into account of optimal position of damped outriggers and scale coefficient, one displays in Figures 3.11, 3.12, and 3.13, the time histories of traversal displacement, acceleration, control force, and applied voltage to MR damper at the first, second, and third vibration modes for MF= 9000. The structural response of the outrigger system at the three first vibration modes is shown in Figures 3.11(a), 3.12(a) and 3.13(a). One can see the structural response show two sequences of the vibration.



(a) Displacement and acceleration of the outrigger system
(b) Control force and applied voltage to MR damper

Figure 3.12: Time histories at the second vibration mode



(a) Displacement and acceleration of the outrigger system
(b) Control force and applied voltage to MR damper

Figure 3.13: Time histories at the third vibration mode

The command signal V_c is selected through the control algorithm based on Lyapunov stability illustrated in Equation 3.36. The numerical result of this adopted strategy allows of having Figures 3.11b, 3.12b, and 3.13b at the first, second, and third vibration modes. The observed separating time interval between $\tau = 170$ and $\tau = 460$ indicates that the controller is in passive-off mode. Since in this relaxation time, the structure did not receive the input produced by earthquake, as a result, the system cease to exhibit the vibration. All the same, this explains the dynamic behaviour of the control device because this is depended on the structural response.

3.4 On the mechanical system with self-control of vibration

3.4.1 Modelling of the dynamics of self-controlled mechanical system

3.4.1.1 Description of the model

The system study here is modelled as an inverted pendulum rigid bar with branches whose are responsible of the dissipation of the energy receive from load apply to the entire structure. Each branches are linked to the rigid bar by rotational springs and viscous dampers, supported masses to their ends. By appreciating the performance of our system to reduce amplitude, we will study first our system without any branch and the next step with one branch, two and three branches. In each step we will compare the time-history response of our system with the last one. The mechanism found here is based similarly to the tuned-mass damper mechanism described by [124]

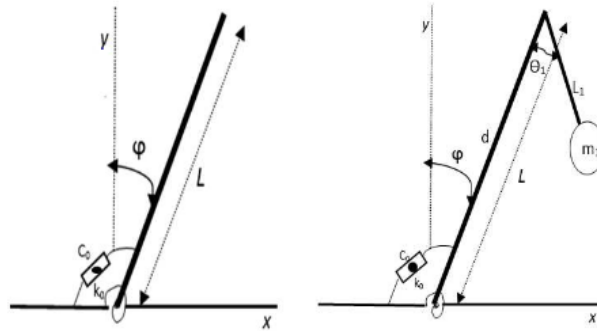


Figure 3.14: System without any branch and with one branch

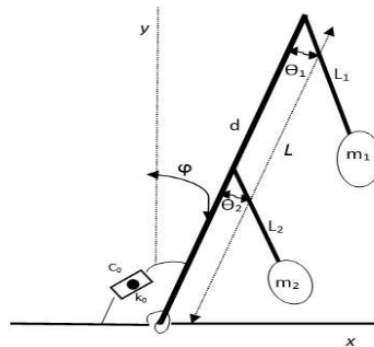


Figure 3.15: System with two branches

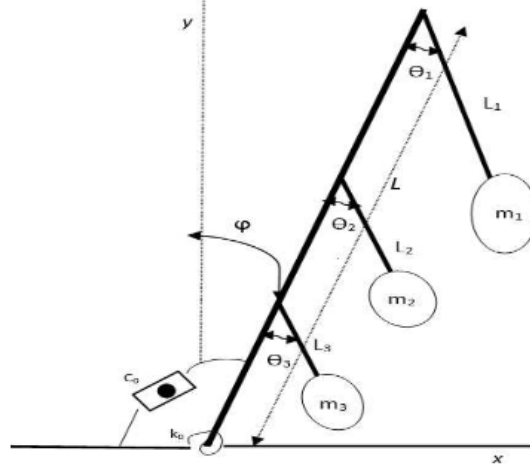


Figure 3.16: System with three branches

3.4.1.2 Mathematical formalism

In this part, we focused on the system with one branch and by using the same analysis, we can obtain the other equations of motion for system with two and three branches.

The positions of the center column (x, y) and the branch (x_1, y_1) is obtained easily [125]:

$$\begin{cases} x = l \sin(\varphi), & y = l \cos(\varphi) \\ x_1 = l_1 \sin(\theta - \varphi) + d \sin(\varphi) \\ y_1 = d \cos(\varphi) - l_1 \cos(\theta - \varphi) \end{cases} \quad (3.37)$$

The kinetic energy T , the potential energy V and the dissipative energy D_E are expressed as follow:

$$\left\{ \begin{array}{l} T = \frac{1}{2}m(\dot{x}^2 + \dot{y}^2) + \frac{1}{2}m_1(\dot{x}_1^2 + \dot{y}_1^2) \\ = \frac{1}{2}m l^2 \dot{\varphi}^2 + \frac{1}{2}m_1 l_1^2 (\dot{\theta} - \dot{\varphi})^2 + \\ \frac{1}{2}m_1 d_1^2 \dot{\varphi}^2 + m_1 l_1 d \dot{\varphi} (\dot{\theta} - \dot{\varphi}) \cos(\theta) \\ V = mgy + m_1 g y_1 \\ = mgl \cos(\varphi) + m_1 g [d \sin(\varphi) + l_1 \sin(\theta - \varphi)] + \\ \frac{1}{2}k_0 \varphi^2 + \frac{1}{2}k_1 \theta^2 \\ D_E = c_0 \dot{\varphi}^2 + c_1 \dot{\theta}^2 \end{array} \right. \quad (3.38)$$

When the structure is excited by external load $F(t)$, the equations of motion are derived using Lagrange equations:

$$\left\{ \begin{array}{l} [ml^2 + m_1(l_1^2 + d^2) - 2m_1 l_1 d \cos(\theta)] \ddot{\varphi} + (m_1 l_1 d \cos(\theta) - m_1 l_1^2) \ddot{\theta} = \\ F(t) - c_0 \dot{\varphi} - k_0 \varphi + mgl \sin(\varphi) + m_1 g [d \sin(\varphi) + l_1 \sin(\theta - \varphi)] + m_1 l_1 d \dot{\theta}^2 \sin(\theta) - 2m_1 l_1 d \dot{\varphi} \dot{\theta} \sin(\theta) \\ m_1 l_1^2 \ddot{\theta} + [m_1 l_1 d \cos(\theta) - m_1 l_1^2] \ddot{\varphi} = -c_1 \dot{\theta} - k_1 \theta - m_1 g l_1 \sin(\theta - \varphi) + m_1 l_1 d \dot{\varphi} \dot{\theta} \sin(\theta) \end{array} \right. \quad (3.39)$$

After some rearrangements, we obtain

$$\left\{ \begin{array}{l} k_a \ddot{\varphi} + c_0 \dot{\varphi} + k_0 \varphi - mgl \sin(\varphi) = F(t) - k_b \ddot{\theta} + \\ m_1 g [d \sin(\varphi) + l_1 \sin(\theta - \varphi)] + \\ m_1 l_1 d \dot{\theta}^2 \sin(\theta) - 2m_1 l_1 d \dot{\varphi} \dot{\theta} \sin(\theta) \\ m_b \ddot{\theta} + c_1 \dot{\theta} + k_1 \theta = -m_a \ddot{\varphi} - \\ m_1 g l_1 \sin(\theta - \varphi) - m_1 l_1 d \dot{\varphi} \dot{\theta} \sin(\theta) \end{array} \right. \quad (3.40)$$

$$\text{with : } k_a = ml^2 + m_1(l_1^2 + d^2) - 2m_1 l_1 d \cos(\theta);$$

$$k_b = m_1 l_1 d \cos(\theta) - m_1 l_1^2;$$

$$m_a = m_1 l_1 d \cos(\theta) - m_1 l_1^2; \quad m_b = m_1 l_1^2$$

Introducing the dimensionless coefficients

$$\tau = \omega t; \quad \Phi(\tau) = \varphi(t) \sqrt{\frac{l}{l_1}}; \quad \Theta(\tau) = \theta(t)$$

The dimensionless system is given by:

$$\left\{ \begin{array}{l} \ddot{\Phi}(\tau) + \gamma_1 \dot{\Phi}(\tau) + \gamma_2 \Phi(\tau) = F(\tau) - \gamma_3 \ddot{\Theta}(\tau) + \\ \gamma_4 [d \sin(\Phi(\tau)) + l_1 \sin(\Theta - \Phi)] + \gamma_5 \dot{\Theta}^2(\tau) - \\ \gamma_6 \dot{\Phi}(\tau) \dot{\Theta}(\tau) + \gamma_7 \\ \ddot{\Theta}(\tau) + \lambda_1 \dot{\Theta}(\tau) + \lambda_2 \Theta(\tau) = -\lambda_3 \ddot{\Phi}(\tau) - \\ \lambda_4 \dot{\Phi}(\tau) \dot{\Theta}(\tau) - \lambda_5 \end{array} \right. \quad (3.41)$$

Where the dimensionless parameters are:

$$\begin{aligned} \gamma_1 &= \frac{c_0}{k_a \omega}, \quad \gamma_2 = \frac{k_0}{k_a \omega^2}, \quad F(\tau) = \frac{F(t)}{k_a \omega^2} \sqrt{\frac{l}{l_1}}, \\ \gamma_3 &= \frac{k_b}{k_a} \sqrt{\frac{l}{l_1}}, \quad \gamma_4 = \frac{m_1 g}{k_a \omega^2} \sqrt{\frac{l}{l_1}}, \quad \gamma_5 = \frac{m_1 l_1 d}{k_a} \sqrt{\frac{l}{l_1}} \\ \gamma_6 &= \frac{m_1 l_1 d \sin(\Theta(\tau))}{k_a}, \quad \gamma_7 = \frac{m g l \sin(\Phi(\tau))}{k_a \omega^2} \sqrt{\frac{l}{l_1}} \\ \lambda_1 &= \frac{c_1}{m_b \omega}, \quad \lambda_2 = \frac{k_1}{m_b \omega^2}, \quad \lambda_3 = \frac{m_a}{m_b} \sqrt{\frac{l}{l_1}}, \\ \lambda_4 &= \frac{m_1 l_1 d \sin(\Theta(\tau))}{m_b} \sqrt{\frac{l}{l_1}}, \\ \lambda_5 &= \frac{m_1 l_1 g \sin(\Theta(\tau) - \Phi(\tau))}{m_b \omega^2} \end{aligned}$$

3.4.2 Dynamics explanations

In this section, we study the robustness of our system driven firstly by wind load and secondly by earthquake excitation.

3.4.2.1 System subjected to wind excitation

When the turbulent wind flow acts on a system, it brings three kinds of forces, namely self, parametric and external excitations. The steady part of the wind flow causes self-excitation while the parametric and external excitation are caused by the unsteady part

of wind flow. A turbulent wind flow can be modelled by a drag wind force and a lift wind force [126].

For this study, we focus our attention to the wind force (lift wind force) which blows orthogonally to the structure with time-dependent velocity $U(t)$. It express as [127]:

$$F_L = \frac{1}{2}\rho U^2 b \left[A_0 + A_1 \left(\frac{\dot{y}}{U} \right) + A_2 \left(\frac{\dot{y}}{U} \right)^2 + A_3 \left(\frac{\dot{y}}{U} \right)^3 \right] \quad (3.42)$$

Where, $A_j(j=1,2,3)$ are the aerodynamic coefficients relevant to square sections, ρ is the air mass density, b is the diameter of the cross-sectional area of the beam. The wind velocity can be decomposed as $U(t)=\bar{U}+u(t)$, where \bar{U} is a constant (average) part, representing the steady component and $u(t)$ is a periodically time-dependent part representing the turbulence. Considering that the turbulent part are small compared to the steady component, $\frac{u(t)}{\bar{U}} \gg 1$ and using the Taylor's expansion, the lift wind force in (3.42) will become:

$$\left\{ \begin{array}{l} F_L = \frac{1}{2}\rho b [c_0 + c_1\dot{y} + c_2\dot{y}^2 + c_3\dot{y}^3] \\ \text{with : } c_0 = A_0 \left(\bar{U}^2 + 2\bar{U}u(t) \right) \\ c_1 = A_1 (\bar{U} + u(t)) \\ c_2 = A_2 \\ c_3 = A_3 \left(\frac{1}{\bar{U}} - \frac{u(t)}{\bar{U}^2} \right) \end{array} \right. \quad (3.43)$$

Applying lift wind load as external excitation in our system in Figures 3.14, 3.15 and 3.16, we obtained after some rearrangements, the equations of motion which will be used for numerical simulation using RK4 algorithm and Matlab.

It can be seen in Fig. 3.17 that amplitude of vibration of the system is a little bit reduced when we added one branch at the top of the initial structure. Let us remember that, the branches are responsible of the dissipation of energy. So from the response of the

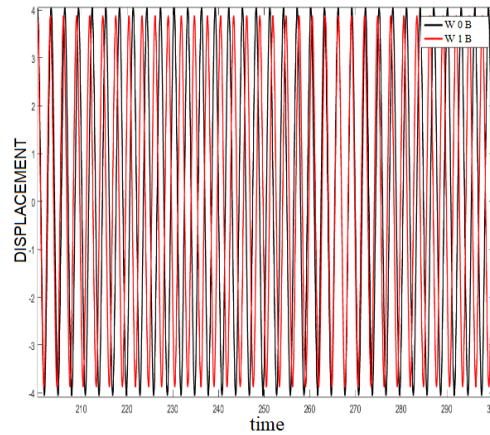


Figure 3.17: Time-histories response of the structure without and with one branch.

system, one added branch help our structure to reduce his amplitude of vibration even if this reduction is not to considerable.

The goal is to better control the vibration amplitude of the made structure, the idea of increase the damping ratio by adding others masses come out. By doing so, Fig. 3.18 and Fig. 3.19 give the behavior of the system for applied lift wind load as external force.

In Fig. 3.18, we observe on the response of the system that the amplitude of vibration when two branches (curve in blue) are added is well reduced compared to amplitude of system with one branch (red curve) and without branch (curve in black). One obtain an amplitude reduction of about 75% compare to the structure without any attached mass.

The numerical simulation of the equation of motion for the system in Fig. 3.16 is given by Fig. 3.19. The effect of three added branches is here shown, and after two branches, a reduction of amplitude is too denote. We observe that the displacement of the system with three branches represent by green curve is well-reduced.

One can by this test of vibration, make a great observation : for a pendulum system, added masses operate as factor of damping fluctuation for the system vibration. And by having a look on Fig. 3.17, Fig. 3.18 and Fig. 3.19, it is not only the amplitude of vibration that has change; the period of oscillations tends towards larger values. Which is

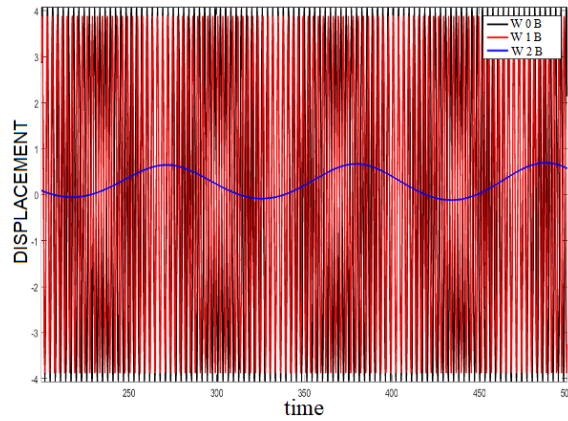


Figure 3.18: Time-histories response of the structure without and with one branch and two branches

too a control because structures are less exposed to damage when the period of oscillations around its equilibrium is large [128, 129].

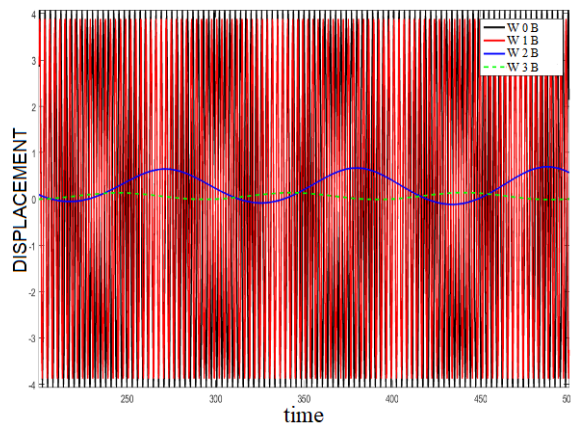


Figure 3.19: Time-histories response of the structure without and with one branch, two branches and three branches

3.4.2.2 System subjected to earthquake excitation

One of the biggest natural disasters, earthquake causes big destruction. Earthquakes are the movement of the earth's crust, which are characterized by three-dimensional vibrations and caused by tectonic movements. So control of earthquakes is impossible and prediction

of them is quite difficult. However we can resist to destructive effects of earthquakes.

The earthquake signal can be modelled as filtered white noise process while the filter design is based on a prescribed spectrum of ground motion [130]. Here, the Kanai-Tajimi spectral description of the ground motion is used:

$$S(\omega) = S_0 \frac{\omega_g^4 + 4\omega_g^2 \zeta_g^2 \omega^2}{(\omega^2 - \omega_g^2)^2 + 4\omega_g^2 \zeta_g^2 \omega^2} \quad (3.44)$$

Where ω_g , ζ_g and S_0 are parameters which depend on the soil characteristics and seismic intensity. An equivalent expression for the evolutionary of earthquake excitation for elastic plastic single-degree-of-freedom structures has been presented by [8, 131–133].

That generated earthquake is applied on the structure, for the same systems as in the last section; the simple pendulum without any tie, the system with one branch, two branches and three branches. One obtain numerical results shown in Fig. 3.20.

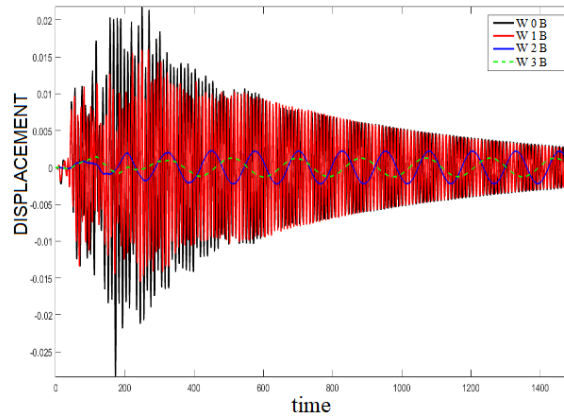


Figure 3.20: Time-histories response of the structure without and with one branch, two branches and three branches

The observation of Fig. 3.20 shows that by adding branches, the amplitude of vibration of the system is reduced compared to amplitude without branch. And the reduction of amplitude is function of the number of attached branch. For one branch, the amplitude reduce but not considerably; and for two branches and three branches, the time-history

response of the system is well-reduced and one can notice that the period of oscillations changes too and expand.

3.4.2.3 Effect of design parameter of the system

This section is devoted to the analysis of the effect of the length of branch on the reduction of the amplitude of vibration of the proposed system in Figs. 3.14 to 3.16 subjected to wind load. The Fig. 3.21 represent the vibration of the system for the inverted pendulum with one added branch at his top for different value of the length of fixed mass. l_1 where varies from dimensionless values of 0.0 to 0.2. A remark can directly be done; to collect the lowest value of the amplitude of vibration at every time of the simulation, l_1 should varie with time and follow the green part of the figure.

For the system with 3 added masses in Fig. 3.16, l_1 and l_2 are fixed, and a variation of the value of length l_3 is done from dimensionless values of 0.0 to 0.2. The result are shown in Fig. 3.22, one observe that, the amplitude of vibration is reduced for small values of the length l_3 and increase when l_3 increase too.

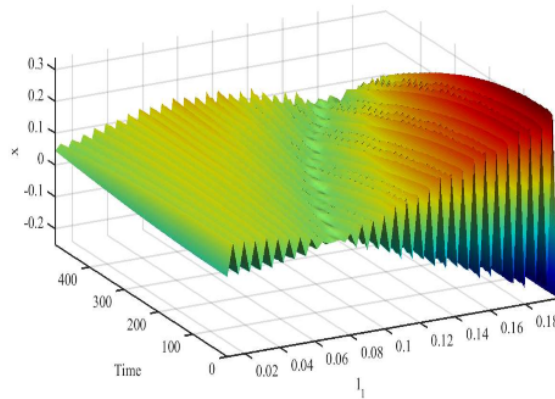
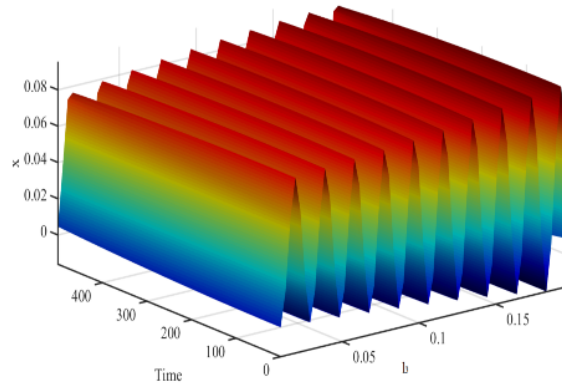


Figure 3.21: Effect of length l_1

Figure 3.22: Effect of length l_3

3.5 An inverted pendulum with multi-branching view as self-controlled system: modelling and vibration absorber capacity

3.5.1 General mathematical formalism of an inverted pendulum with multi-branching

The model shown in Figure 3.23 consists of an inverted pendulum of finite length $l_{n_{max}}$ (n_{max} is the maximum value of n according to the structure configuration : from one level up to five level) and mass M as a rigid rod is connected to the soil by a spring K_1 and dashpot (viscous damper) C_1 according to the reaction of the soil related to its mechanical properties, with massless rigid bars linked on that central column. Those masses are attached at different length l_n of the central column, with $n = 1, 3, \dots, 9$. Each level is two symmetrical bars of length l_i with $i = 2, 4, \dots, 10$, forming an angle ϕ_0 with imaginary horizontale line. These bars are linked to the central column by a rotational spring K_j and viscous damper C_j with $j = 2, 3, \dots, 6$, and support masses m_k with $k = 1, \dots, 5$ the indicator of the level . The motion of the rod is defined by the angle θ , and we consider

only the symmetrical motion of the levels defined by the angle ϕ_k with $k = 1, \dots, 5$. The inclination of the main rod must be less than the critical amplitude, if not the structure will break.

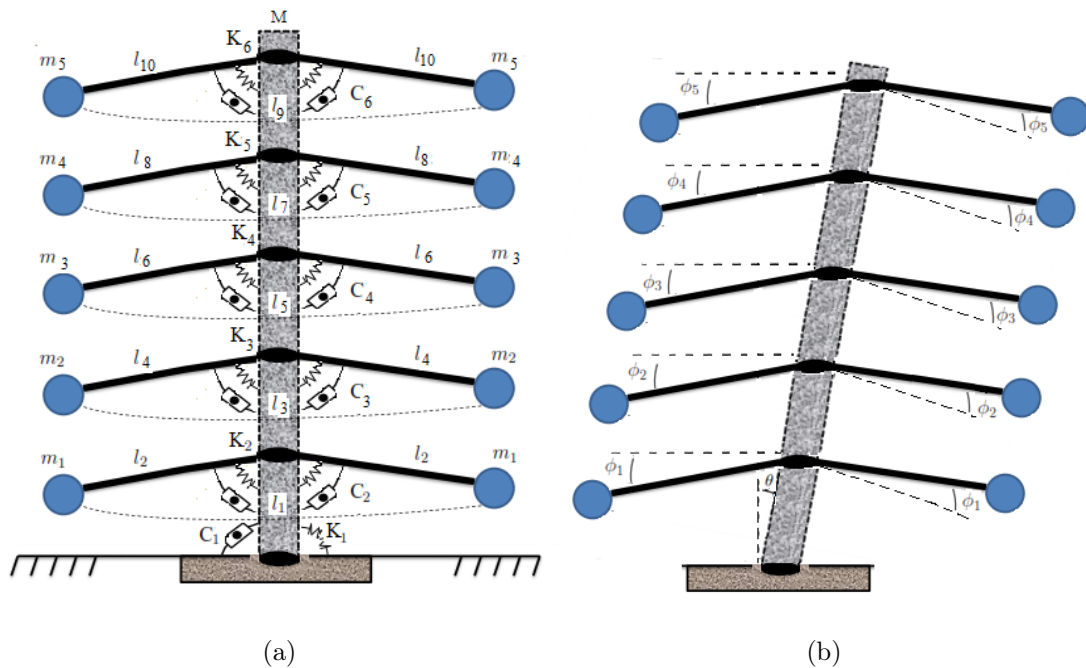


Figure 3.23: (a) Physical model of pendulum with multi-branched at rest, (b) Disturbed system.

To deal with this system of a central column and five levels attached branches, it is divided in 6 subsystems of one degree of freedom (DOF) each one. Kinetic and potential energies of the whole system give the system (3.45) of equations of motion which is derived using Lagrangian formalism:

$$\left\{ \begin{aligned}
& A(\phi_k)\ddot{\theta} + B(\dot{\phi}_k, \phi_k)\dot{\theta} + D(\phi_k)\dot{\theta}^2 + K_1\theta + gE \sin \theta + C_2 \left(\frac{l_1}{l_2} \cos \phi_0 \sin \phi_1 - 1 \right) \dot{\phi}_1 \\
& + C_3 \left(\frac{l_3}{l_4} \cos \phi_0 \sin \phi_2 - 1 \right) \dot{\phi}_2 + C_4 \left(\frac{l_5}{l_6} \cos \phi_0 \sin \phi_3 - 1 \right) \dot{\phi}_3 + C_5 \left(\frac{l_7}{l_8} \cos \phi_0 \sin \phi_4 - 1 \right) \dot{\phi}_4 \\
& + C_6 \left(\frac{l_9}{l_{10}} \cos \phi_0 \sin \phi_5 - 1 \right) \dot{\phi}_5 + 2K_2 \left(\frac{l_1}{l_2} \cos \phi_0 \sin \phi_1 - 1 \right) \phi_1 + 2K_3 \left(\frac{l_3}{l_4} \cos \phi_0 \sin \phi_2 - 1 \right) \phi_2 \\
& + 2K_4 \left(\frac{l_5}{l_6} \cos \phi_0 \sin \phi_3 - 1 \right) \phi_3 + 2K_5 \left(\frac{l_7}{l_8} \cos \phi_0 \sin \phi_4 - 1 \right) \phi_4 + 2K_6 \left(\frac{l_9}{l_{10}} \cos \phi_0 \sin \phi_5 - 1 \right) \phi_5 \\
& - 2m_1l_1l_2\dot{\phi}_1^2 \cos \phi_0 \cos \phi_1 - 2m_2l_3l_4\dot{\phi}_2^2 \cos \phi_0 \cos \phi_2 - 2m_3l_5l_6\dot{\phi}_3^2 \cos \phi_0 \cos \phi_3 \\
& - 2m_4l_7l_8\dot{\phi}_4^2 \cos \phi_0 \cos \phi_4 - 2m_5l_9l_{10}\dot{\phi}_5^2 \cos \phi_0 \cos \phi_5 - m_1l_1g \sin 2\phi_0 \sin \phi_1 \sin (\theta + \phi_1) \\
& - m_2l_3g \sin 2\phi_0 \sin \phi_2 \sin (\theta + \phi_2) - m_3l_5g \sin 2\phi_0 \sin \phi_3 \sin (\theta + \phi_3) \\
& - m_4l_7g \sin 2\phi_0 \sin \phi_4 \sin (\theta + \phi_4) - m_5l_9g \sin 2\phi_0 \sin \phi_5 \sin (\theta + \phi_5) = 0 \\
& 2m_1l_2^2\ddot{\phi}_1 + C_2\dot{\phi}_1 + 2K_2\phi_1 - \left(2m_1gl_2 \sin \phi_0 \right) \sin (\theta + \phi_1) + \left(2m_1l_1l_2\dot{\theta}^2 \cos \phi_0 \right) \cos \phi_1 \\
& \hspace{15em} = \left(2m_1l_1l_2 \cos \phi_0 \sin \phi_1 - 2m_1l_2^2 \right) \ddot{\theta} \\
& 2m_2l_4^2\ddot{\phi}_2 + C_3\dot{\phi}_2 + 2K_3\phi_2 - \left(2m_2gl_4 \sin \phi_0 \right) \sin (\theta + \phi_2) + \left(2m_2l_3l_4\dot{\theta}^2 \cos \phi_0 \right) \cos \phi_2 \\
& \hspace{15em} = \left(2m_2l_3l_4 \cos \phi_0 \sin \phi_2 - 2m_2l_4^2 \right) \ddot{\theta} \\
& 2m_3l_6^2\ddot{\phi}_3 + C_4\dot{\phi}_3 + 2K_4\phi_3 - \left(2m_3gl_6 \sin \phi_0 \right) \sin (\theta + \phi_3) + \left(2m_3l_5l_6\dot{\theta}^2 \cos \phi_0 \right) \cos \phi_3 \\
& \hspace{15em} = \left(2m_3l_5l_6 \cos \phi_0 \sin \phi_3 - 2m_3l_6^2 \right) \ddot{\theta} \\
& 2m_4l_8^2\ddot{\phi}_4 + C_5\dot{\phi}_4 + 2K_5\phi_4 - \left(2m_4gl_8 \sin \phi_0 \right) \sin (\theta + \phi_4) + \left(2m_4l_7l_8\dot{\theta}^2 \cos \phi_0 \right) \cos \phi_4 \\
& \hspace{15em} = \left(2m_4l_7l_8 \cos \phi_0 \sin \phi_4 - 2m_4l_8^2 \right) \ddot{\theta} \\
& 2m_5l_{10}^2\ddot{\phi}_5 + C_6\dot{\phi}_5 + 2K_6\phi_5 - \left(2m_5gl_{10} \sin \phi_0 \right) \sin (\theta + \phi_5) + \left(2m_5l_9l_{10}\dot{\theta}^2 \cos \phi_0 \right) \cos \phi_5 \\
& \hspace{15em} = \left(2m_5l_9l_{10} \cos \phi_0 \sin \phi_5 - 2m_5l_{10}^2 \right) \ddot{\theta}
\end{aligned} \right. \tag{3.45}$$

With $A(\phi_k) = \frac{1}{4}Ml_9^2 + 2m_1l_1^2 + 2m_2l_3^2 + 2m_3l_5^2$

$$+ 2m_4l_7^2 + 2m_5l_9^2 - 2m_1l_1^2 \cos^2 \phi_0 \sin^2 \phi_1 - 2m_2l_3^2 \cos^2 \phi_0 \sin^2 \phi_2 - 2m_3l_5^2 \cos^2 \phi_0 \sin^2 \phi_3 - 2m_4l_7^2 \cos^2 \phi_0 \sin^2 \phi_4 - 2m_5l_9^2 \cos^2 \phi_0 \sin^2 \phi_5$$

$$B(\dot{\phi}_k, \phi_k) = C_1 - 4m_1l_1l_2\dot{\phi}_1 \cos \phi_0 \cos \phi_1 - 4m_2l_3l_4\dot{\phi}_2 \cos \phi_0 \cos \phi_2 - 4m_3l_5l_6\dot{\phi}_3 \cos \phi_0 \cos \phi_3 - 4m_4l_7l_8\dot{\phi}_4 \cos \phi_0 \cos \phi_4 - 4m_5l_9l_{10}\dot{\phi}_5 \cos \phi_0 \cos \phi_5$$

$$D(\phi_k) = 2m_1l_1^2\cos^2\phi_0 \cos \phi_1 \sin \phi_1 + 2m_2l_3^2\cos^2\phi_0 \cos \phi_2 \sin \phi_2 + 2m_3l_5^2\cos^2\phi_0 \cos \phi_3 \sin \phi_3 + 2m_4l_7^2\cos^2\phi_0 \cos \phi_4 \sin \phi_4 + 2m_5l_9^2\cos^2\phi_0 \cos \phi_5 \sin \phi_5 - 2m_1l_1l_2 \cos \phi_0 \cos \phi_1 - 2m_2l_3l_4 \cos \phi_0 \cos \phi_2 - 2m_3l_5l_6 \cos \phi_0 \cos \phi_3 - 2m_4l_7l_8 \cos \phi_0 \cos \phi_4 - 2m_5l_9l_{10} \cos \phi_0 \cos \phi_5$$

$$E = 2m_1l_1 + 2m_2l_3 + 2m_3l_5 + 2m_4l_7 + 2m_5l_9 - \frac{1}{2}Ml_9$$

with g the acceleration of terrestrial gravity.

Because the equations of motion of the central column and each branch are coupled by nonlinear terms, energy can be exchanged between them [33]. As one can see, the movement of branches are independent each other but all induced by the motion of the main rod. Therefore, the dissipation in the branches may damp the energy received from the central column, resulting in an effective damping of the whole structure.

3.5.2 Effects of branches on the damping of the central column vibration

3.5.2.1 Free vibration case

The central column is moved from its equilibrium point ($\theta = 0$) with an initial value of 1.57 rad for θ_0 and 1.047 rad for ϕ_{i_0} for branches. And for vibration test and behavior observation, the amplitude of vibration of the central column is plotted for five different cases: one level branches, two, three, four and five level branches at different positions.

Figure 3.24 (a) shows that the angular displacement of the central column is surely a damped oscillated motion around its equilibrium position which is here 0. While Figure

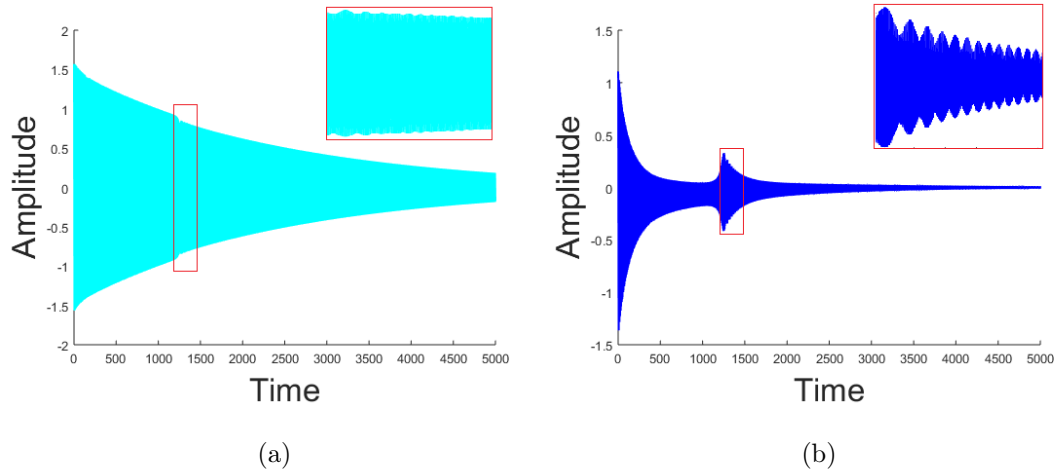


Figure 3.24: Angular displacement (a) θ for the central column, (b) ϕ_1 for the first level branches

3.24 (b) exhibits in addition to vibration an appearance of one pack of peaks of bursting oscillation which consequently reduce with a high effect the amplitude of vibration of the central column. It is well observed around the dimensionless time of [1250, 1500]. As main results here, it is important to mention that as the central column give its motion to attached branches, this denote to the energy exchange between the two subsystem [33].

In Figure 3.25, the effect of the number of attached branches is pointed out by a gradual reduction of the amplitude of vibration of the central column which is plotted here. Figure 3.25 (a) is the comparison between one attached level branches and two, Figure 3.17 (b) between two and three, Figure 3.25 (c) three and four and finally Figure 3.25 (d) four and five levels of attached branches. The observation is not debatable, the more the branches are added, the amplitude the central rod is reduced, and one can see a reduction of up to 50% during the time going of the simulation.

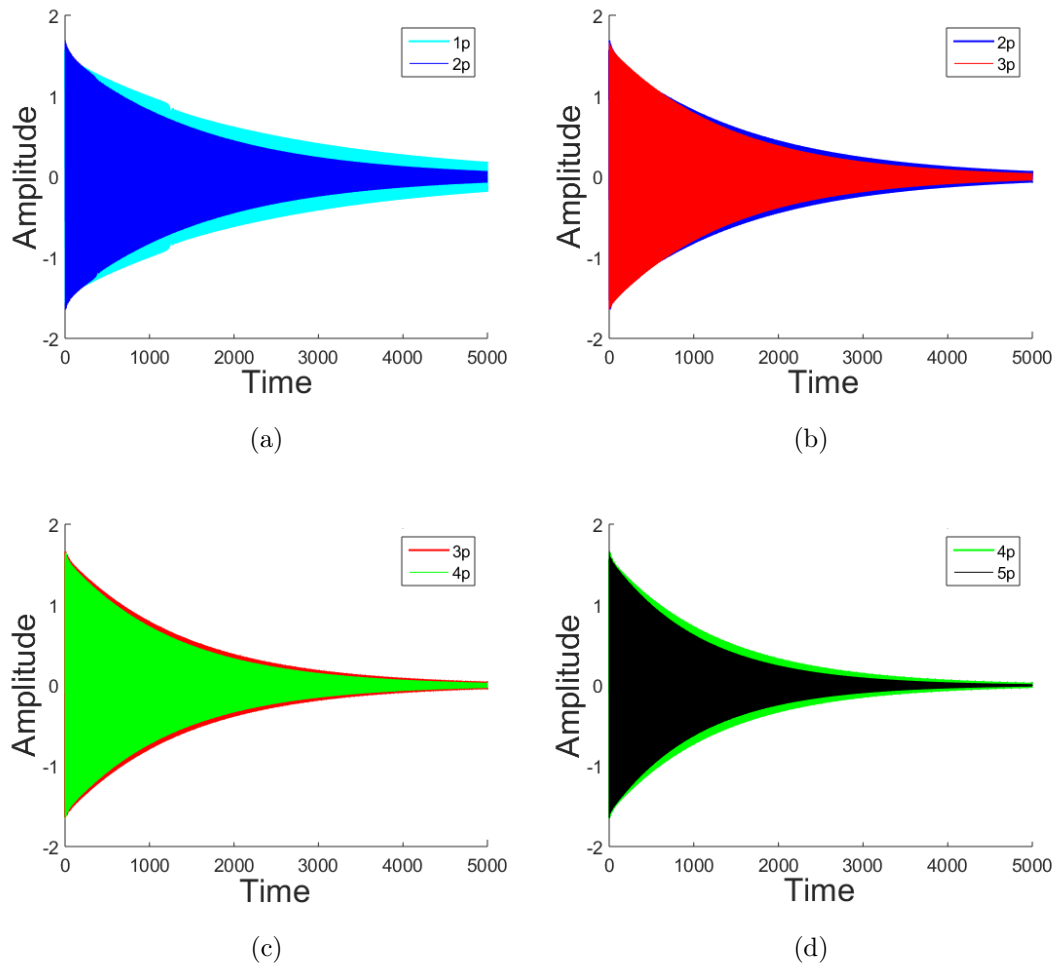


Figure 3.25: Angular displacement of Central column with (a)One-Two, (b)Two-Three, (c)Three-Four, (d)Four-Five levels of attached branches

3.5.2.2 Under earthquake excitation

In this section, an external force (here the earthquake) appears on the base of the central rod. That earthquake loads is numerically generated according to Kanai Tajimi model [116, 117]: a nonstationary ground acceleration with a random function which takes the form of a filtered Gaussian stationary white noise modulated by a deterministic envelope function. The physical and geometrical properties of the central column, are those of a wooden structure [40]. And we aim to determine if the previous results are the same.

The ground acceleration \ddot{u}_g is assumed to be represented by

$$\ddot{u}_g = e_0(e^{-\beta_1 t} - e^{-\beta_2 t})\ddot{w}(t) \quad (3.46)$$

with the spectral density given by :

$$S_{\ddot{w}}(\omega) = S_0 \frac{\omega_g^4 + (2\zeta_g \omega_g \omega)^2}{(\omega_g^2 - \omega^2)^2 + (2\zeta_g \omega_g \omega)^2} \quad (3.47)$$

where S_0 is the intensity of the white noise process at the rock level, ω_g is the dominant frequency of the soil site and ζ_g is the associated damping ratio of the soil strata.

The system submitted to earthquake load is shown in figure 3.26:

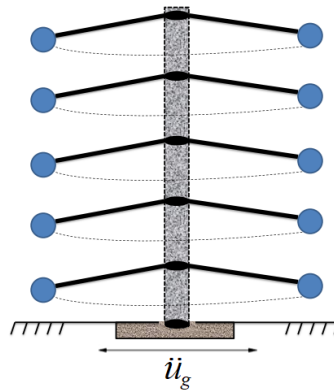


Figure 3.26: The model of a set of pendulums under earthquake loads

Figure 3.27 is the generated acceleration of the ground \ddot{u}_g .

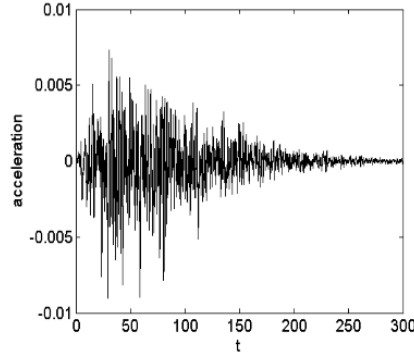


Figure 3.27: Dimensionless ground acceleration

From the system of equations 3.45, the central column is directly affected by the appearance of earthquake as it is the only part of the structure which is attached to the soil. And its equation of motion become:

$$\begin{aligned}
& A(\phi_k)(\ddot{\theta} + \ddot{u}_g) + B(\dot{\phi}_k, \phi_k)\dot{\theta} + D(\phi_k)\dot{\theta}^2 + K_1\theta \\
& + gE \sin \theta + C_2 \left(\frac{l_1}{l_2} \cos \phi_0 \sin \phi_1 - 1 \right) \dot{\phi}_1 \\
& + C_3 \left(\frac{l_3}{l_4} \cos \phi_0 \sin \phi_2 - 1 \right) \dot{\phi}_2 + C_4 \left(\frac{l_5}{l_6} \cos \phi_0 \sin \phi_3 - 1 \right) \dot{\phi}_3 \\
& + C_5 \left(\frac{l_7}{l_8} \cos \phi_0 \sin \phi_4 - 1 \right) \dot{\phi}_4 + C_6 \left(\frac{l_9}{l_{10}} \cos \phi_0 \sin \phi_5 - 1 \right) \dot{\phi}_5 \\
& + 2K_2 \left(\frac{l_1}{l_2} \cos \phi_0 \sin \phi_1 - 1 \right) \phi_1 + 2K_3 \left(\frac{l_3}{l_4} \cos \phi_0 \sin \phi_2 - 1 \right) \phi_2 \\
& + 2K_4 \left(\frac{l_5}{l_6} \cos \phi_0 \sin \phi_3 - 1 \right) \phi_3 + 2K_5 \left(\frac{l_7}{l_8} \cos \phi_0 \sin \phi_4 - 1 \right) \phi_4 \\
& + 2K_6 \left(\frac{l_9}{l_{10}} \cos \phi_0 \sin \phi_5 - 1 \right) \phi_5 - 2m_1 l_1 l_2 \dot{\phi}_1^2 \cos \phi_0 \cos \phi_1 \\
& - 2m_2 l_3 l_4 \dot{\phi}_2^2 \cos \phi_0 \cos \phi_2 - 2m_3 l_5 l_6 \dot{\phi}_3^2 \cos \phi_0 \cos \phi_3 \\
& - 2m_4 l_7 l_8 \dot{\phi}_4^2 \cos \phi_0 \cos \phi_4 - 2m_5 l_9 l_{10} \dot{\phi}_5^2 \cos \phi_0 \cos \phi_5 \\
& - m_1 l_1 g \sin 2\phi_0 \sin \phi_1 \sin (\theta + \phi_1) - m_2 l_3 g \sin 2\phi_0 \sin \phi_2 \sin (\theta + \phi_2) \\
& - m_3 l_5 g \sin 2\phi_0 \sin \phi_3 \sin (\theta + \phi_3) - m_4 l_7 g \sin 2\phi_0 \sin \phi_4 \sin (\theta + \phi_4) \\
& - m_5 l_9 g \sin 2\phi_0 \sin \phi_5 \sin (\theta + \phi_5) = 0
\end{aligned} \tag{3.48}$$

By adding the earthquake, the central column exhibit a behavior which follows the earthquake displacement and by so doing induced vibrations of each of branches as it

appears in Figure 3.28.

Each level of attached branches vibrates exactly as the central column Figure 3.28 (b), (c), (d), (e) and (f) for the five floors and the amplitude of vibration is according to the intensity of earthquake that is transmitted to its through the rigid main rod.

To point out the influence of branches on the vibration of the central column which is the main supported branch of the system, the amplitude of vibration of the system is drawn taking into account the number of attached branches levels, from one attached branches level up to five. The results are those of Figure 3.29.

For one floor, the attached masses are at the top of the main rigid rod, while for more than two floors which is more than two different positions of attached masses, one pair of masses is attached at the top of the central column and others are somewhere between the base and the top of that central column.

After the appearance of earthquake, one can notice that the vibration of each floor affect considerably the vibration of the central column, and it is by so doing that the system reduce the amplitude of vibration during the earthquake excitation.

A deep observation of Figures 3.28 (a) and 3.29 do not shows an appearance of peaks of bursting oscillation firstly because as it was shown in the first part Section 3.4.2, it cannot be visible for more than two levels of attached branches; secondly, the earthquake behave particularly as a disorder and by that it is not possible to observe such kind of phenomenun. Furthermore, the results of Figure 3.29 come to confirm those of Figure 3.25, and a report of a damping of up to 33% of vibration is highlighted. And by adding branches from one to five levels, one can obtain a total damping of around 50% and more comparative to the amplitude of vibration when the structure is just a central column with only one level of attached branches. To resume this part, one can say that, up to Five levels in an inverted pendulum with multi-branching, the damping phenomenun increase

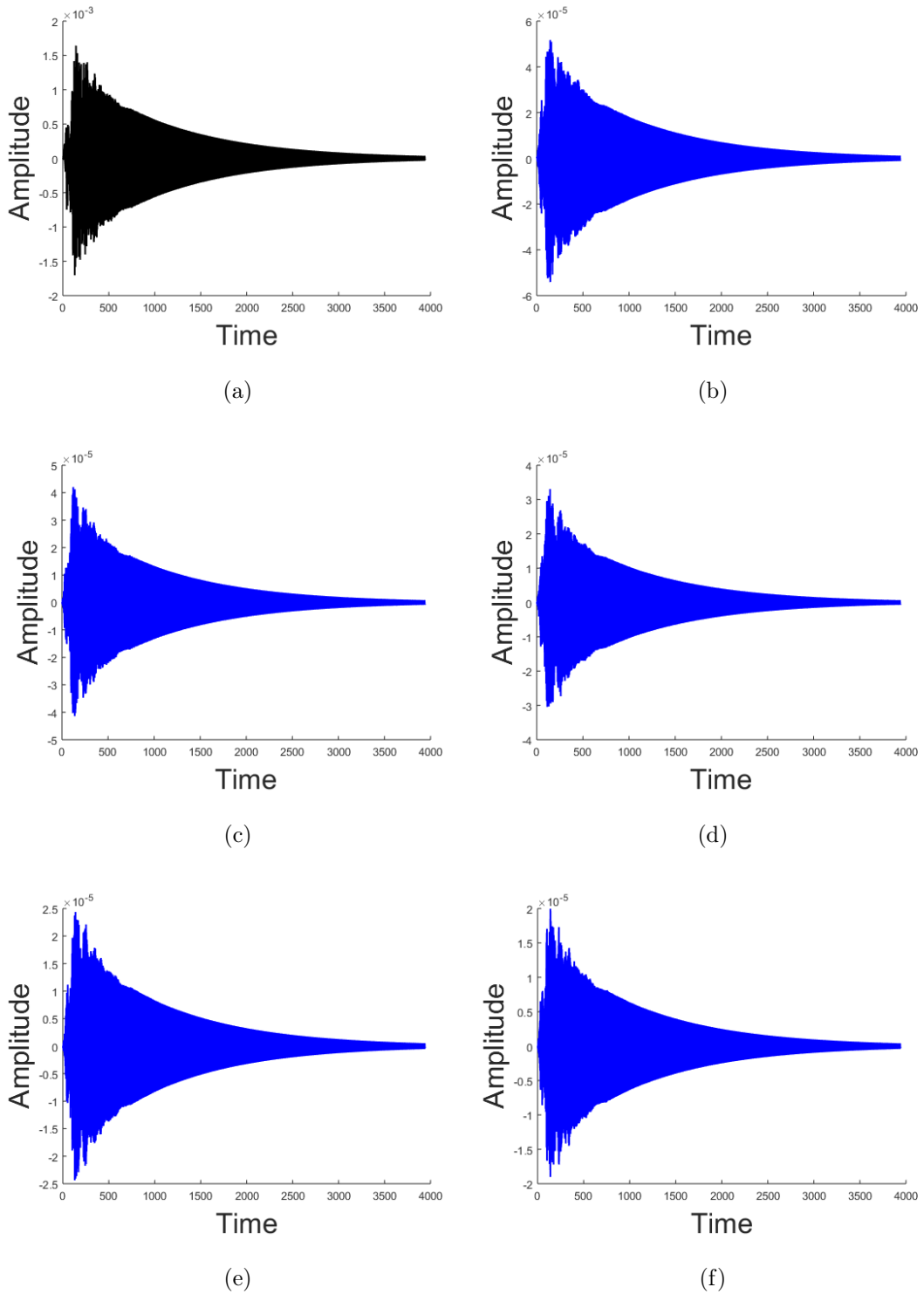


Figure 3.28: Angular displacement of (a) Central column θ , (b) First floor ϕ_1 , (c) Second floor ϕ_2 , (d) Third floor ϕ_3 , (e) Fourth floor ϕ_4 , (f) Fifth floor ϕ_5

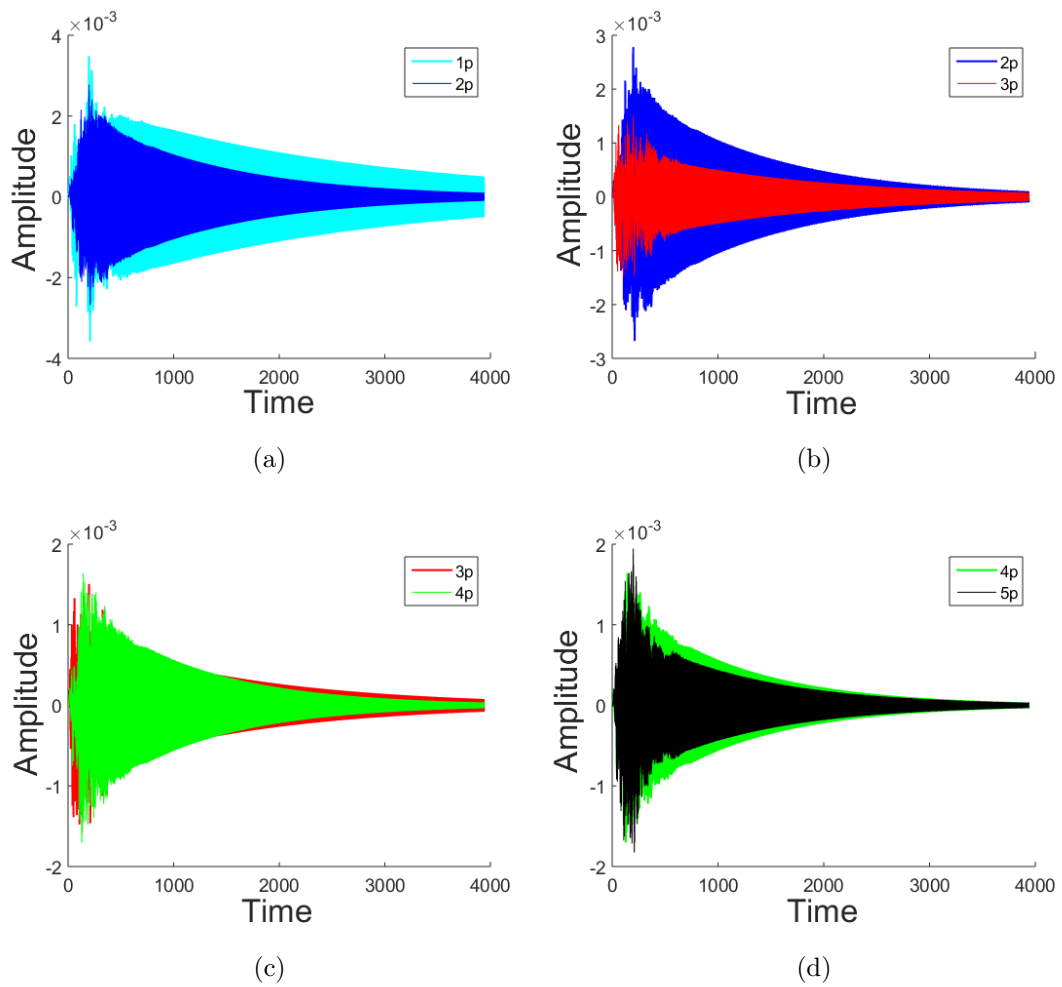


Figure 3.29: Angular displacement of Central Column according to the number of floors
(a)1 and 2, (b)2 and 3, (c)3 and 4, (d)4 and 5

with the number of added branches.

3.5.3 Energy tranfer leading to damping effect of branches

Let us come back to the autonomous case. Many others consideration have been made as: $l_{n_{max}} = l_9 = 5l_1$ because a five story is chosen. In addition to that, $l_3 = 2l_1$, $l_5 = 3l_1$, $l_7 = 4l_1$, $l_2 = l_4 = l_6 = l_8 = l_{10}$, $m_1 = m_2 = m_3 = m_4 = m_5$, $C_2 = C_3 = C_4 = C_5 = C_6$, $K_2 = K_3 = K_4 = K_5 = K_6$ so that the structure have at different levels the same masses values added.

With ϕ_k , $k = 1, \dots, 5$ for each floors up to 5, and by taking as coefficients :

$$\Gamma = \frac{2m_1 l_1^2 \cos^2 \phi_0}{J_\Delta}; \quad J_\Delta = \frac{25}{4} M l_1^2 + 110 m_1 l_1^2; \quad J_{\phi_1} = \sin^2 \phi_1;$$

$$J_{\phi_2} = 4 \sin^2 \phi_2; \quad J_{\phi_3} = 9 \sin^2 \phi_3; \quad J_{\phi_4} = 16 \sin^2 \phi_4;$$

$$J_{\phi_5} = 25 \sin^2 \phi_5; \quad \Omega_1^2 = \frac{K_1}{J_\Delta}; \quad \Omega_2^2 = \frac{K_2}{m_1 l_2^2}$$

$$\beta_1^2 = \frac{(30m_1 - \frac{5}{2}M)gl_1}{J_\Delta}; \quad \beta_2^2 = \frac{g}{l_2} \sin \phi_0; \quad K_{\phi_1} = \frac{m_1 g l_1 \sin(2\phi_0) \sin \phi_1}{J_\Delta}$$

$$K_{\phi_2} = \frac{2m_1 g l_1 \sin(2\phi_0) \sin \phi_2}{J_\Delta}; \quad K_{\phi_3} = \frac{3m_1 g l_1 \sin(2\phi_0) \sin \phi_3}{J_\Delta}$$

$$K_{\phi_4} = \frac{4m_1 g l_1 \sin(2\phi_0) \sin \phi_4}{J_\Delta}; \quad K_{\phi_5} = \frac{5m_1 g l_1 \sin(2\phi_0) \sin \phi_5}{J_\Delta}$$

The system of equations 3.45 lead to the new system of motion which is given by equations 3.49.

$$\left\{ \begin{array}{l}
A'(\phi_k)\ddot{\theta} + B'(\dot{\phi}_k, \phi_k)\dot{\theta} + D'(\phi_k)\dot{\theta}^2 \\
+ K_1\theta + \left(30m_1 - \frac{5}{2}M\right) gl_1 \sin \theta + \left(\frac{l_1}{l_2} \cos \phi_0 \sin \phi_1 - 1\right) C_2\dot{\phi}_1 \\
+ \left(2\frac{l_1}{l_2} \cos \phi_0 \sin \phi_2 - 1\right) C_2\dot{\phi}_2 + \left(3\frac{l_1}{l_2} \cos \phi_0 \sin \phi_3 - 1\right) C_2\dot{\phi}_3 \\
+ \left(4\frac{l_1}{l_2} \cos \phi_0 \sin \phi_4 - 1\right) C_2\dot{\phi}_4 + \left(5\frac{l_1}{l_2} \cos \phi_0 \sin \phi_5 - 1\right) C_2\dot{\phi}_5 \\
+ \left(\frac{l_1}{l_2} \cos \phi_0 \sin \phi_1 - 1\right) 2K_2\phi_1 + \left(2\frac{l_1}{l_2} \cos \phi_0 \sin \phi_2 - 1\right) 2K_2\phi_2 \\
+ \left(3\frac{l_1}{l_2} \cos \phi_0 \sin \phi_3 - 1\right) 2K_2\phi_3 + \left(4\frac{l_1}{l_2} \cos \phi_0 \sin \phi_4 - 1\right) 2K_2\phi_4 \\
+ \left(5\frac{l_1}{l_2} \cos \phi_0 \sin \phi_5 - 1\right) 2K_2\phi_5 \\
- 2m_1l_1l_2 \cos \phi_0 \begin{pmatrix} \dot{\phi}_1^2 \cos \phi_1 + 2\dot{\phi}_2^2 \cos \phi_2 \\ + 3\dot{\phi}_3^2 \cos \phi_3 + 4\dot{\phi}_4^2 \cos \phi_4 \\ + 5\dot{\phi}_5^2 \cos \phi_5 \end{pmatrix} \\
- m_1gl_1 \sin(2\phi_0) \begin{bmatrix} \sin \phi_1 \sin(\theta + \phi_1) + 2 \sin \phi_2 \sin(\theta + \phi_2) + \\ 3 \sin \phi_3 \sin(\theta + \phi_3) + 4 \sin \phi_4 \sin(\theta + \phi_4) \\ + 5 \sin \phi_5 \sin(\theta + \phi_5) \end{bmatrix} = 0 \\
2m_1l_2^2\ddot{\phi}_k + C_2\dot{\phi}_k + 2K_2\phi_k - \begin{pmatrix} 2m_1gl_2 \\ \sin \phi_0 \end{pmatrix} \sin(\theta + \phi_k) \\
+ \begin{pmatrix} 2(k)m_1l_1l_2 \\ \dot{\theta}^2 \cos \phi_0 \end{pmatrix} \cos \phi_k = 2 \begin{pmatrix} (k)m_1l_1l_2 \cos \phi_0 \sin \phi_k \\ -m_1l_2^2 \end{pmatrix} \ddot{\theta}
\end{array} \right. \quad (3.49)$$

With news coefficients: $A'(\phi_k) = \frac{25}{4}Ml_1^2 + 110m_1l_1^2$
 $- 2m_1l_1^2 \cos^2 \phi_0 (\sin^2 \phi_1 + \sin^2 \phi_2 + \sin^2 \phi_3 + \sin^2 \phi_4 + \sin^2 \phi_5)$

$$\begin{aligned}
B'(\dot{\phi}_k, \phi_k) &= C_1 - 4m_1l_1l_2 \cos \phi_0 (\dot{\phi}_1 \cos \phi_1 \\
&+ 2\dot{\phi}_2 \cos \phi_2 + 3\dot{\phi}_3 \cos \phi_3 \\
&+ 4\dot{\phi}_4 \cos \phi_4 + 5\dot{\phi}_5 \cos \phi_5)
\end{aligned}$$

$$\begin{aligned}
D'(\phi_k) &= 2m_1 l_1^2 \cos^2 \phi_0 (\cos \phi_1 \sin \phi_1 + 4 \cos \phi_2 \sin \phi_2 \\
&+ 9 \cos \phi_3 \sin \phi_3 + 16 \cos \phi_4 \sin \phi_4 \\
&+ 25 \cos \phi_5 \sin \phi_5) - 2m_1 l_1 l_2 \sin \phi_0 (\sin \phi_1 + 2 \sin \phi_2 \\
&+ 3 \sin \phi_3 + 4 \sin \phi_4 + 5 \sin \phi_5)
\end{aligned}$$

The total mechanical energy is given by:

$$\begin{aligned}
E_m &= [1 - 2\Gamma (J_{\phi_1} + J_{\phi_2} + J_{\phi_3} + J_{\phi_4} + J_{\phi_5})] \dot{\theta}^2 + \Omega_1^2 \theta^2 - 2\beta_1^2 \cos \theta \\
&+ 2K_{\phi_1} \cos (\theta + \phi_1) + 2K_{\phi_2} \cos (\theta + \phi_2) + 2K_{\phi_3} \cos (\theta + \phi_3) \\
&+ 2K_{\phi_4} \cos (\theta + \phi_4) + 2K_{\phi_5} \cos (\theta + \phi_5) \\
&+ \Gamma \left[\begin{aligned} &\dot{\phi}_1^2 + \dot{\phi}_2^2 + \dot{\phi}_3^2 + \dot{\phi}_4^2 + \dot{\phi}_5^2 + \Omega_2^2 (\phi_1^2 + \phi_2^2 + \phi_3^2 + \phi_4^2 + \phi_5^2) \\ &+ 2\beta_2^2 [\cos (\theta + \phi_1) + \cos (\theta + \phi_2) + \cos (\theta + \phi_3) + \cos (\theta + \phi_4) + \cos (\theta + \phi_5)] \end{aligned} \right]
\end{aligned} \tag{3.50}$$

In Figures 3.30 (a) and (b) , we display the energy of the whole system after a brief displacement (autonomous case), in function of the time for one level of attached branches and two, this to have an idea on the dissipation phenomenon inside the system. There is a good agreement with the previous observation, because one can notice that the energy of the system rapidly reduce with the number of added branches. When the number of branches increase, one observes that reduction of energy is more important [8, 134].

As observation, we notice that the pack of peaks of bursting oscillation (red circle) that was pointed out during the vibration test is too expose by a pack of peaks of bursting oscillation too on energy time history. Figures 3.30 (a) and (b) illustrate well the fact that bursting oscillation see its amplitude reduce and move near the started time of simulation until that phenomenon disappear when the number of attached branches increase.

To confirm the results of rapid dissipation due to branches, the comparison of the energy of the system in four cases was shown in Figure 3.31. The initial energy of the

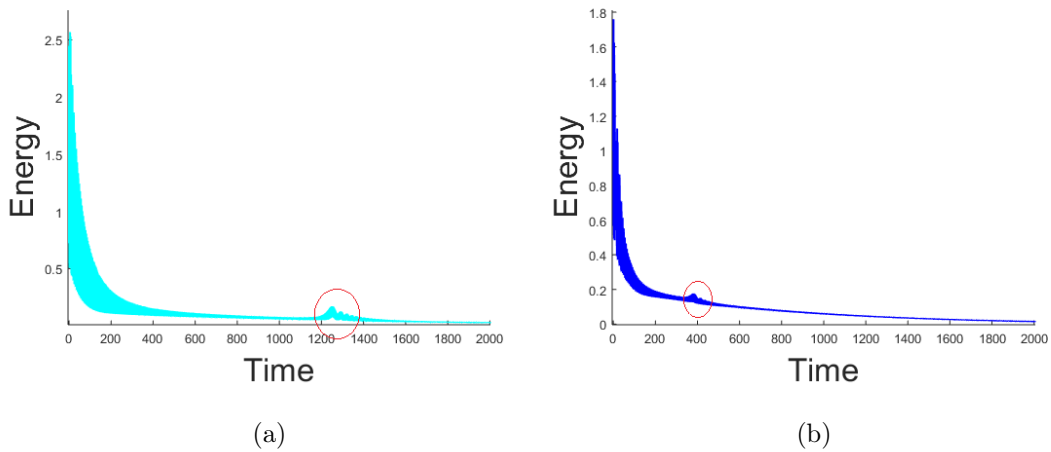


Figure 3.30: Energy of the system for (a)One and (b)Two levels branches

system was normalized at 1, to have a well appreciation on the control of vibration involved in the system. Gradually, from (a) to (d), the comparison between One and two levels, two and three levels, three and four levels and finally four and five levels are drawn. To return to its initial position, the structure need to dissipate all the received energy from external excitation; and one can clearly says that the point zero of energy is quickly reached for a larger number of branches.

Figure 3.32 (a) presents the energy of system during the vibration phenomenon as fonction of the weight m_1 of the central column and the time. One can bring out one main point : when the central column weight is high, the energy of the system at the beginning at the inverse is reduce. It is the same observation on Figures 3.32 (b), (c) and (d) which show the influence of main rod length l_1 , the attached mass weight m_2 and the distance between that attached mass and the central column l_2 . The main results to retain is that for each parameters of the system, up to the plotted taken value, when they increase, the total energy of the system decrease and this has not effect on time history of the energy. Only for the length l_2 , when its high value is really welpful for the structure because the most it increase then the structure dissipate quicly the energy and even the

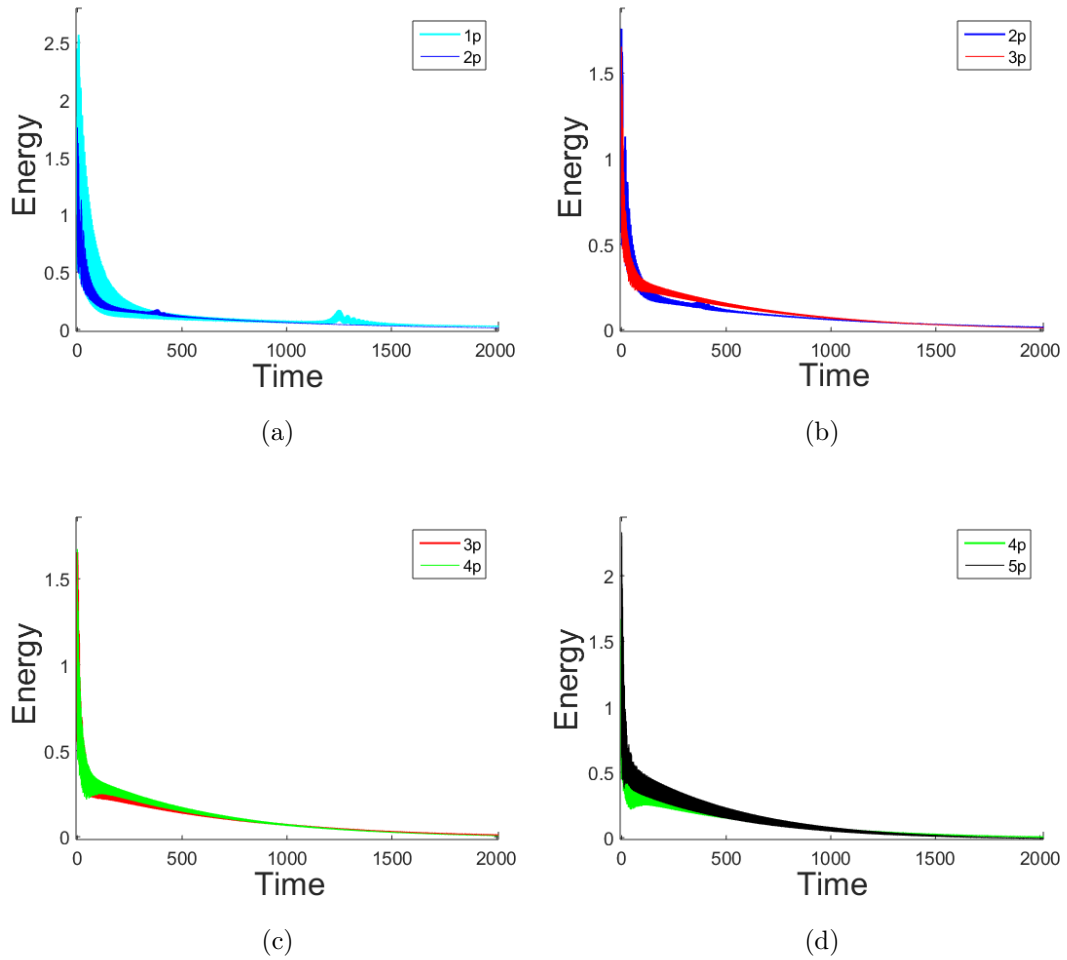


Figure 3.31: Energy of the system for (a)One-Two, (b)Two-Three, (c)Three-Four, (d)Four-Five levels branches

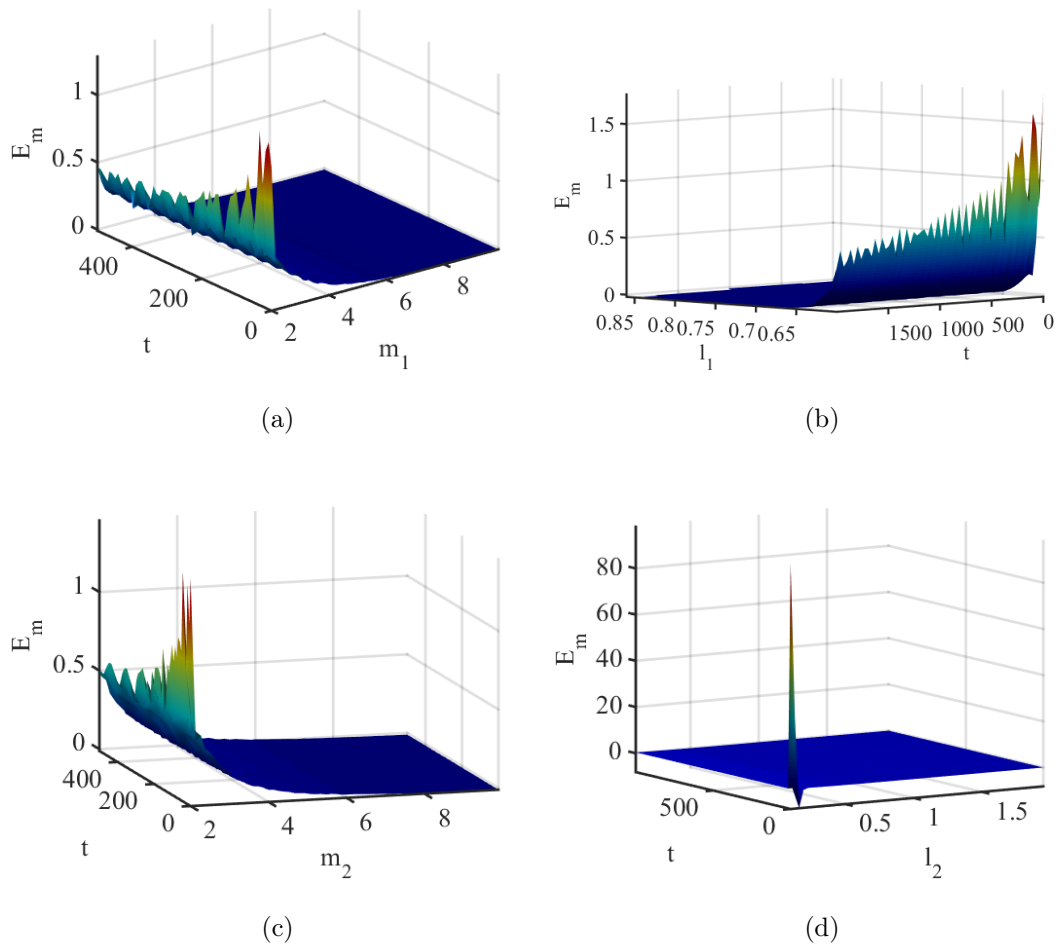


Figure 3.32: Effects of the design parameters on the energy of the system : (a)mass of central rod, (b)length of central rod, (c)level masses, (d)level length

time history is quiet affected by its value. A nullification of the energy of the system is rapidly denoted. Therefore, the system return quickly to its initial position by dissipating its energy when the length of its branches are considerable. Particularly for the length of location of the mass (l_2), the highest value is fonction of the length of the central column to avoid the fact that, masses will touch the ground or touch each others. And to make sure that, this condition will be taken into account, the length should satisfy : $l_2 < \frac{l_1}{\sin(\phi_0)}$.

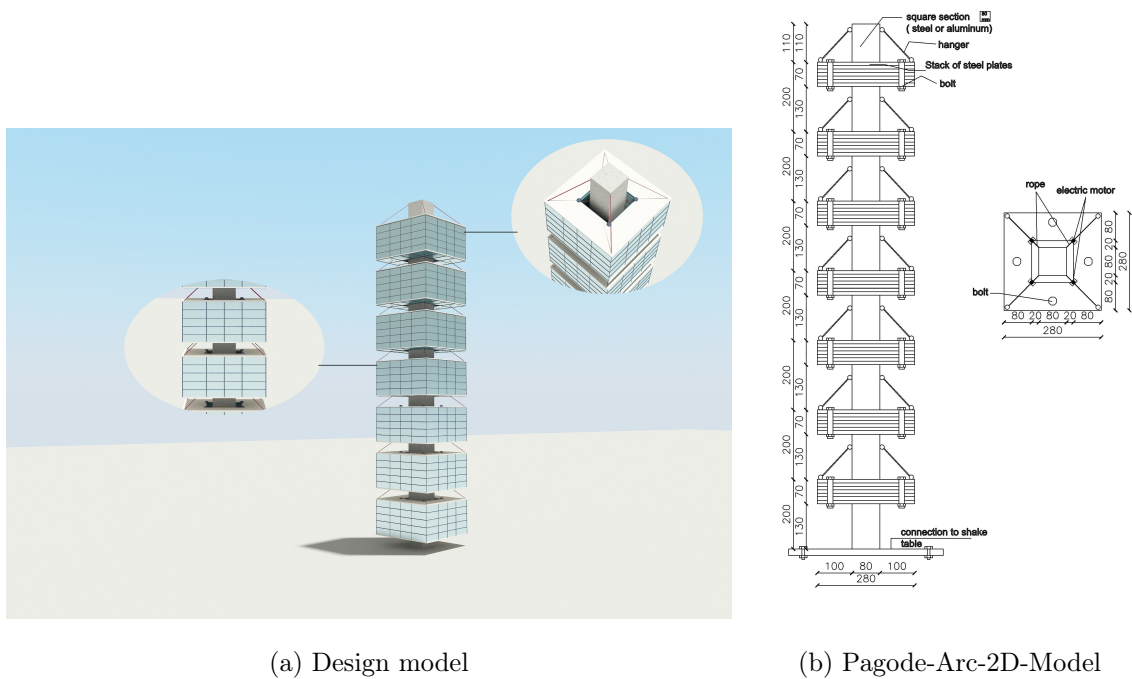


Figure 3.33: Model of a building view as a set of pendulum with multi-branched

3.6 Conclusion

The present chapter has presented the results obtained in this thesis work. Firstly, The effect of the disposition of many damped outriggers attached on a high-rise structure is investigated. A partial differential equation governing the vibration is proposed and deduced from a Bernoulli-Euler beam where the geometrical non-linearity is taken into

account. The analysis shows that, the right position to locate an outrigger on a cantilever beam is near the top level only for the first mode. When the number of outrigger increase, the damping ratio of the system increase too and the vibrations are reduced. The disposition of the outrigger affect considerably the amplitude of vibration according to the considered mode. Secondly, The nonstationary random approach is employed to simulate seismic events. The Timoshenko beam approach is used to model the frame-core tube linked at a point of its length by the damped outriggers, therefore are connected vertically two magnetorheological damper devices. To evaluate the performance of the control system, the control algorithm based on Lyapunov stability theory is adopted to seek the input voltage leading to the reduction of vibration. Finally, two models of self-controlled of vibration systems were proposed and their dynamic evaluations were given leading to the conclusion that there are good candidates for earthquake protection of mechanical structures.

General conclusion

The present thesis has treated the problem of modelling of an elastic structure where outriggers systems are located along its length, modelling of a rigid body structure where masses are attached at different levels as a structural control system, dynamic of such structures with the effect of outriggers and masses on their vibrations in the autonomous case (an impulsion move the structure from its initial position) and also when they are subjected to earthquake loads or wind flows.

Inspired by pagoda system which is among the best technics of earthquake protection, this work had as aim to give a mathematical modeling of a system that can fit the dynamics of pagoda's system with its damping factors.

The first chapter presented the state of art on the modelling and the generalities on the dynamics of Euler-Bernoulli and Timoshenko beam using the dynamics fundamental relationship approach. Then the generalities on vibration control systems are presented, by a review on some structural control methods before the problematic of the thesis.

In the second chapter, externals excitations which induce vibration in the system are generated and, methods and techniques used to solve the problematic of the thesis has been described. Such as the modal approximation, the fourth order Runge-Kutta method and the stochastic fourth order Runge-Kutta method are used, for solving equations. Earthquake and wind loads are defined here in details.

The third chapter is devoted to the results obtained in the thesis. We proposed models, by using the specificities of their ways of building, firstly for structures with more than one outrigger systems attached, secondly for sets of pendulums view as self-controlled systems inspired by trees vibration and pagoda system. Those models in this work were studied, and with a view on the dynamic shows off:

- One can assert that they fit the real dynamic of those mechanical structures,

– A located outrigger near the top of a Cantilever beam is the best position for the damped outrigger only for the first mode of vibration, and we could not have a suitable position of one outrigger for the five first modes where the amplitude of vibration will be the smallest one. A comparison of displacements of the structure under earthquake, between the 0.9 position of an outrigger and a five outriggers system with same parameters, denote that the addition of the number of outriggers (until five outriggers) is quite beneficial for the structure to reduce the amplitude of vibration of all the first five modes. We realise also that for the second, the fourth and the fifth modes for a defined length the non equidistance positions of the five levels is the best configuration but for the third mode of vibration the equidistance positions of levels reduce more significantly the vibrations. Not only the number of moving loads, but their disposition affects too the mean amplitude of the beam,

– And in the third part, it appears that all position of outriggers cannot lead to optimal minimization of the seismic vibration of the structural system. On top of that, the best scale coefficient MF of the parameter of the MR device leading to the maximum force by maintaining the efficient control has been determined. Lyapunov stability theory based on semi active control has been used to select the suitable voltage that operate MR damper. The repeated sequence of the input voltage response reveals that this strategy has been adequate for the control devices.

– For the second mechanical proposed system with self-control of vibration, the results obtained in a numerical simulation show that by adding only one branch, that branch increase the damping ratio of the system but the vibration is just a little bit reduced. For more than one branch, the amplitude of vibration is well reduced. The influence of design parameter of the system is analyzed,

– It was shown after dynamics evaluation in the fourth part that, when a set of pendulum view as self-controlled system inspired by trees vibration and pagoda system is moved from its initial and equilibrium position, the energy received by the central column is distributed to the different branches of the structure leading to a self vibration control of the system; branches have a damping effect on the structure. All that results were confirmed even when the structure faces an external force like earthquake loads. It was also found that one can increase or decrease the damping ratio according to the length and the weight of the central rod and even the length and the mass of branches. One also deduct that to keep that configuration of the structure, the limit value acceptable of l_2 is fonction of the length of the central column l_1 and the angle ϕ_0 of its position. A real representation of this structure is proposed in this work called “Modern pagoda system”. A structure which is robust, reliable and fit most our environnement.

This work leads to some prospective works which could be the improvement of the proposed model of this work by the adding of friction damper and tuned mass damper to the modelling. This investigation will be helpful to analyse the evolution and/or the proportionality of the considered devices of control in beam structures. And this result will be more interesting in term of design and technologies in industry, mechanical, aerospace and civil engineering.

Bibliography

Bibliography

- [1] E. Kujawski, Y. Tang, (2009), Simultaneous calculation of direct and indirect levelling in investigating deformations of Pagoda-Type building, *Reports on Geodesy*.
- [2] A.S. Oumarou, B.R. Nana Nbandjo, P. Wofo, (2011), Appearance of horseshoes chaos on a buckled beam controlled by disseminated couple forces, *Communications in Nonlinear Science and Numerical Simulation* 16 3212-3218.
- [3] J. Metsebo, B.R. Nana Nbandjo, P. Wofo, (2016), Dynamic responses of a hinged-hinged Timoshenko beam with or without a damage subject to blast loading, *Mechanics Research Communications* 71 38-43.
- [4] <https://m.investiraucameroun.com>.
- [5] N.D. Anh, N.X. Nguyen and N.H. Quan, (2016), Global-local approach to the design of dynamic vibration absorber for damped structures, *Journal of Vibration and Control* 22(14) 3182-3201.
- [6] D.C. Tsobgni-Fozap, A. Kenfack-Jiotsa, E. Tala-Tebue, M. Motchongom-Tingue, T.C. Kofané, (2018), The effectiveness of a new tuned mass damper to control the dynamics of a mass interacting in a nonsinusoidal Remoissenet-Peyrard potential, *Engineering Structures* 176 303-313.

-
- [7] C.A. Kitio Kwuimy, B.R. Nana Nbandjo, P. Wofo, (2006), Optimization of electromechanical control of beam dynamics: Analytical method and finite differences simulation, *Journal of Sound and Vibration* 298 180-193.
- [8] B.P. Ndemanou, E.R. Fankem, B.R. Nana Nbandjo, (2017) Reduction of vibration on a Cantilever Timoshenko beam subjected to repeated sequence of excitation with Magneto-rheological Outriggers, *Structural Design of Tall and Special Buildings* 26(18) e1393.
- [9] H. Kim, J. Kang, (2017), Smart outrigger damper system for response reduction of tall buildings subjected to wind and seismic excitations, *International Journal of Steel Structures* 17(4) 1263-1272.
- [10] B.P. Ndemanou, B.R. Nana Nbandjo, U.E. Dorka, (2016), Quenching of vibration modes on two interconnected buildings subjected to seismic loads using magneto rheological device, *Mechanics Research Communications* 78 6-12.
- [11] A.A. Nanha Djanan, B.R. Nana Nbandjo and P. Wofo, (2015), Self-synchronization of two motors on a rectangular plate and reduction of vibration, *Journal of Vibration and Control* 21(11) 2114-2123.
- [12] S. Krenk, (2000), Vibrations of a taut cable with an external damper, *Journal of Applied Mechanics* 67(4) 772-776.
- [13] J.D. Hartog, (2007), Mechanical Vibrations, *Dover, New York*.
- [14] B.R. Nana Nbandjo, P. Wofo, (2007), Active control with delay of horseshoes chaos using piezoelectric absorber on a buckled beam under parametric excitation, *Chaos, Solitons and Fractals* 32(1) 73-79.

-
- [15] B.R. Nana Nbandjo, U. Dorka, (2015), Mathematical modelling, *Humboldt meeting Bremen, Kassel, Deutschland, Avril 15-17*.
- [16] A. Preumont, (2002), Responsive systems for active vibration control, *Springer Science & Business Media*.
- [17] P.M.B.R.K. Nanduri, B. Suresh and M.D.I. Hussain, (2013), Optimum position of outrigger system for high-rise reinforced concrete buildings under wind and earthquake loadings, *American Journal of Engineering Research (AJER) 2(8) 76-89*.
- [18] Z. Bayati, M. Mahdikhani, A. Rahaei,(2008), Optimized use of multi-outriggers system to stiffen tall buildings, *in: Proc. 14th World Conference on Earthquake Engineering, Beijing, China, October 12-17*.
- [19] Z. Wang, C. Chang, B.F Spencer Jr., Z. Chen, (2010), Controllable outrigger damping system for highrise building with MR dampers, *Sensors and Smart Structures Technologies for Civil, Mechanical, and Aerospace Systems, Proc. Of SPIE 7647 76473Z*.
- [20] U.E. Dorka, (2004), Erdbebensicherung durch structural control, *Stahlbau 73 661-667*.
- [21] U.E. Dorka, (2014), Seismic control for elevated roads, *Building materials and structures 57 9-20*.
- [22] B.R. Nana Nbandjo, U.E. Dorka, (2016), Effect of tendon structural control on the appearance of horseshoes chaos on a cantilever beam due to seismic action, *Advances in Mechanical Engineering DOI: 10.1177*.
- [23] Y. Wu, X. Song, X. Gu, L. Luo, (2018), Dynamic performance of a multi-story traditional timber pagoda, *Engineering Structures, 159 277-285*.

- [24] T. Bock, T. Linner, S. Miura, (2011), Robotic High-Rise Construction of Pagoda Concept: innovative earthquake-proof Design for the Tokyo Sky Tree, *CTBUH World Conference, Seoul, Korea, 2011*.
- [25] T. Hanazato, D. Ayaki, Y. Ogiwara, R. Uchida, Sato, M. Misu, M. Takayama, I. Sakamoto, (2012), Seismic Design and Construction of a Traditional Timber-Made Five-Storeyed Pagoda by Applying Coupled Vibration Control, *15th World Conference on Earthquake Engineering, LISBOA*.
- [26] A. Ueda et al, (1996), Why five story pagodas hardly collapsed, *Shincho-sha., Japan*.
- [27] K. Nakahara, T. Hisatoku, Y. Takahashi, T. Nagase, (2000), Earthquake response of ancient five-story Pagoda structure of Horyu-ji Temple in Japan, *12th World Conference on Earthquake Engineering, 1229/11/A*.
- [28] H. Omori, (1921), About the seismic vibration of five-story pagodas, *Journal of Architecture and Building Science 415 219-226*.
- [29] K. Muto, (1949), Five-Story Pagodas and Earthquake Resistance, *Journal of the Disaster Prevention 11*.
- [30] R. Tanabashi, (1960), Earthquake Resistance of Traditional Japanese Wooden Structure, *Special lecture of 2WCEE, Japan, July*.
- [31] S. Ishida, (1993), The critical behavior of the wooden pagoda under earthquakes, *Technical report No. 15 71-85*.
- [32] C. Minowa, N. Kawai, H. Maekawa, K. Nitto, T. Hanazato, Y. Niitsu, (2010), Observation of wind and earthquake responses of national heritage five story wooden Pagoda, *World Conference on Timber Engineering*.

- [33] B. Theckes, E. de Langre, X. Boutillon, (2011), Damping by branching: a bioinspiration from trees, *Bioinspiration & Biomimetics* 6(4) 046010.
- [34] S.M. Han, H.B. and T. Wan, (1999), Dynamics of transversely vibrating beams using four engineering theories, *Journal of Sound and Vibration* 225(5) 935-988.
- [35] S.P. Timoshenko, (1921), On the correction for shear of the differential equation for transverse vibrations of bars of uniform cross-section, *Philosophical Magazine*, 744.
- [36] S.P. Timoshenko, (1922), On the transverse vibrations of bars of uniform cross-section, *Philosophical Magazine*, 125.
- [37] A.H. Nayfeh, D.T. Mook, (1979), Nonlinear oscillations, *John Wiley, New York*, 704.
- [38] S. Timoshenko and J. M. Gere, (1961), Theory of Elastic Stability, *McGraw-Hill New York*.
- [39] A. AL Majid, (2002), Dissipation de l'énergie en mécanique vibratoire : Opérateur d'hystérésis, Phénomène métrique, PhD Thesis, *Institut National des Sciences Appliquées de Lyon*, 169.
- [40] B.R. Nana Nbandjo, (2004), Dynamics and active control with delay of the dynamics of unbounded monostable mechanical structures with ϕ^6 potential, PhD Thesis in Non-linear Mechanics, *University of Yaoundé 1, Yaoundé, Cameroon*.
- [41] S. Kulkarni, D. Jadhav and P. Khadke, (2012), Passive control systems for tall structures, *International Journal on Theoretical and Applied Research in Mechanical Engineering* 1(2) 2319-3182.
- [42] T.T. Soong, (1950), Active Structural Control: Theory and Practice, *John Wiley & Sons, Inc, New York*.

- [43] C.R. Fuller, S.J. Eliot, P.A. Nelson, (1997), Active control of vibration, *London Academic*.
- [44] T.T. Soong and B.F. Spencer, (2000), Active, Semi-Active and Hybrid Control of Structures, *Conference 12WCEE*.
- [45] B. R. Nana Nbandjo, (2013), “Cours de PHY 440 : Contrôle des structures”, Master 1 de Physique, Option : Modélisation et Simulation en Ingénierie et Bio-ingénierie, *Département de Physique, Université de Yaoundé I*.
- [46] B.F. Spencer and S. Nagarajaiah, (2003), State of the Art of Structural Control, *Journal of Structural Engineering* 129 845-856.
- [47] U.E. Dorka, (2014), Introduction to Earthquake Engineering: Introduction to Seismic Control, *published October 2014*.
- [48] T.E. Saaed, G. Nikolakopoulos, J.E. Jonasson and H. Hedlund, (2015), A state-of-the-art review of structural control systems, *Journal of Vibration and Control* 21(5) 919-937.
- [49] U.E. Dorka, (1994), Hysteretic device systems for earthquake protection of buildings, *Proc. 5th US nat. conf. on earthq. eng., Chicago, USA, 775-785*.
- [50] U.E. Dorka and G.A. Conversano, (1995), Seismic retrofit of Allstate Building, *IABSE symposium, San Francisco, USA, 145-150*.
- [51] I.S. Idrizi, U.E. Dorka and Z.S. Idrizi, (2012), Application of HYDE structural control system for RC buildings, *15th World Conference on Earthquake Engineering, LISBOA 2012*.

- [52] D. Okuyucu, U.E. Dorka and M. Sharifi, (2009), Tendon Systems for Seismic Upgrading of Historical Masonry Buildings, A Preliminary Feasibility Study: Erzurum Double Minaret Madrasah, *Symposium with International Participation on Strengthening and Preserving Historical Buildings and Cultural Heritage - II, Diyarbakir, Turkey, 15th-17th October 2009*.
- [53] M.G. Castellano, M. Indirli, A. Martelli, J.J Azedevo, G.E. Sincarian, D. Tirelli, V. Renda, G. Croci, M. Biritognolo, A. Bonci, A. Viskovic, (1999), Seismic Protection of Cultural Heritage Using Shape Memory Alloy Devices-An EC Funded Project (ISTECH), *International Post-SmiRT Conference Seminar on Seismic Isolation, Passive Energy Dissipation and Active Control of Vibration of Structures, Cheju, Korea*.
- [54] Y. Wu, X. Song, X. Gu, L. Luo, (2018), Dynamic performance of a multi-story traditional timber pagoda, *Engineering Structures*, 159 277-285.
- [55] T. Hanazato, D. Ayaki, Y. Ogiwara, R. Uchida, Sato, M. Misu, M. Takayama, I. Sakamoto, (2012), Seismic Design and Construction of a Traditional Timber-Made Five-Storeyed Pagoda by Applying Coupled Vibration Control, *15th World Conference on Earthquake Engineering, LISBOA*.
- [56] T. Bock, T. Linner, S. Miura, (2011), Robotic High-Rise Construction of Pagoda Concept: innovative earthquake-proof Design for the Tokyo Sky Tree, *CTBUH 2011 World Conference, Seoul, Korea*.
- [57] K. Kamath, N. Divya, A.U. Rao, (2012), A study on static and dynamic behavior of outrigger structural system for tall buildings, *Bonfring International Journal of Industrial Engineering and Management Science* 2(4) 15-20.

-
- [58] R.J. Smith and M.R. Willford, (2007), The damped outrigger concept for tall buildings, *Structural Design of Tall and Special Buildings* 16, 501-517.
- [59] T. Speck, O. Speck, N. Beheshti and AC. McIntosh, (2008), Process sequences in biomimetic research, *Design and nature IV* 114 3-11.
- [60] P. Gruber, (2011), Biomimetics in Architecture : Architecture of Life and Buildings, *Springer Vienna Architecture*.
- [61] G. Jeronimidis and AG. Atkins, (1995), Mechanics of biological materials and structures : Nature's lessons for the engineer, *Proceedings of the Institution of Mechanical Engineers, Part C : Journal of Mechanical Engineering Science 1989-1996* 209(43) 221-235.
- [62] T. Speck, R. Luchsinger, S. Busch, M. Rüggeberg and O. Speck, (2006), Selfhealing processes in nature and engineering : self-repairing biomimetic membranes for pneumatic structures, *Design and nature* 3 105-114.
- [63] S.H. Yoon and S. Park, (2011), A mechanical analysis of woodpecker drumming and its application to shock-absorbing systems, *Bioinspiration & Biomimetics* 6(1) 016003.
- [64] F.W. Telewski, (2006), A unified hypothesis of mechanoperception in plants, *American Journal of Botany* 93(10) 1466-1476.
- [65] B. Moulia, C. Coutand, and C. Lenne, (2006), Posture control and skeletal mechanical acclimation in terrestrial plants : implications for mechanical modeling of plant architecture, *American Journal of Botany* 93(10) 1477-1489.
- [66] MS. Watt, JR. Moore and B. McKinlay, (2005), The influence of wind on branch characteristics of pinus radiata, *Trees-Structure and Function* 19(1) 58-65.

- [67] F. Gosselin, E. de Langre and B.A. Machado-Almeida, (2010), Drag reduction of flexible plates by reconfiguration, *Journal of Fluids Mechanics* 650 319-341.
- [68] S. Vogel, (1984), Drag and flexibility in sessile organisms, *American Zoologist* 24(1) 37-44.
- [69] E. de Langre, (2012), Methodological advances in predicting flow-induced dynamics of plants using mechanical-engineering theory, *The Journal of Experimental Biology* 215(6) 914-921.
- [70] H.C. Spatz, A. Emanns and O. Speck, (2004), The structural basis of oscillation damping in plant stems-biomechanics and biomimetics, *Journal of Bionics Engineering* 1(3) 149-158.
- [71] F. Brüchert, and B. Gardiner, (2006), The effect of wind exposure on the tree aerial architecture and biomechanics of sitka spruce (*picea sitchensis*, pinaceae), *American journal of botany* 93(10) 1512-1521.
- [72] J.R. Moore and D.A. Maguire, (2007), Simulating the dynamic behavior of douglas-fir trees under applied loads by the finite element method, *Tree Physiology* 28(1) 75-83.
- [73] M.J. Jonsson, A. Foetzki, M. Kalberer, T. Lundström, W. Ammann and V. Stöckli, (2007), Natural frequencies and damping ratios of norway spruce (*picea abies* (L.) karst) growing on subalpine forested slopes, *Trees-Structure and Function* 21(5) 541-548.
- [74] S. Castro-García, G.L. Blanco-Roldán, J.A. Gil-Ribes and J. Agüera-Vega, (2008), Dynamic analysis of olive trees in intensive orchards under forced vibration, *Trees-Structure and Function* 22(6) 795-802.

- [75] D. Schindler, R. Vogt, H. Fugmann, M. Rodriguez, J. Schönborn, and H. Mayer, (2010), Vibration behavior of plantation-grown scots pine trees in response to wind excitation, *Agricultural and Forest Meteorology* 150(7) 984-993.
- [76] T. Speck and I. Burgert, (2011), Plant stems : functional design and mechanics, *Annual Review of Materials Research* 41 169-193.
- [77] K.R. James, N. Haritos and P.K. Ades, (2006), Mechanical stability of trees under dynamic loads, *American Journal of Botany* 93(10) 1522-1530.
- [78] M. Rodriguez, E. de Langre and B. Moulia, (2008), A scaling law for the effects of architecture and allometry on tree vibration modes suggests a biological tuning to modal compartmentalization, *American Journal of Botany* 95(12) 1523-1537.
- [79] Y. Wu, X. Song, X. Gu, L. Luo, (2018), Dynamic performance of a multi-story traditional timber pagoda, *Engineering Structures* 159 277-285.
- [80] K. Nakahara, T. Hisatoku, Y. Takahashi, T. Nagase, (2000), Earthquake response of ancient five-story Pagoda structure of Horyu-ji Temple in Japan, *12th World Conference on Earthquake Engineering*, 1229/11/A.
- [81] www.yourarticlelibrary.com/earthquake/earthquakes-definitioncauses-measures-and-other-details-with-diagram/31854.
- [82] K. Lu, M. Hou, Z. Jiang, Q. Wang, G. Sun and J. Liu, (2018), Understanding earthquake from the granular physics point of view Causes of earthquake, earthquake precursors and predictions, *International Journal of Modern Physics B* 32 1850081.
- [83] www.google.com/search?q=definition+of+earthquake.
- [84] K. Kumar, Basic Geotechnical Earthquake Engineering, *New Age International*.

- [85] <https://www.worldvision.org/disaster-relief-news-stories/2016-ecuador-earthquake-facts>.
- [86] C. Scawthorn and W.F. Chen, (2002), Earthquake Engineering Handbook, *CRC press*.
- [87] B. Mohraz and F. Sadek, (2001), Chapter 2: Earthquake ground motion and response spectra, *F. Naeim (ed.), The seismic Design Handbook, Kluwer Academic Publishers*.
- [88] S.Y. Kung, D.A. Pecknold, (1982), Effect of ground motion characteristics on the seismic response of torsionally coupled elastic systems, *Thesis, University of Illinois at Urbana-Champaign Urbana, Illinois*.
- [89] Y.K. Lin, Y. Yong, (1987), Evolutionary kanai-tajimi earthquake models, *Journal of engineering mechanics 113 1119-1137*.
- [90] F.R. Rofooei, A. Mobarake, G. Ahmadi, (2001), Generation of artificial earthquake records with a nonstationary Kanai-Tajimi model, *Engineering Structures 33 827-837*.
- [91] M.M. Kahan, Approches Stochastiques pour le Calcul des Ponts aux Séismes, *Thèse de Doctorat de l'Ecole Nationale des ponts et Chaussées*.
- [92] P.C. Jennings, G.W. Housner, N.C. Tsai, (1968), Simulated earthquake motions, *California Institute of Technology*.
- [93] M. Boore, (1983), Stochastic simulation of high-frequency ground motions based on Seismological models of the radiated spectra, *Bulletin of the Seismological Society of America 73 1865-1894*.

-
- [94] R. Saragoni and G. Hart, (1974), Simulation of artificial earthquakes, *Earthquake Engineering and Structural Dynamics* 2 249-267.
- [95] G. Alotta, S.D. Lorenzo, M.D. Paola, A. Pirrotta, (2013), Earthquake ground motion artificial simulations through Fractional Tajimi-Kanai Model, *Aimeta*.
- [96] A.M Abbas, I. Takewaki, (2011), Response of nonlinear single-degree-offreedom structures to random acceleration sequences, *Engineering Structures* 33 1251-1258.
- [97] <https://en.m.wikipedia.org/wiki/wind>
- [98] JetStream, (2008), How to read weather maps, *National weather service*, *Archived from original on 2012-06-22, Retrieved 2009-05-16*.
- [99] Glossary of Meteorology (2009), Wind vane, *American Meteorology Society*, *Archived from the original on 2007-10-18, Retrieved 2009-03-17*.
- [100] Glossary of Meteorology, (2009), Anemometer, *American Meteorology Society*, *Archived from the original on 2011-06-06, Retrieved 2009-03-17*.
- [101] D.A. Ascânio, E.J.R. Parteli, T. Pöschel, J.S. Andrade Jr. and H.J. Herrmann, (2013), Numerical modeling of the wind flow over a transverse dune, *Scientific reports* 3 2858.
- [102] <https://www.google.com/search?q=images+of+structure+destroyed+by+wind+effect>.
- [103] <https://www.google.com/search?q=images+of+wind+effect+on+structure>.
- [104] A. Kareem, (1987), Wind effects on structures: a probabilistic viewpoint, *Probabilistic Engineering Mechanics* 2(4) © 1987 COMPUTATIONAL MECHANICS PUBLICATION.

- [105] M. Sathyamoorthy, (1997), Nonlinear analysis of structures, *CRC press*.
- [106] W.H. Press, S.A. Teukolsky, W.T. Vetterling and B.P. Flannery, (2007), Numerical Recipes: The Art of Scientific Computing, *Cambridge University Press ISBN 0521880688, August*.
- [107] N.J. Kasdin, (1995), Runge-Kutta Algorithm for the Numerical Integration of Stochastic Differential Equations, *Journal of Guidance, Control and Dynamic* 18(1) 114-120.
- [108] Y. K. Lin and G. Q. Cai, (1995), Probabilistic structural dynamics: advanced theory and applications, *McGraw-Hill New York*.
- [109] N.J. Kasdin, (1995), Discrete simulation of colored noise and stochastic processes and $1/f$ power law noise generation, *In proceedings of the IEEE* 83(5) 802-827.
- [110] L.M. Jansen, S.J. Dyke, (2000), Semiactive control strategies for MR dampers: comparative study, *Journal of Engineering Mechanics* 126(8) 795-803.
- [111] C.K. Li, (2006), A review on the products of distributions, *Mathematical methods in engineering*, K. Tas, J. A. Tenreiro Machado, D. Baleanu, eds., Springer, Dordrecht, The Netherlands, 71-96.
- [112] C. Chang, Z. Wang, B.F. Spencer Jr., Z. Chen, Z.,(2013), Semi-active damped outriggers for seismic protection of high-rise buildings, *Smart Structures and Systems* 11(5) 435-451.
- [113] Y. Chen, D.M. McFarland, Z. Wang, B.F. Spencer Jr., L.A. Bergman, (2010), Analysis of tall buildings with damped outriggers, *Journal of Structural Engineering* 136(11) 1435-1443.

- [114] B.R. Nana Nbandjo, P. Wofo,(2011), Modelling of the dynamics of Euler's beam by ϕ_6 potential, *Mechanics Research Communications* 38(8) 542-545.
- [115] K. Fujita, T. Hanazato, I. Sakamoto, (2004), Earthquake response monitoring and seismic performance of five storied timber pagoda, *13th World Conference on Earthquake Engineering* 54, Vancouver, B.C., Canada. August 1-6.
- [116] Y.K. Lin and Y. Yong, (1987), Evolutionary Kanai-tajimi earthquake models, *Journal of Engineering Mechanics* 113(8) 1119-1137.
- [117] J.C. Ramallo, E.A. Johnson, B.F. Spencer Jr.,(2002), "Smart" base isolation systems, *Journal of Engineering Mechanics* 128(10) 1088-1099.
- [118] Cowper, (1966), The shear coefficient in Timoshenko's beam theory, *Journal of Applied Mechanics* 33 335-340.
- [119] A.F. Mosaad, (1999), *Computational Structure* 71 663-670.
- [120] B.F. Spencer, S.J. Dyke, M. K. Sain, J. D. Carlson, (1996), Phenomenological model for magnetorheological dampers, *Journal of Engineering Mechechanics*, 123(3) 230-238.
- [121] H.S. Park, S. Lee, S.W. Choi, B. Kwan oh, T. Cho, Y. Kim, (2016), *Engineering Structures*, 117 496-505.
- [122] H.J. Jung, B.F. Spencer Jr, I.W. Lee, (2003), Control seismically excited cable-stayed bridge employing magnetorheological fluid dampers, *Journal of Structural Engineering* 129(7) 873-883.
- [123] B. Erkus, M. Abe, Y. Fujino, (2002), Investigation of semi-active control for seismic protection of elevated highway bridges, *Engineering Structure* 24(3) 281-293.

- [124] H. Spatz, F. Bruchert, J. Pfisterer, (2007), *American Journal of Botany* (94) 1603.
- [125] N.D. Anh, H. Matsuhisa, L. D. Viet and M. Yasuda, (2007), Vibration control of an inverted pendulum type structure by passive mass-spring-pendulum dynamic vibration absorber, *Journal of Sound and Vibration* 307(1-2) 187-201.
- [126] M. Abdel-Rohman, (2001), Effect of unsteady wind flow on galloping of tall prismatic structures, *Nonlinear Dynamic* 26(3) 233-254.
- [127] L. Angelo and Z. Daniele, (2001), Parametric, external and self-excitation of a tower under turbulent wind flow, *Journal of Sound and Vibration* 330 3057.
- [128] H. Zhu, B. He and X. Chen, (2005), *WUJHS: Wuhan University Journal of Natural Sciences* 10(6) 1069.
- [129] O.S. Salawu, (1997), Detection of structural damage through changes in frequency: a review, *Engineering Structures* 19(9) 718-723.
- [130] G. Mei, A. Kareem and J. C. Kantor, (2001), Real-time model predictive control of structures under earthquakes, *Earthquake Engineering and Structural Dynamics* 30(7) 995.
- [131] A.M. Abbas and C. Manohar, (2002), Investigations into critical earthquake load models within deterministic and probabilistic frameworks, *Earthquake Engineering and Structural Dynamics* 31(4) 813-832.
- [132] A.M. Abbas, (2006), Critical seismic load inputs for simple inelastic structures, *Journal of Sound and Vibration* 296(4-5) 949-967.

-
- [133] B.P. Ndemanou, J. Metsebo, B.R. Nana Nbandjo and P. Wofo, (2014), Dynamics and magneto-rheological control of vibration of cantilever Timoshenko beam under earthquake loads, *Nonlinear Dynamic* 78 163-173.
- [134] R.N. Iyengar and M. Shinozuk, (1972), Effect of self-weight and vertical acceleration on the behaviour of tall structures during earthquake, *Earthquake Engineering and Structural Dynamics* 1(1) 69-78.

List of publications

-
- 1- B.P. Ndemanou, **E.R. Fankem**, B.R. Nana Nbandjo, (2017), Reduction of vibration on a Cantilever Timoshenko beam subjected to repeated sequence of excitation with Magneto-rheological Outriggers, *The Structural Design of Tall and Special Buildings* 2017:e1393.
 - 2- **E.R. Fankem**, B.R. Nana Nbandjo, P. Wofo, U. Dorka, (2020), An inverted pendulum with multi-branching view as self-controlled system: Modelling and vibration absorber capacity, *Journal of Vibration and Control*, DOI: 10.1177/1077546320908141.

Collection of the published papers

RESEARCH ARTICLE

Reduction of vibration on a cantilever Timoshenko beam subjected to repeated sequence of excitation with magnetorheological outriggers

Buris Peggy Ndemanou¹  | Eliane Raïssa Fankem¹ | Blaise Romeo Nana Nbandjo^{1,2}

¹Laboratory Modeling and Simulation in Engineering, Biomimetism and Prototypes, Department of physics, Faculty of science, University of Yaounde I, Yaounde, Cameroon
²Steel and Composite structures, University of Kassel, Germany

Correspondence

Buris Peggy Ndemanou, Laboratory of Modeling and Simulation in Engineering, Biomimetism and Prototypes, Department of physics, Faculty of science, University of Yaounde I, P. Box 812, Yaounde, Cameroon.
Email: ndemanoupeggy@gmail.com

Funding information

Alexander von Humboldt Foundation

Summary

This paper deals with the statistical effects of an outrigger system on a cantilever beam under seismic excitation. The nonstationary random approach is employed to simulate seismic events. The Timoshenko beam approach is used to model the frame-core tube linked at a point of its length by the damped outriggers, therefore are connected vertically two magnetorheological damper devices. The peak root-mean-square values of displacement responses is employed as a best measure effective to specify the optimal locations of outriggers according to different vibration modes. To evaluate the performance of the control system, the control algorithm based on Lyapunov stability theory is adopted to seek the input voltage leading to the reduction of vibration.

KEYWORDS

Lyapunov stability, MR dampers, nonstationary random, outriggers, peak RMS, Timoshenko beam

1 | INTRODUCTION

Since several decades, researchers and engineers do not cease to multiply the intensive research efforts, in view of reinforcing the degree of energy dissipation of tall buildings to further resist to the energy from the external disturbances. Due to the vulnerability of those structures to environmental dynamic loads, various alternatives in this sense carried out, with a view to increase structural safety in minimizing the damage effects that could lead to a premature collapse. The configuration of these ones is done such as the dynamic forces are transferred upon one another in such manner that they work as a group.^[1] As the further element, the passive, active, and semiactive devices are inserted into those structures to enhance control performance by providing energy dissipation. In the same view, another designed way to improve efficiency of tall buildings such as the outrigger system, which is consisted of a core wall, external columns, and outriggers, was developed and implemented. Smith and Willford^[2] described that structural system like a new concept for the structural design of high-rise buildings. The authors mentioned that the performance of this type of system depends on the flexural and shear stiffness of various core or wall and also of the axial stiffness of the perimeter columns and their distance from the core. In this regard, Tan et al.^[3] presented the experimental work on the outrigger damping system. They showed that the damped outrigger system can achieve a better performance than the outrigger structure in reducing the seismic response of the structure. Asai et al.^[4] defined that new structural concept like a novel energy dissipation system, which can mostly be used to protect high rise and tall buildings against the hazard loads, such as severe earthquakes and strong winds. Chang et al.^[5] has indicated that outrigger system provides additional damping that can reduce structural response, and that the bending deformation of the building is transformed into shear deformation across dampers placed between the outrigger and the perimeter column. Park et al.^[6] studied an optimal design method for minimizing the volume of the primary structural members. According to authors, the flexural rigidity of the core wall and the axial rigidity of the external column vary linearly with respect to height. Some investigations about outrigger damping systems employing the magnetorheological (MR) dampers, which are inserted vertically between the outriggers, and the perimeter columns studied by previous studies.^[5,7,8] The particularities of MR devices are due to its semiactive nature, inherent stability, mechanical simplicity, large temperature operating range, and require a low voltage to achieve high control performance.^[9] In the present paper, outrigger system will be constituted of a core and outriggers equipped of the two MR dampers installed vertically at the ends, This signifies, in other words, that the influence of the perimeter columns is neglected. All these illustrated assumptions lead us to have the signifies model.^[10,11]

To investigate the dynamic responses, the different approaches were employed by the authors to model the outrigger system such as the elastic flexural deformation beam,^[4, 10–12] known on the name of the Euler–Bernoulli beam, the shear-flexural cantilever.^[13] Thus, it is important to mention that up to now, there is a lack of research work in the literature that takes into account the combination of shear-type deformation and rotary inertia effects in the dynamic behaviours in investigating transverse vibration of the structure. As a result, the core tube adopted here is a cantilever beam in which the influence of the shear deformation and rotary inertia is taken into account in the modelling. Timoshenko^[14] was the first to demonstrate the importance of shear deformation and rotational inertia effect in the dynamics of elastic beams. That model is a mathematical expansion of the Euler–Bernoulli theory associated with the quoted effects.

In this work, the frame-core tube is considered as a continuum cantilever Timoshenko beam theory characterized by a set of partial differential equations. As damped element, two MR dampers are installed vertically at the ends of each outrigger, which are fixed at one point of the mentioned core structure. The whole structure is adopted to mitigate the earthquake sequence response. The main objective is to find the suitable location of outriggers at the first three modes by varying the distance of these ones from the core, in order to evaluate the effective response of the structural system. These results are obtained through the passive-on strategy. It is important to note that the employed optimisation principle is very necessary to minimize the earthquake-induced structural vibration.

2 | DESCRIPTION OF PHYSICAL SYSTEM

The physical model represented in Figure 1 is a structural system that is constituted of an uniform cantilever beam and one outrigger truss. The set of the system is subjected to the same environmental dynamic force in the horizontal direction denoted ground excitation, which is considered to

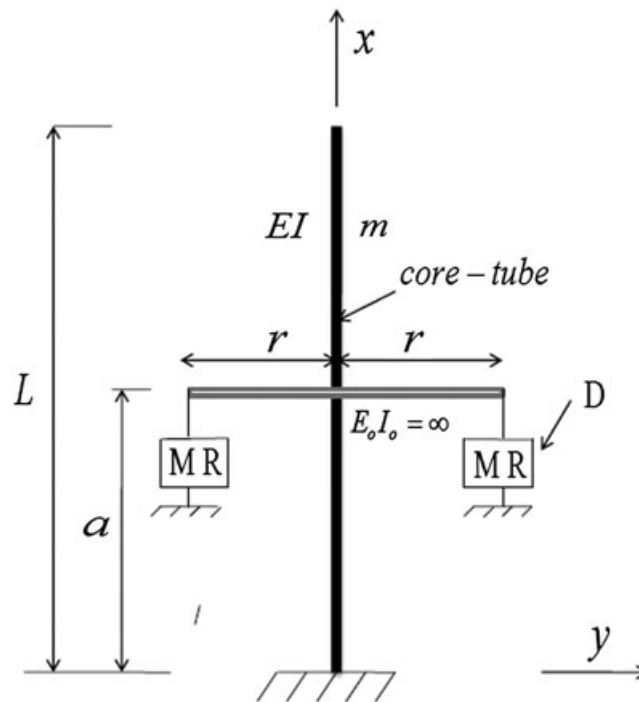


FIGURE 1 Cantilever beam with magnetorheological (MR) outriggers

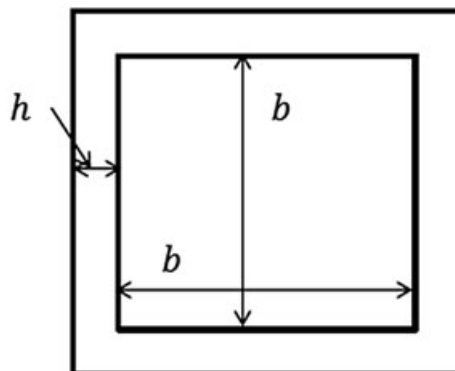


FIGURE 2 Cross-section of the core tube

simulate a seismic motion. The outriggers and the exterior columns have commonly a high stiffness. In this context, they are assumed to be infinitely rigid. As a result, the outrigger behaves as a rigid body and is located at a point a from the end of the core tube. In view of increasing the capacity of the dynamic response of the structural system to resist of the better way against the nonstationary excitation, two semiactive devices dubbed MR dampers (D) are installed vertically and symmetrically; therefore, the generated forces are applied to the core tube through the outriggers.

2.1 | Dynamic model formulation

The mass per unit length is m_1 ; I is the moment of inertia of the cross-section about the neutral axis, E is the Young's modulus; G is the shear modulus of elasticity; r_a is the radius of gyration. These geometrical characteristics are assumed constant. Thus, the lateral displacement is defined by $y(x, t) = y$, which varies with the coordinate along the beam x and with time t . The control device f_d is generated by a MR damper. The influence of the perimeter columns on the dynamics of the core is not taken into consideration. As a result, the governing equations describing the dynamics of the cantilever Timoshenko beam with one damped outrigger under the earthquake loadings can be written as

$$m_1 \frac{\partial^2 y}{\partial t^2} + EI \frac{\partial^4 y}{\partial x^4} - m_1 r_a^2 \left(1 + \frac{E}{k_s G} \right) \frac{\partial^4 y}{\partial x^2 \partial t^2} = -m_1 \ddot{x}_g(t) + \frac{\partial M_a}{\partial x}, \quad (1)$$

where the distributed moment generated by the MR dampers is

$$M_a = 2\delta(x - a) r f_d(t), \quad (2)$$

in which $\delta(x - a)$ denotes the Dirac function. This one indicates that the point a is the place where the damped outriggers is installed. The distance from the control devices to the centre of the core is denoted r . The dimensionless quantity k_s is the shear coefficient depending on the geometric of the cross section of the beam and depend on as well as of the Poisson's ratio. It is assumed in this paper that the dimensional ratio of the width on the area to the thickness is very small, reason why the core tube is considered like a beam being the cross section at the small thickness. This analysis leads us to adopt that, the expression of this mentioned coefficient associated with the cross-section of the core tube is given by Cowper^[15]:

$$k_s = \frac{20(1 + \nu)}{48 + 39\nu}. \quad (3)$$

ν is the Poisson's ratio coefficient, it is clearly seen that k_s is connected with that coefficient, which its value depends solely on the material property. In what follows, the moment of inertia and area of the cross-section can be formulated as (Figure 2)

$$A = (b + 2h)^2 - b^2; \quad I = \frac{(b + 2h)^4}{12} - \frac{b^4}{12}.$$

In this formulation in Equation 1, the first two terms correspond to the classical Bernoulli-Euler beam model. The third term represents the correction for rotary inertia, and the fourth term represents the shear deformation effect.^[16] For convenience in the present study, the joint action of rotary inertia and shear deformation effects is neglected. Thereafter, the bending stiffness for the outriggers is assumed to be infinite.^[10]

The mathematical model of the nonstationary ground acceleration $\ddot{x}_g(t)$ of n sequences proposed by Abbas and Takewakib^[17] is adopted in this paper. According to the authors, ground acceleration of multiplied sequences could result in more damage to the structure than a single ordinary event. This is because the structure gets damaged in the first sequence, and additional damage accumulates from secondary sequence before any repair is possible. As a result, this random function is assumed to take the form of a filtered Gaussian stationary white noise modulated by a deterministic envelope function under the sequence form. Expression of this term is defined in Equation 4 as follows:

$$\ddot{u}_g(t) = \begin{cases} e_1(t) \ddot{w}_1(t) & 0 \leq t \leq T_1 \\ 0 & T_1 \leq t \leq \sum_{i=1}^2 T_i \\ e_2(t - \sum_{i=1}^2 T_i) \ddot{w}_2(t) & \sum_{i=1}^2 T_i \leq t \leq \sum_{i=1}^3 T_i \\ 0 & \sum_{i=1}^3 T_i \leq t \leq \sum_{i=1}^4 T_i \\ \dots & \dots \\ e_n \left(t - \sum_{i=1}^{n-1} T_i \right) \ddot{w}_n(t) & \sum_{i=1}^{n-1} T_i \leq t \leq \sum_{i=1}^{n+2} T_i \end{cases}, \quad (4)$$

where $e_1(t), e_2(t), \dots, e_n(t)$ are the envelope functions associated with the acceleration sequences 1, 2, ..., n , $\ddot{w}_1(t), \ddot{w}_2(t), \dots, \ddot{w}_n(t)$ are stationary random processes, T_1, T_3, \dots, T_{n+2} are the time durations of the acceleration sequences, and T_2, T_4, \dots, T_{n+1} are the time intervals separating these sequences. Thus, the envelope function for the i th sequence is expressed as

$$e_i(t) = e_{0i} \left(t - \sum_{i=1}^n T_i \right) \exp \left[-\alpha_i \left(t - \sum_{i=1}^n T_i \right) \right]; \quad \sum_{i=1}^{n+1} T_i \leq t \leq \sum_{i=1}^{n+2} T_i, \quad (5)$$

where e_{0i} and α_i are $2n$ positive constants that control the intensity and the nonstationarity trend of the i th acceleration sequence.

The phenomenological model, which is based on Bouc-Wen modified version, proposed by Spencer et al.^[18] is adopted here to describe the dynamic of the control device in order to predict its response. This model can exhibit a wide variety of hysteretic behaviours. To valid their mathematical model, authors have done a comparative approach between these analytical data and those obtained experimental results. The analysis of that study on the basis of their results have pointed out the approach numerically tractable and effectively portrays the behaviour of the MR damper. In other words, the proposed mathematical model describes the dynamic behaviour of the MR damper very well. As a result, the equation governing force f_d generated by the control device:

$$f_d(t) = c_1 \dot{y}_1 + k_1(y(a, t) - y_0). \quad (6)$$

The internal displacement y_1 is illustrated:

$$\dot{y}_1 = \frac{1}{(c_0 + c_1)} (\alpha z + c_0 \dot{y}(a, t) + k_0(y(a, t) - y_1)), \quad (7)$$

and z is an evolutionary variable given by

$$\dot{z} = -\gamma |\dot{y}(a, t) - \dot{y}_1| |z|^{n-1} + (\delta_1 - \beta |z|^n)(\dot{y}(a, t) - \dot{y}_1), \quad (8)$$

where c_0 and c_1 are the viscous damping at larger and low velocities, respectively; k_1 is the accumulator stiffness; k_0 represents the stiffness at large velocity; γ , δ_1 and β are the shape parameters of the hysteresis loops. Moreover some of these parameters depend on the command voltage u_1 , which are given by

$$c_0 = c_{0a} + c_{0b}u_1, \quad c_1 = c_{1a} + c_{1b}u_1, \quad \alpha = \alpha_a + \alpha_bu_1, \quad (9)$$

where the command voltage u_1 is accounted for through the first order filter:

$$\dot{u}_1 = \eta_p(u_1 - v_c). \quad (10)$$

v_c is the maximum applied voltage that is associated with the saturation of the magnetic field in the MR damper, and η_p is a positive number that reflects the delay time of the MR damper.

Introducing the new parameters, one has the expressions defined as follows:

$$Y = \frac{y}{L}, \quad \tau = \frac{t}{T}, \quad \delta_a = \delta_1 L, \quad \gamma_L = \gamma L, \quad \zeta_a = \frac{2r}{L}, \quad \ddot{y}_g(\tau) = \frac{T^2}{L} \ddot{x}_g(t); \quad a_1 = \frac{EIT^2}{mL^4}, \quad a_2 = \frac{r_a^2}{L^2} \left(1 + \frac{E}{k_s G}\right),$$

$$C_0 = \frac{c_0}{c_0 + c_1}, \quad K_0 = \frac{k_0 T}{c_0 + c_1}, \quad \alpha_b = \frac{\alpha T}{(c_0 + c_1)L}, \quad C_1 = \frac{c_1 T}{mL}, \quad K_1 = \frac{k_1 T^2}{mL}, \quad T = L \sqrt{\frac{\rho}{k_s G}}, \quad Y_0 = \frac{y_0}{L}.$$

The relationship between the parameters leads to new reformulation, which is described by the below equation:

$$\frac{\partial^2 Y}{\partial \tau^2} + a_1 \frac{\partial^4 Y}{\partial X^4} + a_2 \frac{\partial^4 Y}{\partial X^2 \partial \tau^2} = -\ddot{y}_g(\tau) + \zeta_a F_d(\tau) \frac{\partial}{\partial X} \delta(X - X_0). \quad (11)$$

The dimensionless equation of the MR damper force is rewritten as

$$F_d(\tau) = C_1 \dot{Y}_1 + K_1(Y(X_0, \tau) - Y_0). \quad (12)$$

Y_1 and Z are governed by the below equations:

$$\dot{Y}_1 = \alpha_b Z + C_0 \dot{Y}(X_0, \tau) + K_0(Y(X_0, \tau) - Y_1), \quad (13)$$

$$\dot{z} = -\gamma_L |\dot{Y}(X_0, \tau) - \dot{Y}_1| |Z|^{n-1} + (\delta_1 - \beta |Z|^n)(\dot{Y}(X_0, \tau) - \dot{Y}_1), \quad (14)$$

where X_0 is the location of the damped outriggers. By observing closely the Equations 12, 13, and 14, one can notice that these depend on the quoted location point. This shows that the outrigger position is an important issue in terms of ensuring the efficiency of lateral displacement control.^[6] For the sake of simplicity, it is necessary to assess the dynamic responses of the structural system through the modal properties.

2.2 | Modal equations

To reduce the partial differential equations to a set of ordinary differential equations, in order to assess the dynamic behaviour response of the structural system. Thus, the general solution of the Equation 11 can be written as separation variables of $\chi(\tau)$, which is the time dependent function and the shape function $\Phi(X)$:

$$Y = \sum_{j=1}^{n_m} \Phi_j(X) \chi_j(\tau). \quad (15)$$

n_m is the total of modes with

$$\Phi(X) = \left(d_1^j \sin(\delta_1^j X) + \cos(\delta_1^j X) - d_3^j \sinh(\epsilon_1^j X) - \cosh(\epsilon_1^j X) \right). \quad (16)$$

The spatial function is obtained from Equation 11 without the right member. The superscript j represents the j th mode.

The coefficients d_1^j and d_3^j are obtained by using the boundary conditions of the cantilever Timoshenko beam^[19,20]:

$$d_1^j = \frac{\cos(\delta_1^j) + \frac{(\epsilon_1^{j2} + \mu_1 \delta_1^{j2})}{(\delta_1^{j2} + \mu_1 \epsilon_1^{j2})} \cosh(\epsilon_1^j)}{-\left(\sin(\delta_1^j) + \frac{\delta_1^j}{\epsilon_1^j} \sinh(\epsilon_1^j)\right)}, \quad d_3^j = -\left(\frac{\delta_1^j + \mu_1 \frac{\epsilon_1^{j2}}{\delta_1^j}}{\epsilon_1^j + \mu_1 \frac{\delta_1^{j2}}{\epsilon_1^j}}\right) d_1^j.$$

In which δ_1^j and ϵ_1^j are eigenvalues defined at the j^{th} mode of the vibration. Impossible to adopt an analytical consideration, these quoted eigenvalues are obtained from Equation 17, by using an numerical appropriate algorithm:

$$\begin{cases} \left[\left(\delta_1^{j2} + \Gamma_1 \epsilon_1^{j2} \right)^2 + \left(\epsilon_1^{j2} + \Gamma_1 \delta_1^{j2} \right)^2 \right] \cos(\delta_1^j) \cosh(\epsilon_1^j) - \left(\delta_1^{j2} + \Gamma_1 \epsilon_1^{j2} \right) \left(\epsilon_1^{j2} + \Gamma_1 \delta_1^{j2} \right) \times \\ \left(-2 + \frac{(\delta_1^{j2} - \epsilon_1^{j2})}{\delta_1^j \epsilon_1^j} \sin(\delta_1^j) \sinh(\epsilon_1^j) \right) = 0 \\ \left(\delta_1^{j2} - \epsilon_1^{j2} \right) \Gamma_2^2 - \left(1 + \frac{1}{\Gamma_1} \right) \delta_1^{j2} \epsilon_1^{j2} = 0, \end{cases} \quad (17)$$

with $\Gamma_1 = \frac{E}{k_s G}$, $\Gamma_2 = L \frac{k_s GA}{EI}$.

In what follows, by using the mode decomposition of the illustrated expression in Equation 15 and substituting them into Equation 11, multiplying by the different spatial expression and performing the integration from 0 to 1, by adding the damping coefficient. One gets the modal forms of above equations that can be expressed as follows:

$$\ddot{\chi}_j(\tau) + \zeta_j \dot{\chi}_j(\tau) + \varsigma_j \chi_j(\tau) = -\sigma_j \ddot{y}_g(\tau) - \zeta_a \eta_j F_d(\tau). \quad (18)$$

The dimensionless equation of the force generated by the MR device is satisfied by the illustrated expressions as follows:

$$F_d(\tau) = C_1 \dot{Y}_1 + K_1 (\chi_j(\tau) \Phi_j(X_0) - Y_0), \quad (19)$$

where Y_h and Z can be rewritten as

$$\dot{Y}_1 = \alpha_6 Z + C_0 \dot{\chi}_j(\tau) \Phi_j(X_0) + K_0 (\chi_j(\tau) \Phi_j(X_0) - Y_1), \quad (20)$$

$$\dot{z} = -\gamma_L |\dot{\chi}_j(\tau) \Phi_j(X_0) - \dot{Y}_1| Z |Z|^{n-1} + (\delta_L - \beta_L |Z|^n) (\dot{\chi}_j(\tau) \Phi_j(X_0) - \dot{Y}_1). \quad (21)$$

The applied voltage to the control device is defined by the dimensionless expression which is given by

$$U = \eta_T (U - Vc), \quad (22)$$

with

$$\varsigma_j = \frac{a_1 b_3}{b_1 + a_2 b_2}, \quad \eta_j = \frac{\Phi_j'(X_0)}{b_1 + a_2 b_2}, \quad \sigma_j = \frac{b_4}{b_1 + a_2 b_2},$$

in which

$$b_1 = \int_0^1 \Phi_j(X)^2 dX, \quad b_2 = \int_0^1 \Phi_j''(X) \Phi_j(X) dX, \quad b_3 = \int_0^1 \Phi_j''''(X) \Phi_j(X) dX, \quad b_4 = \int_0^1 \Phi_j(X) dX.$$

Equations 18- 22 describe the time evolution of the concrete core tube which is fixed at the point X_0 by the damped outriggers. It is useful to observe that the parameter of the Equation 18 varied at each vibration mode and that the force generated by MR device depends on the attachment point of the damped outriggers on core tube. All these results indicate that outrigger locations could modify the structural response at the different vibration mode and can provide a better understanding of the outrigger design.

2.3 | Semiactive controller

With a view to obtain the optimal input voltage corresponding to the desired damper force and to assess the performance of control system, the control algorithm as an effective mean used in semiactive control based on the Lyapunov stability theory^[9] is employed. Because the control device is not directly controllable and that only applied voltage can be adjusted. Also the mentioned control algorithm is developed for characterizing adequately the damper's intrinsic nonlinear behaviour.^[18] Thus, the Lyapunov function denoted $L_v(\mathbf{W})$ must be a positive function of the state of the system, \mathbf{W} . According to the Lyapunov stability theory, if the rate of change of lyapunov function, $\dot{L}_v(\mathbf{W})$, is negative semidefinite, the origin is stable.

Lyapunov function is chosen of the form

$$L_y = \frac{1}{2} \|\mathbf{W}\|_p^2, \quad (23)$$

where $\|\Sigma\|_p$ = p -norm of the states defined by

$$\|\Sigma\|_p = [\Sigma' \mathbf{P}_L \Sigma]^{1/2}, \quad (24)$$

where \mathbf{P}_L is real, symmetric, positive definite matrix. \mathbf{P}_L is found using Lyapunov equation.

$$\Sigma' \mathbf{P}_L + \mathbf{P}_L \Sigma = -\mathbf{Q}_p \quad (25)$$

\mathbf{Q}_p is a positive definite matrix. The derivative of the Lyapunov function for a solution of the state-space equation is

$$\dot{L}_y = -\frac{1}{2} \mathbf{W}' \mathbf{Q}_p \mathbf{W} + \mathbf{W}' \mathbf{P}_L \mathbf{B}_1 F_d + \mathbf{W}' \mathbf{P}_L \mathbf{B}_2 \ddot{y}_g, \quad (26)$$

The above parameters are defined as follows:

$$\mathbf{W} = \begin{bmatrix} \dot{x}_j \\ \dot{x}_j \end{bmatrix}, \Sigma = \begin{bmatrix} 0 & 1 \\ -\zeta_j & -\zeta_j \end{bmatrix}, \mathbf{B} = \begin{bmatrix} 0 \\ -\sigma_j \end{bmatrix}, \mathbf{B}_1 = \begin{bmatrix} 0 \\ -\zeta_a \eta_j \end{bmatrix}.$$

The control law which will minimize \dot{L}_y

$$V_c = V_{max} H(-\mathbf{W}' \mathbf{P}_L \mathbf{B}_1 F_d), \quad (27)$$

where V_{max} is the maximum voltage and $H(\cdot)$ is Heaviside step function. When this function is greater than zero, the voltage (V_c) applied to the damper should be maximum (V_{max}), otherwise, the command voltage is set to zero.

3 | RESULTS AND DISCUSSIONS

To investigate efficiency of the simplified model, the concrete core is assumed to be $12m \times 12m$ with a $0.5m$ thickness, and with the height of $210m$.^[5] The mass per unit length is $m_1 = 62500K_g/m$. The eigenvalues are obtained from Equation 17 through the Newton-Raphson numerical. These results obtained through this method are illustrated in Table 1.

The listed parameter values in Table 2 when MF= 1.0 are those obtained from the analysis of experimental data and theoretical results by Jung et al.^[21] As it is difficult to have an MR damper with the obtained parameters experimentally that will lead to the optimal minimization of excessive vibration of mechanical structures. To avoid this drawback, it is observed from this Table 2 that some parameters depend on MF, named, the modification factor that allows of multiplying the damping; stiffness and hysteretic constants of the model magnify the damper force. In this regard, the objective here is to modify the properties of the damper, in view of having the parameter values for a large scale MR damper, enable to control the mechanical structure.^[22]

TABLE 1 Parameters of the structural system

Parameter	First	Second	Third
δ_1^j	1.873	4.649	7.752
ϵ_1^j	1.860	4.465	6.979
d_1^j	-0.743	-1.127	-1.283
d_3^j	-0.731	-1.023	-0.998
ζ_1^j	0.039	1.579	13.918

TABLE 2 Model parameters of the magnetorheological damper

Parameter	Value	Parameter	Value
δ_a	1107.2	n_1	2
$\gamma(m^{-2})$	164.0×10^4	$\eta_p(s^{-1})$	190
$\beta(m^{-2})$	164.0×10^4	$k_1(N/m)$	9.7 MF
$k_0(N/m)$	2 MF	$Y_0(m)$	0.0
$\alpha_a(N/m)$	46.2×10^3 MF	$\alpha_b(N/mV)$	41.2×10^3 MF
$c_{0a}(Ns/m)$	11×10^4 MF	$c_{0b}(Ns/mV)$	114.3×10^3 MF
$c_{1a}(Ns/m)$	8359.2×10^3 MF	$c_{1b}(Ns/mV)$	7482.9×10^3 MF

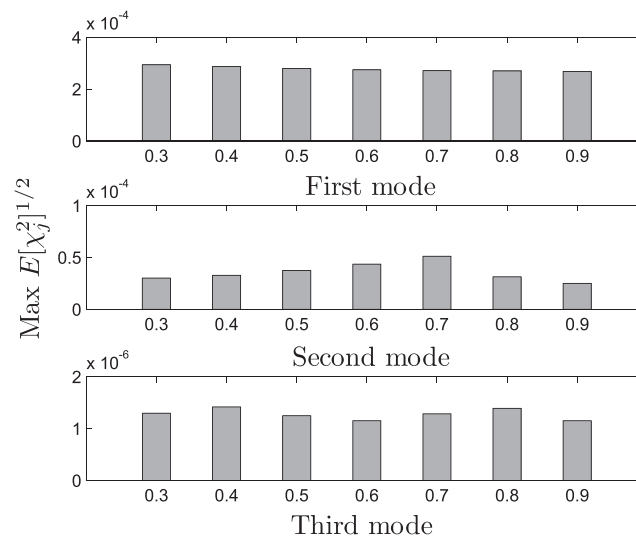


FIGURE 3 Optimal position of damped outriggers, $\zeta_a = 0.762$ and $MF=1.0$

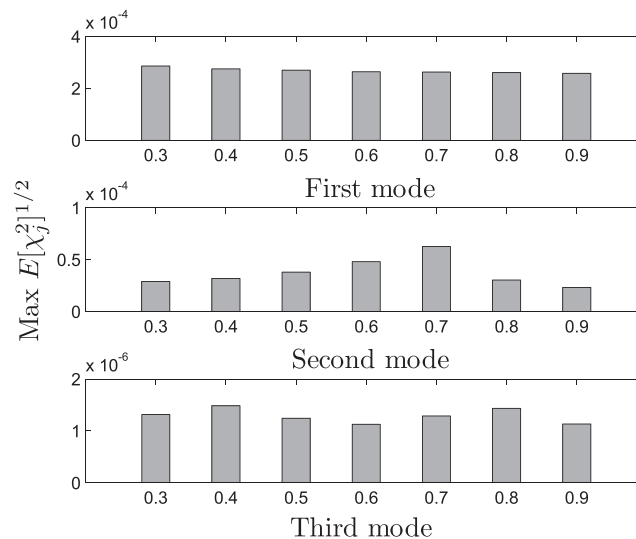


FIGURE 4 Optimal position of damped outriggers, $\zeta_a = 0.095$ and $MF=1.0$

To assess the optimal position of outriggers on the core tube, the passive-on strategy of the controller is employed. Thus, Figures 3 and 4 display the peak RMS versus locations of outriggers on the structure.

Figure 3 presents at the first mode, a slight variation between the amplitude at the different position of outriggers on the core tube. For that, one can realize that the positions 0.7, 0.8, and 0.9 at this quoted mode are the location points of damped outriggers where the displacement of the structural system is reduced slightly in relation to other positions. The second mode exhibits only one best position of outriggers on the core tube which is 0.9. It is well-seen that at this point the vibration amplitude is reduced dramatically. As regards the third mode, the optimal positions are 0.6 and 0.9. In these points, the peak amplitude of the structure are reduced than other positions. The global analysis of different observations from Figure 3 leads us to mention that the optimal attachment point of outriggers benefits for the three vibration modes is 0.9.

The same observation from Figure 3 is illustrated in Figure 4, that is to say that the point 0.9 stays only the best position of outriggers on the frame core tube. Analysing these figures, as can be seen, the point 0.9 is better attachment point of damped outriggers on the frame-core tube favourable for the three first vibration mode. Moreover, the variation of the length of each outrigger does not affect the value of its optimal attachment point on the beam.

As mentioned before, it is difficult to have the best parameters from experimental results of the MR damper, which incorporated into the structure leading to efficient control. For that, Figure 5 displays the peak RMS versus the scale coefficient MF at the first three vibration modes. It is observed from this figure that the increasing of this quoted coefficient affects the performance of damped outrigger in reducing the seismic response of the structure. It is important to note that the choice of MF is done such as the control device cannot increase the mechanical energy in the structural system. In other words, the control device should reinforce the stability of the structure in order to avoid their premature destruction.

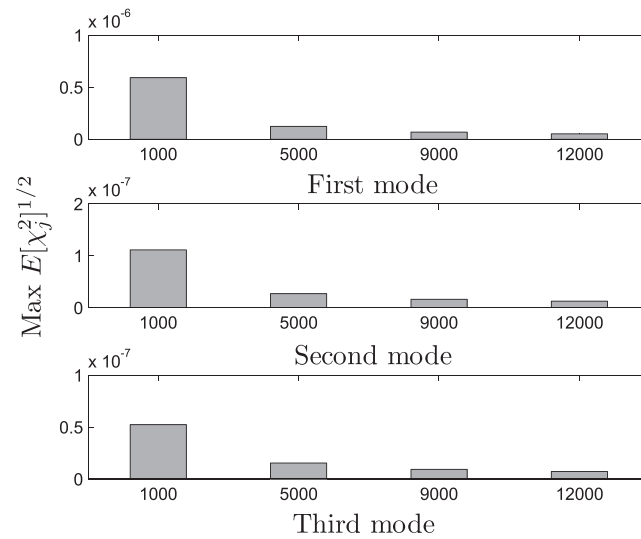


FIGURE 5 Optimal scale coefficient MF

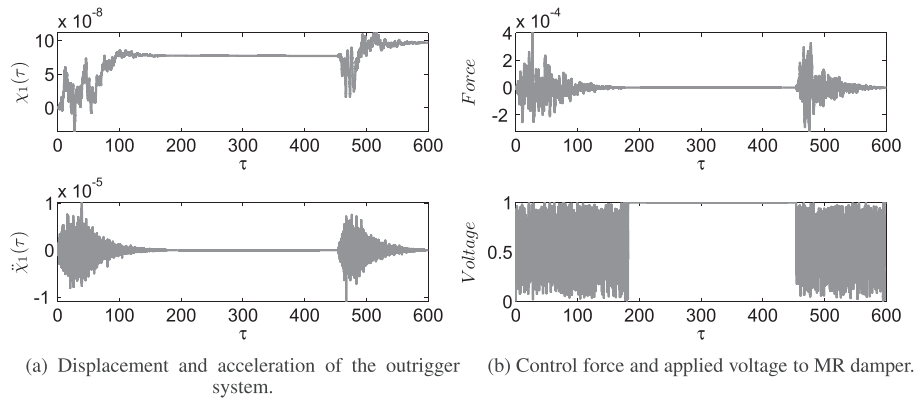


FIGURE 6 Time histories at the first vibration mode

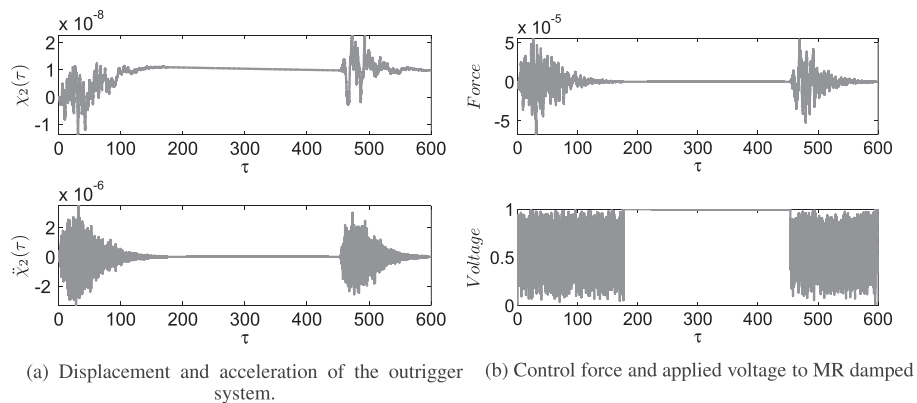


FIGURE 7 Time histories at the second vibration mode

By taking into account of optimal position of damped outriggers and scale coefficient, one displays in Figures 6, 7, and 8, the time histories of traversal displacement, acceleration, control force, and applied voltage to MR damper at the first, second, and third vibration modes for MF= 9,000. The structural response of the outrigger system at the three first vibration modes is shows in Figures 6(a), 7(a) and 8(a). One can see the structural response show two sequences of the vibration.

The command signal V_c is selected through the control algorithm based on Lyapunov stability illustrated in Equation 27. The numerical result of this adopted strategy allows of having Figures 6b, 7b, and 8b at the first, second, and third vibration modes. The observed separating time interval between $\tau = 170$ and $\tau = 460$ indicates that the controller is in passive-off mode. Since in this relaxation time, the structure did not receive the

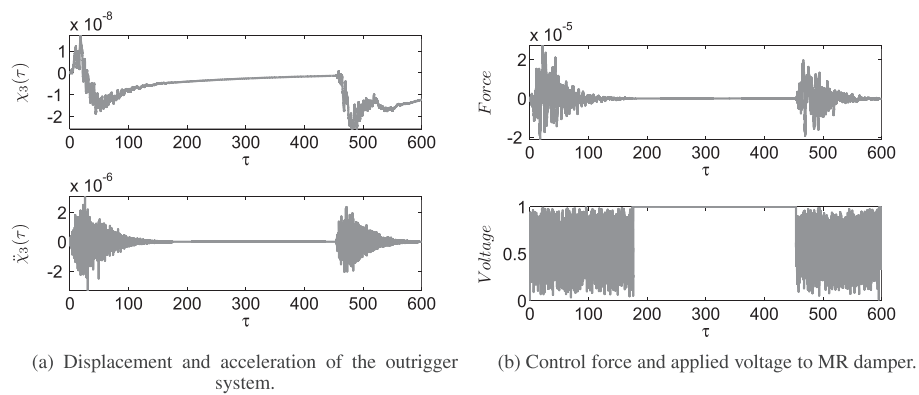


FIGURE 8 Time histories at the third vibration mode

input produced by earthquake, as a result, the system cease to exhibit the vibration. All the same, this explains the dynamic behaviour of the control device because this is depended on the structural response.

4 | CONCLUSION

In this present paper, the dynamic response of the outrigger system under the two sequences of the nonstationary stochastic ground motion has been investigated. The adopted outrigger system is constituted of a core-tube and outriggers employing the MR dampers, which are inserted vertically. Timoshenko beam theory, which takes into account the combination of shear type deformation and rotary inertia effects, has been considered to model the dynamic behaviours of the outrigger system. The statistical analysis through the peak root mean square displacement of the structural system has been employed, to evaluate the influence of optimal attachment points of outriggers on the core tube. The obtained results show that the analytical investigation of other modes is really necessary to seek the optimal position of outriggers. By taking into account of this strategy, it is observed all position of outriggers can not lead to optimal minimization of the seismic vibration of the structural system. On top of that, the best scale coefficient MF of the parameter of the MR device leading to the maximum force by maintaining the efficient control has been determined. Lyapunov stability theory based on semiactive control has been used to select the suitable voltage that operate MR damper. The repeated sequence of the input voltage response reveals that this strategy has been adequated for the control devices.

ACKNOWLEDGEMENTS

BP Ndeமானou. He is grateful to ICTP for invitation and for financial support. Part of this work was completed during a research visit of Pr Nana Nbenjo at the University of Kassel in Germany. He is grateful to the Alexander von Humboldt Foundation for financial support within the Georg Forster Fellowship.

REFERENCES

- [1] M. E. Sandoval, L. B. Ugarte, B. F. Spencer, in Proceeding of the 15th WCEE, Lisbon, Portugal **2012**, 1–10.
- [2] R. J. Smith, M. R. Willford. *The Struct. Design Tall Spec. Build.* **2007**, *16*, 501–517.
- [3] P. Tan, C. J. Fang, W. R. Tu, F. L. Zhou, Y. Wang, M. Jiang, in Proceeding of the 15th WCEE, Lisbon, Portugal **2012**, 1–7.
- [4] T. Asai, C. M. Chang, B. M. Phillips, B. F. Spencer. *Eng. Struct.* **2013**, *57*, 177–188.
- [5] C. M. Chang, Z. Wang, B. F. Spencer, Z. Chen. *Smart Struct. Syst.* **2013**, *11*, 435–451.
- [6] H. S. Park, S. Lee, S. W. Choi, B. Kwan oh, T. Cho, Y. Kim. *Eng. Struct.* **2016**, *117*, 496–505.
- [7] C. M. Chang, T. Asai, Z. Wang, B. F. Spencer, Z. Chen, in Proceedings of the 15th WCEE, Lisbon, Portugal **2012**, 1–10.
- [8] Z. Wanga, C. M. Chia-Ming Chang, B. F. Spencer, Z. Chen. *Proc. SPIE* **2010**, 7647[[SPI-AQ6]].
- [9] M. Laura, S. J. Dyke. *J. Eng. Mech.* **2000**, *126*, 795–803.
- [10] Y. Chen, D. M. McFarland, Wang Z., B. F. Spencer, L. A. Bergman. *J. Struct. Eng.* **2010**, *136*, 1435–1443.
- [11] K. Deng, P. Pan, A. Lam, Y. Xue, in *The Structural Design of tall and Special Buildings* **2013**, 1158–1170.
- [12] T. Ping, F. Chuangjie, Z. Fulin. *Earthquake Eng. Eng. Vibr.* **2014**, *13*, 293–304.
- [13] J. Lee, M. Bang, J. Y. Kim. *The Struct. Design Tall Spec. Build.* **2008**, *17*, 839–851.
- [14] S. P. Timoshenko. *Philos. Mag.* **1921**, *41*, 744–746.
- [15] Cowper. *J. Appl. Mech.* **1966**, *33*, 335–340.
- [16] A. F. Mosaad. *Comput. Struct.* **1999**, *71*, 663–670.
- [17] M. Abbas, I. Takewakib. *Eng. Struct.* **2011**, *33*, 1251–1258.

- [18] B. F. Spencer, S. J. Dyke, M. K. Sain, J. D. Carlson. *J. Eng. Mech.* **1997**, 123, 230–238.
- [19] J. Xie, Z. Wen, in *Proceeding of the 14th WCEE*, Beijing **2008**, 1–13.
- [20] B. P. Ndeமானou, J. Metsebo, B. R. Nana Nbandjo, P. Woafo. *Nonlinear Dyn.* **2014**, 78, 163–171.
- [21] H. J. Jung, B. F. Spencer, I. W. Lee. *J. Struct. Eng.* **2003**, 129, 873–883.
- [22] B. Erkus, M. Abe, Y. Fujino. *Eng. Struct.* **2002**, 24, 281–291.

Buris Peggy Ndeமானou obtained his MS degree in 2012 at University of Yaoundé I, Cameroon. He got his bachelor degree in 2010 at University of Yaoundé I. Currently, he is a Ph.D. candidate at University of Yaoundé I and his research interests include modelling and simulation of non-linear mechanical systems, adaptive control.


Eliane Raïssa Fankem got her MS degree at University of Yaoundé I, Cameroon. She got his bachelor degree at University of Douala, Cameroon. Currently, she is a Ph.D. candidate at University of Yaoundé I and her research interests include structural health monitoring using dynamic's evaluation particularly on cantilever beam.

Blaise Romeo Nana Nbandjo Received is PhD in Nonlinear Mechanics in 2004 at University of Yaoundé I, Cameroon. He is currently an Associate Professor at the same University. His research interests include Nonlinear Dynamics and control.

How to cite this article: Ndeமானou BP, Fankem ER, Nana Nbandjo BR. Reduction of vibration on a cantilever Timoshenko beam subjected to repeated sequence of excitation with magnetorheological outriggers. *Struct Design Tall Spec Build.* 2017:e1393. <https://doi.org/10.1002/tal.1393>

An inverted pendulum with multibranching view as self-controlled system: Modelling and vibration absorber capacity

Eliane Raïssa Fankem¹, Blaise Romeo Nana Nbandjo^{1,2} , Paul Wofo¹ and Uwe Dorka²

Journal of Vibration and Control
2020, Vol. 0(0) 1–11
© The Author(s) 2020
Article reuse guidelines:
sagepub.com/journals-permissions
DOI: 10.1177/1077546320908141
journals.sagepub.com/home/jvc


Abstract

The design and performance evaluation of a self-controlled system are investigated. An autonomous set of pendulums with different branches is considered. A mathematical model is derived, and the damping mechanism due to the transfer of energy between the central column and its attached branches is pointed out. The case of earthquake loads has been tested. Dynamics study shows that the energy received by the central column is distributed to the different branches, leading to a self-vibration control of the system. It is also found that one can increase the damping ratio according to the physical characteristics of the structure. This is a good candidate for earthquake protection of mechanical structures.

Keywords

Pendulums, trees vibration, bioinspiration, earthquake excitation, vibration control

1. Introduction

After they have been built, tall and slender structures require permanent monitoring of the deformations that take place with the time. The causes of the deformations include external factors such as strong winds, earthquakes, and floods, accompanied by the natural process of ageing (Kujawski and Tang, 2009; Metsebo et al., 2016; Oumarou et al., 2011). Two main consequences of the monitoring are the reparation of the damages suffered by the material structures and the utilization of control methods (Anh et al., 2016), some of which require external devices (Avossa et al., 2018) and energy (Djanan et al., 2015; Kim and Kang, 2017; Kitio Kwuimy et al., 2006; Ndemanou et al., 2016, 2017). Since many years, numbers of structural concepts (Dorka, 2004) that allow rigid body control has been identified, and four concepts (base isolation, hysteretic device system, tendon system, and pagoda system) have been suggested for seismic control (Dorka, 2014; Nana Nbandjo and Dorka, 2016). Our aim was to construct a structure design that incorporates a set of pendulums (a central rigid column with branches at different levels) and to bring out their proficiencies to resist earthquakes and strong winds.

The pagoda system, inspired by high seismic performance of old-built pagoda structures, is one of the most powerful design structures which reacts positively when they face earthquake (Bock et al., 2011; Hanazato et al.,

2012; Ueda et al., 1996; Wu et al., 2018). Fujita et al. (2004) discussed on the seismic performance of traditional timber five-story pagoda based on the results of microtremor measurement, free vibration test, and earthquake response monitoring. The experiment was subjected to a newly built five-story timber pagoda in Japan. They found that the natural frequency of vibration was approximately 1.5 Hz and the damping factor 5%, the results of which are consistent with those of the preceding experimental research studies. With the same idea, earthquake and strong wind responses of Hokekyou-ji five-story wood pagoda were monitored and recorded. The observations were that the deformation is nearly 4 cm under strong wind of about 25 m/s, and by supposing the strong wind about 60 m/s, the deformation of nearly 20 cm would be brought. Hokekyou-ji five-story pagoda has good damping of 5%–10%

¹Laboratory of Modelling and Simulation in Engineering, Biomimetics and Prototypes, Faculty of Science, University of Yaoundé I, Cameroon

²Steel and Composite Structures, University of Kassel, Germany

Received: 17 September 2019; accepted: 8 January 2020

Corresponding author:

Blaise Romeo Nana Nbandjo, Laboratory of Modelling and Simulation in Engineering, Biomimetics and Prototypes, Faculty of Science, University of Yaoundé I, P.O. Box 812, Yaoundé, Cameroon.
Email: nananbandjo@yahoo.com

(Minowa et al., 2010). And after many analyses, some assumptions were proposed to explain that resistance (Nakahara et al., 2000); it was indicated that the good resistance is due to the combined actions of different mechanisms: base isolation, slip joint, friction damper, snake dance, Shinbashira, and tuned mass damper, which makes that structures so resistant to earthquakes. Omori (1921) proposed that the compound pendulum system, the center column and the main structure, gives a tuned mass damper effect after investigations on pagodas in Senso-ji temple and Nikko-ji temple. And the friction damping effect of the wooden joints (pieces of wood are assembled using tenons and mortises) was an important factor in making them earthquake resistant (Muto, 1949). According to the analyses conducted by Tanabashi (1960), the factors increasing the resistance of the structure were the scale effect of the five-story structure, a characteristic of the flexible structure and the wood joint capacity for allowing plastic deformations through slipping or gaps in them. Some years after, it was proposed that the center column acts as a bolt fastening the whole structure and adding a restraint effect of shearing deformations among individual stories (Ishida, 1993). Ueda et al. (1996) considered that each structurally independent stories mounted on top of the other was able to allow each one to act like a balancing toy, cancelling the inertia force of each story out among them.

Because more investigations and theoretical analyses are still required to clarify the five-story pagoda behavior (Minowa et al., 2010), an attention was carried out on the slip joint and Shinbashira from the pagoda system, and on the damping mechanism by branching studied by Theckes et al. (2011) where they found that significant levels of damping achieved via branching with typically 30% of

the energy being dissipated in one oscillation for two bio-inspired architectures. From the combination of that previous devices, one propose in this work a model of structure that has good abilities.

The article is organized as follows. After the Introduction, the physical model of the system which takes into account the balancing toy and central column is illustrated in Section 2. There, the system of equations of motion of each part of the system is also obtained. Section 3 is devoted to the behavior of the structure when it is moved from its equilibrium point (Section 3.1) and when an earthquake appears on it (Section 3.2); and the influence of branches is pointed out. In Section 4, the results of the study of the energy dissipation in the system are presented and described. The self-controlled behavior of the system is denoted here, and the effect of length and masses on the damping ratio is investigated. Concluding remarks end this work in Section 5.

2. General mathematical formalism of an inverted pendulum with multibranching

The model shown in Figure 1 consists of an inverted pendulum of finite length $l_{n_{\max}}$ (n_{\max} is the maximum value of n according to the structure configuration: from one level up to five levels) and mass M as a rigid rod is connected to the soil by a spring K_1 and dashpot (viscous damper) C_1 according to the reaction of the soil related to its mechanical properties, with massless rigid bars linked on that central column. Those masses are attached at different length l_n of the central column, with $n = 1, 3, \dots, 9$. Each level is two symmetrical bars of length l_i with $i = 2, 4, \dots, 10$, forming an angle ϕ_0 with imaginary horizontal line. These bars are linked to the central column by a rotational spring K_j and

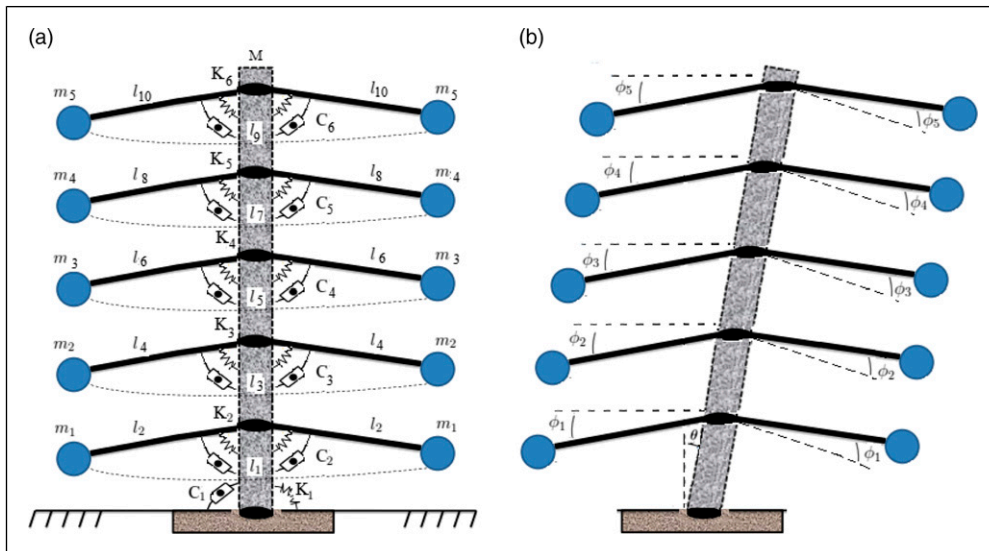


Figure 1. (a) Physical model of the pendulum with multibranching at rest and (b) disturbed system.

viscous damper C_j with $j = 2, 3, \dots, 6$ and support masses m_k with $k = 1, \dots, 5$, the indicator of the level. The motion of the rod is defined by the angle θ , and we consider only the symmetrical motion of the levels defined by the angle ϕ_k with $k = 1, \dots, 5$. The inclination of the main rod must be less than the critical amplitude, if not the structure will break.

To deal with this system of a central column and five levels attached branches, it is divided into six subsystems of one degree of freedom each. Kinetic and potential energies of the whole system give the system (1) of equations of motion which is derived using Lagrangian formalism.

with g the acceleration of terrestrial gravity.

Because the equations of motion of the central column and each branch are coupled by nonlinear terms, energy can be exchanged between them (Theckes et al., 2011). As one can see, the movement of branches is independent of each other but is induced by the motion of the main rod. Therefore, the dissipation in the branches may damp the energy received from the central column, resulting in an effective damping of the whole structure.

3. Effects of branches on the damping of the central column vibration

3.1. Free vibration case

The central column is moved from its equilibrium point ($\theta = 0$) with an initial value of 1.57 rad for θ_0 and 1.047 rad for ϕ_{i_0} for branches. And for the vibration test and behavior observation, the amplitude of vibration of the central column is plotted for five different cases: one, two, three, four, and five levels of branches at different positions.

Figure 2(a) shows that the angular displacement of the central column is surely a damped oscillated motion around its equilibrium position which is here 0, while Figure 2(b) exhibits in addition to vibration an appearance of one pack of peaks of bursting oscillation which consequently reduces with a high effect the amplitude of vibration of the central column. It is well observed around the dimensionless time of [1250, 1500]. As main results here, it is important to mention that as the central column gives its motion to attached branches, this denotes to the energy exchange between the two subsystems (Theckes et al., 2011).

$$\left\{ \begin{aligned}
 & A(\phi_k)\ddot{\theta} + B(\dot{\phi}_k, \phi_k)\dot{\theta} + D(\phi_k)\dot{\theta}^2 + K_1\theta + gE \sin \theta + C_2 \left(\frac{l_1}{l_2} \cos \phi_0 \sin \phi_1 - 1 \right) \dot{\phi}_1 + C_3 \left(\frac{l_3}{l_4} \cos \phi_0 \sin \phi_2 - 1 \right) \dot{\phi}_2 \\
 & + C_4 \left(\frac{l_5}{l_6} \cos \phi_0 \sin \phi_3 - 1 \right) \dot{\phi}_3 + C_5 \left(\frac{l_7}{l_8} \cos \phi_0 \sin \phi_4 - 1 \right) \dot{\phi}_4 + C_6 \left(\frac{l_9}{l_{10}} \cos \phi_0 \sin \phi_5 - 1 \right) \dot{\phi}_5 \\
 & + 2K_2 \left(\frac{l_1}{l_2} \cos \phi_0 \sin \phi_1 - 1 \right) \phi_1 + 2K_3 \left(\frac{l_3}{l_4} \cos \phi_0 \sin \phi_2 - 1 \right) \phi_2 + 2K_4 \left(\frac{l_5}{l_6} \cos \phi_0 \sin \phi_3 - 1 \right) \phi_3 \\
 & + 2K_5 \left(\frac{l_7}{l_8} \cos \phi_0 \sin \phi_4 - 1 \right) \phi_4 + 2K_6 \left(\frac{l_9}{l_{10}} \cos \phi_0 \sin \phi_5 - 1 \right) \phi_5 \\
 & - 2m_1 l_1 l_2 \dot{\phi}_1^2 \cos \phi_0 \cos \phi_1 - 2m_2 l_3 l_4 \dot{\phi}_2^2 \cos \phi_0 \cos \phi_2 - 2m_3 l_5 l_6 \dot{\phi}_3^2 \cos \phi_0 \cos \phi_3 - 2m_4 l_7 l_8 \dot{\phi}_4^2 \cos \phi_0 \cos \phi_4 \\
 & - 2m_5 l_9 l_{10} \dot{\phi}_5^2 \cos \phi_0 \cos \phi_5 - m_1 l_1 g \sin 2\phi_0 \sin \phi_1 \sin(\theta + \phi_1) - m_2 l_3 g \sin 2\phi_0 \sin \phi_2 \sin(\theta + \phi_2) \\
 & - m_3 l_5 g \sin 2\phi_0 \sin \phi_3 \sin(\theta + \phi_3) - m_4 l_7 g \sin 2\phi_0 \sin \phi_4 \sin(\theta + \phi_4) - m_5 l_9 g \sin 2\phi_0 \sin \phi_5 \sin(\theta + \phi_5) = 0 \\
 & 2m_1 l_2^2 \ddot{\phi}_1 + C_2 \dot{\phi}_1 + 2K_2 \phi_1 - \left(\frac{2m_1 g l_2}{\sin \phi_0} \right) \sin(\theta + \phi_1) + \left(\frac{2m_1 l_1 l_2}{\dot{\theta}^2 \cos \phi_0} \right) \cos \phi_1 = (2m_1 l_1 l_2 \cos \phi_0 \sin \phi_1 - 2m_1 l_2^2) \ddot{\theta} \\
 & 2m_2 l_4^2 \ddot{\phi}_2 + C_3 \dot{\phi}_2 + 2K_3 \phi_2 - \left(\frac{2m_2 g l_4}{\sin \phi_0} \right) \sin(\theta + \phi_2) + \left(\frac{2m_2 l_3 l_4}{\dot{\theta}^2 \cos \phi_0} \right) \cos \phi_2 = (2m_2 l_3 l_4 \cos \phi_0 \sin \phi_2 - 2m_2 l_4^2) \ddot{\theta} \\
 & 2m_3 l_6^2 \ddot{\phi}_3 + C_4 \dot{\phi}_3 + 2K_4 \phi_3 - \left(\frac{2m_3 g l_6}{\sin \phi_0} \right) \sin(\theta + \phi_3) + \left(\frac{2m_3 l_5 l_6}{\dot{\theta}^2 \cos \phi_0} \right) \cos \phi_3 = (2m_3 l_5 l_6 \cos \phi_0 \sin \phi_3 - 2m_3 l_6^2) \ddot{\theta} \\
 & 2m_4 l_8^2 \ddot{\phi}_4 + C_5 \dot{\phi}_4 + 2K_5 \phi_4 - \left(\frac{2m_4 g l_8}{\sin \phi_0} \right) \sin(\theta + \phi_4) + \left(\frac{2m_4 l_7 l_8}{\dot{\theta}^2 \cos \phi_0} \right) \cos \phi_4 = (2m_4 l_7 l_8 \cos \phi_0 \sin \phi_4 - 2m_4 l_8^2) \ddot{\theta} \\
 & 2m_5 l_{10}^2 \ddot{\phi}_5 + C_6 \dot{\phi}_5 + 2K_6 \phi_5 - \left(\frac{2m_5 g l_{10}}{\sin \phi_0} \right) \sin(\theta + \phi_5) + \left(\frac{2m_5 l_9 l_{10}}{\dot{\theta}^2 \cos \phi_0} \right) \cos \phi_5 = (2m_5 l_9 l_{10} \cos \phi_0 \sin \phi_5 - 2m_5 l_{10}^2) \ddot{\theta}
 \end{aligned} \right. \quad (1)$$

with

$$\begin{aligned}
 A(\phi_k) &= \frac{1}{4}Ml_9^2 + 2m_1l_1^2 + 2m_2l_3^2 + 2m_3l_5^2 + 2m_4l_7^2 + 2m_5l_9^2 - 2m_1l_1^2 \cos^2 \phi_0 \sin^2 \phi_1 - 2m_2l_3^2 \cos^2 \phi_0 \sin^2 \phi_2 \\
 &\quad - 2m_3l_5^2 \cos^2 \phi_0 \sin^2 \phi_3 - 2m_4l_7^2 \cos^2 \phi_0 \sin^2 \phi_4 - 2m_5l_9^2 \cos^2 \phi_0 \sin^2 \phi_5 \\
 B(\dot{\phi}_k, \phi_k) &= C_1 - 4m_1l_1l_2\dot{\phi}_1 \cos \phi_0 \cos \phi_1 - 4m_2l_3l_4\dot{\phi}_2 \cos \phi_0 \cos \phi_2 - 4m_3l_5l_6\dot{\phi}_3 \cos \phi_0 \cos \phi_3 \\
 &\quad - 4m_4l_7l_8\dot{\phi}_4 \cos \phi_0 \cos \phi_4 - 4m_5l_9l_{10}\dot{\phi}_5 \cos \phi_0 \cos \phi_5 \\
 D(\phi_k) &= 2m_1l_1^2 \cos^2 \phi_0 \cos \phi_1 \sin \phi_1 + 2m_2l_3^2 \cos^2 \phi_0 \cos \phi_2 \sin \phi_2 + 2m_3l_5^2 \cos^2 \phi_0 \cos \phi_3 \sin \phi_3 + 2m_4l_7^2 \cos^2 \phi_0 \cos \phi_4 \sin \phi_4 \\
 &\quad + 2m_5l_9^2 \cos^2 \phi_0 \cos \phi_5 \sin \phi_5 - 2m_1l_1l_2 \cos \phi_0 \cos \phi_1 - 2m_2l_3l_4 \cos \phi_0 \cos \phi_2 - 2m_3l_5l_6 \cos \phi_0 \cos \phi_3 \\
 &\quad - 2m_4l_7l_8 \cos \phi_0 \cos \phi_4 - 2m_5l_9l_{10} \cos \phi_0 \cos \phi_5 \\
 E &= 2m_1l_1 + 2m_2l_3 + 2m_3l_5 + 2m_4l_7 + 2m_5l_9 - \frac{1}{2}Ml_9
 \end{aligned}$$

In [Figure 3](#), the effect of the number of attached branches is pointed out by a gradual reduction in the amplitude of vibration of the central column which is plotted here. [Figure 3\(a\)](#) is the comparison between one attached level branches and two, [Figure 3\(b\)](#) between two and three, [Figure 3\(c\)](#) three and four, and finally [Figure 3\(d\)](#) four and five levels of attached branches. The observation is not debatable; the more the branches are added, the amplitude of the central rod is reduced, and one can see a reduction of up to 50% during the time going of the simulation.

3.2. Under earthquake excitation

In this section, an external force (here, the earthquake) appears on the base of the central rod. That earthquake loads are numerically generated according to the Kanai–Tajimi model ([Lin et al., 1987](#)): a nonstationary ground acceleration with a random function which takes the form of a filtered Gaussian stationary white noise modulated by a deterministic envelope function. The physical and geometrical properties of the central column are those of

a wooden structure ([Nana Nbenjjo, 2004](#)). And we aimed to determine whether the previous results are the same.

The ground acceleration \ddot{u}_g is assumed to be represented by

$$\ddot{u}_g = e_0(e^{-\beta_1 t} - e^{-\beta_2 t})\ddot{w}(t) \quad (2)$$

with the spectral density given by

$$S_{\ddot{w}}(\omega) = S_0 \frac{\omega_g^4 + (2\zeta_g \omega_g \omega)^2}{(\omega_g^2 - \omega^2)^2 + (2\zeta_g \omega_g \omega)^2} \quad (3)$$

where S_0 is the intensity of the white noise process at the rock level, ω_g is the dominant frequency of the soil site, and ζ_g is the associated damping ratio of the soil strata.

The system submitted to the earthquake load is shown in [Figure 4](#).

[Figure 5](#) is the generated acceleration of the ground \ddot{u}_g .

From the system of equation (1), the central column is directly affected by the appearance of earthquake, as it is the only part of the structure which is attached to the soil. And its equation of motion become

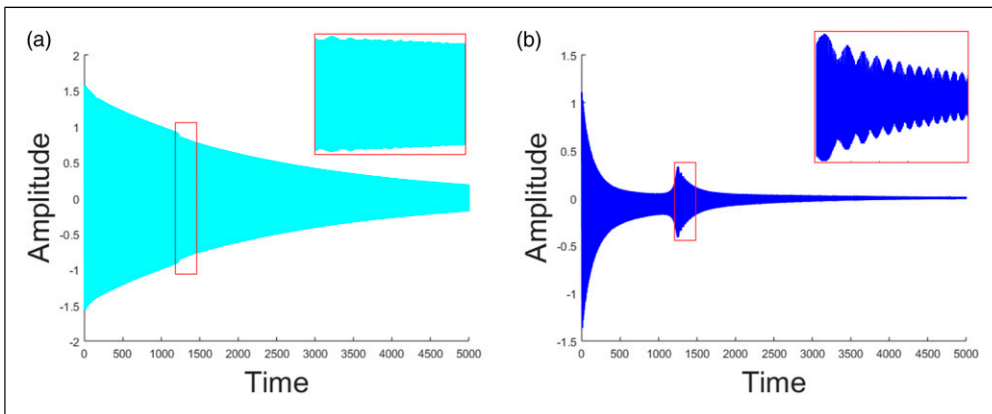


Figure 2. Angular displacement (a) θ for the central column and (b) ϕ_1 for the first level of branches.

$$\begin{aligned}
& A(\phi_k)(\ddot{\theta} + \ddot{u}_g) + B(\dot{\phi}_k, \phi_k)\dot{\theta} + D(\phi_k)\dot{\theta}^2 + K_1\theta + gE \sin \theta + C_2 \left(\frac{l_1}{l_2} \cos \phi_0 \sin \phi_1 - 1 \right) \dot{\phi}_1 + C_3 \left(\frac{l_3}{l_4} \cos \phi_0 \sin \phi_2 - 1 \right) \dot{\phi}_2 \\
& + C_4 \left(\frac{l_5}{l_6} \cos \phi_0 \sin \phi_3 - 1 \right) \dot{\phi}_3 + C_5 \left(\frac{l_7}{l_8} \cos \phi_0 \sin \phi_4 - 1 \right) \dot{\phi}_4 + C_6 \left(\frac{l_9}{l_{10}} \cos \phi_0 \sin \phi_5 - 1 \right) \dot{\phi}_5 \\
& + 2K_2 \left(\frac{l_1}{l_2} \cos \phi_0 \sin \phi_1 - 1 \right) \phi_1 + 2K_3 \left(\frac{l_3}{l_4} \cos \phi_0 \sin \phi_2 - 1 \right) \phi_2 + 2K_4 \left(\frac{l_5}{l_6} \cos \phi_0 \sin \phi_3 - 1 \right) \phi_3 \\
& + 2K_5 \left(\frac{l_7}{l_8} \cos \phi_0 \sin \phi_4 - 1 \right) \phi_4 + 2K_6 \left(\frac{l_9}{l_{10}} \cos \phi_0 \sin \phi_5 - 1 \right) \phi_5 - 2m_1 l_1 l_2 \dot{\phi}_1^2 \cos \phi_0 \cos \phi_1 - 2m_2 l_3 l_4 \dot{\phi}_2^2 \cos \phi_0 \cos \phi_2 \\
& - 2m_3 l_5 l_6 \dot{\phi}_3^2 \cos \phi_0 \cos \phi_3 - 2m_4 l_7 l_8 \dot{\phi}_4^2 \cos \phi_0 \cos \phi_4 - 2m_5 l_9 l_{10} \dot{\phi}_5^2 \cos \phi_0 \cos \phi_5 - m_1 l_1 g \sin 2\phi_0 \sin \phi_1 \sin(\theta + \phi_1) \\
& - m_2 l_3 g \sin 2\phi_0 \sin \phi_2 \sin(\theta + \phi_2) - m_3 l_5 g \sin 2\phi_0 \sin \phi_3 \sin(\theta + \phi_3) - m_4 l_7 g \sin 2\phi_0 \sin \phi_4 \sin(\theta + \phi_4) \\
& - m_5 l_9 g \sin 2\phi_0 \sin \phi_5 \sin(\theta + \phi_5) = 0
\end{aligned} \tag{4}$$

By adding earthquake, the central column exhibits a behavior which follows the earthquake displacement [Figure 6\(a\)](#), and by so doing, induced vibrations of each of branches as it appears in [Figure 6](#).

Each level of attached branches vibrates exactly as the central column [Figure 6\(b\)–\(f\)](#) for the five floors, and the amplitude of vibration is according to the intensity of earthquake that is transmitted to it through the rigid main rod. To point out the influence of branches on the vibration of the central column which is the main supported

branch of the system, the amplitude of vibration of the system is drawn, taking into account the number of attached branch levels, from one attached branch level up to five. The results are those of [Figure 7](#): For one floor, the attached masses are at the top of the main rigid rod, while for more than two floors which is more than two different positions of attached masses: one pair of masses is attached at the top of the central column and others are somewhere between the base and the top of that central column.

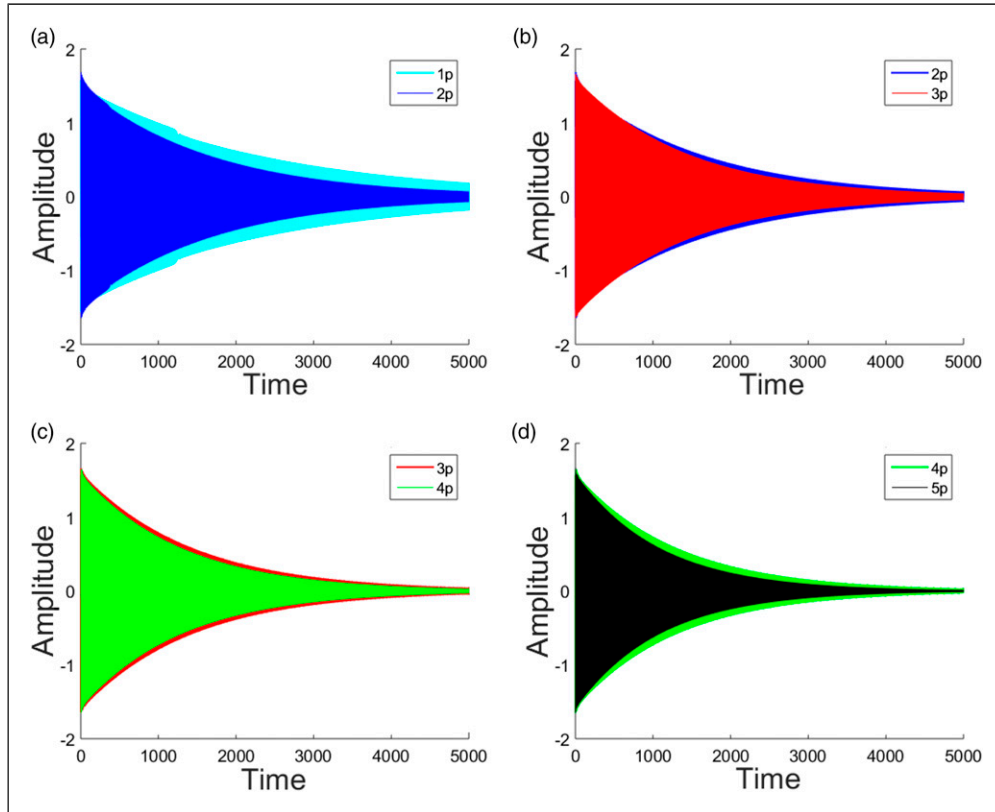


Figure 3. Angular displacement of the central column with (a) one–two, (b) two–three, (c) three–four, and (d) four–five levels of attached branches.

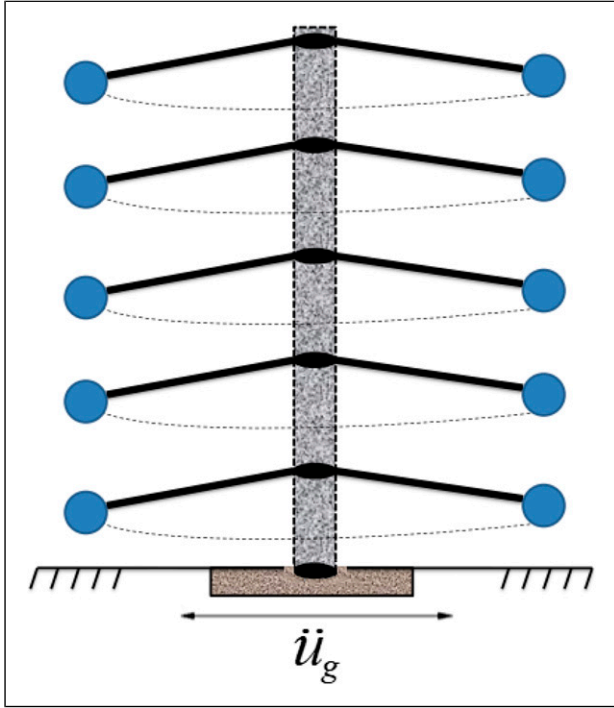


Figure 4. Model of a set of pendulums under earthquake loads.

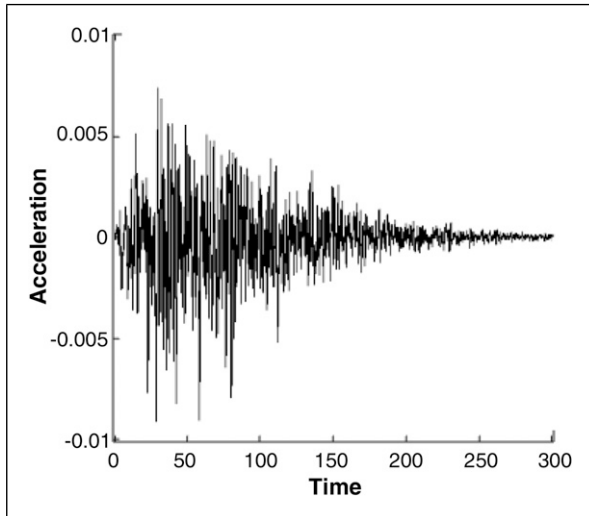


Figure 5. Dimensionless ground acceleration.

After the appearance of earthquake, one can notice that the vibration of each floor affects considerably the vibration of the central column, and it is by so doing that the system reduces the amplitude of vibration during the earthquake excitation.

A deep observation of Figures 6(a) and 7 does not show an appearance of bursting oscillation first because, as it was shown in Section 3.1, it cannot be visible for more than two levels of attached branches; second, the earthquake behaves particularly as a disorder, and by that, it is not possible to observe such kind of phenomenon. Furthermore, the results of Figure 7 come to confirm those of Figure 3,

and a report of a damping of up to 33% of vibration is highlighted. And by adding branches from one to five levels, one can obtain a total damping of around 50% and more compared with the amplitude of vibration when the structure is just a central column, with only one level of attached branches. To resume this part, one can say that up to five levels in an inverted pendulum with multibranching, the damping phenomenon increases with the number of added branches.

4. Energy transfer leading to damping effect of branches

Let us come back to the autonomous case. Many other considerations have been made as: $l_{n_{\max}} = l_9 = 5l_1$ because a five story is chosen. In addition to that, $l_3 = 2l_1$, $l_5 = 3l_1$, $l_7 = 4l_1$, $l_2 = l_4 = l_6 = l_8 = l_{10}$, $m_1 = m_2 = m_3 = m_4 = m_5$, $C_2 = C_3 = C_4 = C_5 = C_6$, $K_2 = K_3 = K_4 = K_5 = K_6$, so that the structure has at different levels the same mass values added.

With ϕ_k , $k = 1, \dots, 5$ for each floors up to five, and by taking as coefficients

$$\Gamma = \frac{2m_1 l_1^2 \cos^2 \phi_0}{J_\Delta}; \quad J_\Delta = \frac{25}{4} M l_1^2 + 110 m_1 l_1^2;$$

$$J_{\phi_1} = \sin^2 \phi_1; \quad J_{\phi_2} = 4 \sin^2 \phi_2; \quad J_{\phi_3} = 9 \sin^2 \phi_3;$$

$$J_{\phi_4} = 16 \sin^2 \phi_4; \quad J_{\phi_5} = 25 \sin^2 \phi_5;$$

$$\Omega_1^2 = \frac{K_1}{J_\Delta}; \quad \Omega_2^2 = \frac{K_2}{m_1 l_2^2}$$

$$\beta_1^2 = \frac{(30m_1 - (5/2)M)gl_1}{J_\Delta}; \quad \beta_2^2 = \frac{g}{l_2} \sin \phi_0;$$

$$K_{\phi_1} = \frac{m_1 gl_1 \sin(2\phi_0) \sin \phi_1}{J_\Delta}; \quad K_{\phi_2} = \frac{2m_1 gl_1 \sin(2\phi_0) \sin \phi_2}{J_\Delta};$$

$$K_{\phi_3} = \frac{3m_1 gl_1 \sin(2\phi_0) \sin \phi_3}{J_\Delta}; \quad K_{\phi_4} = \frac{4m_1 gl_1 \sin(2\phi_0) \sin \phi_4}{J_\Delta};$$

$$K_{\phi_5} = \frac{5m_1 gl_1 \sin(2\phi_0) \sin \phi_5}{J_\Delta}$$

The system of equation (1) leads to the new system of motion which is given by equation (6).

The total mechanical energy is given by

$$E_m = [1 - 2\Gamma(J_{\phi_1} + J_{\phi_2} + J_{\phi_3} + J_{\phi_4} + J_{\phi_5})]\dot{\theta}^2 + \Omega_1^2 \theta^2 - 2\beta_1^2 \cos \theta + 2K_{\phi_1} \cos(\theta + \phi_1) + 2K_{\phi_2} \cos(\theta + \phi_2) + 2K_{\phi_3} \cos(\theta + \phi_3) + 2K_{\phi_4} \cos(\theta + \phi_4) + 2K_{\phi_5} \cos(\theta + \phi_5) + \Gamma \left[\begin{aligned} & \dot{\phi}_1^2 + \dot{\phi}_2^2 + \dot{\phi}_3^2 + \dot{\phi}_4^2 + \dot{\phi}_5^2 \\ & + \Omega_2^2 (\phi_1^2 + \phi_2^2 + \phi_3^2 + \phi_4^2 + \phi_5^2) \\ & + 2\beta_2^2 \left[\begin{aligned} & \cos(\theta + \phi_1) + \cos(\theta + \phi_2) \\ & + \cos(\theta + \phi_3) + \cos(\theta + \phi_4) \\ & + \cos(\theta + \phi_5) \end{aligned} \right] \end{aligned} \right] \quad (5)$$

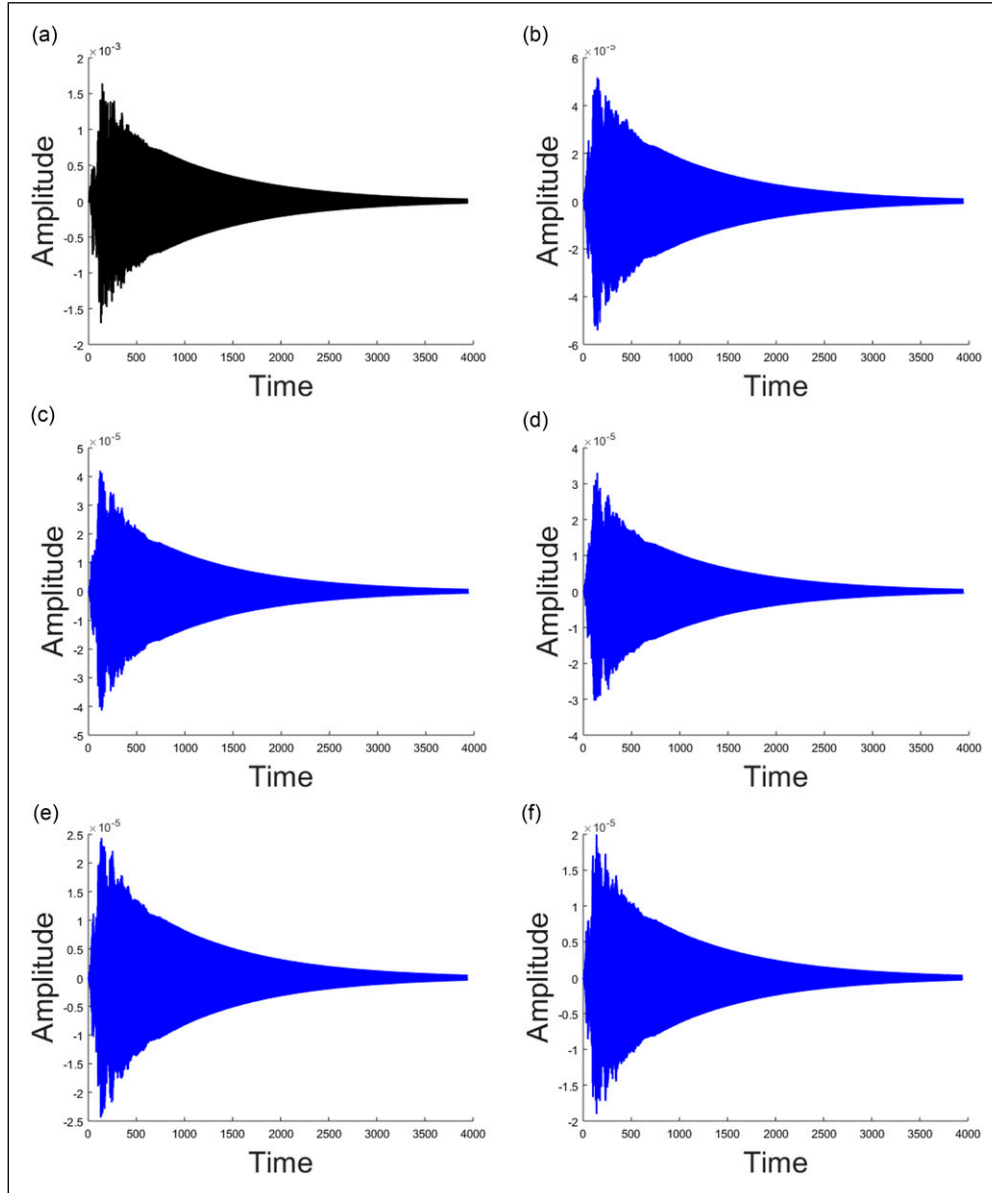


Figure 6. Angular displacement of (a) central column θ , (b) first floor ϕ_1 , (c) second floor ϕ_2 , (d) third floor ϕ_3 , (e) fourth floor ϕ_4 , and (f) fifth floor ϕ_5 .

In [Figure 8\(a\) and \(b\)](#), we display the energy of the whole system after a brief displacement (autonomous case), in function of time for one level of attached branches and two, to have an idea on the dissipation phenomenon inside the system. There is a good agreement with the previous observation because one can notice that the energy of the system rapidly reduces with the number of added branches. When the number of branches increases, one can observe that reduction in energy is more important ([Iyengar and Shinozuka, 1972](#); [Ndemanou et al., 2017](#)).

As an observation, we notice that the pack of peaks of bursting oscillation (black circle) that was pointed out

during the vibration test is too exposed by a pack of peaks of bursting oscillation too on energy time history. [Figure 8\(a\) and \(b\)](#) illustrate well the fact that in bursting oscillation, amplitude reduces and moves near the starting time of simulation until that phenomenon disappears when the number of attached branches increases.

To confirm the results of rapid dissipation due to branches, the comparison of the energy of the system in four cases was shown in [Figure 9](#). The initial energy of the system was normalized at 1 to have a good appreciation on the control of vibration involved in the system. Gradually, from [Figure 9\(a\) to \(d\)](#), the comparison between one and

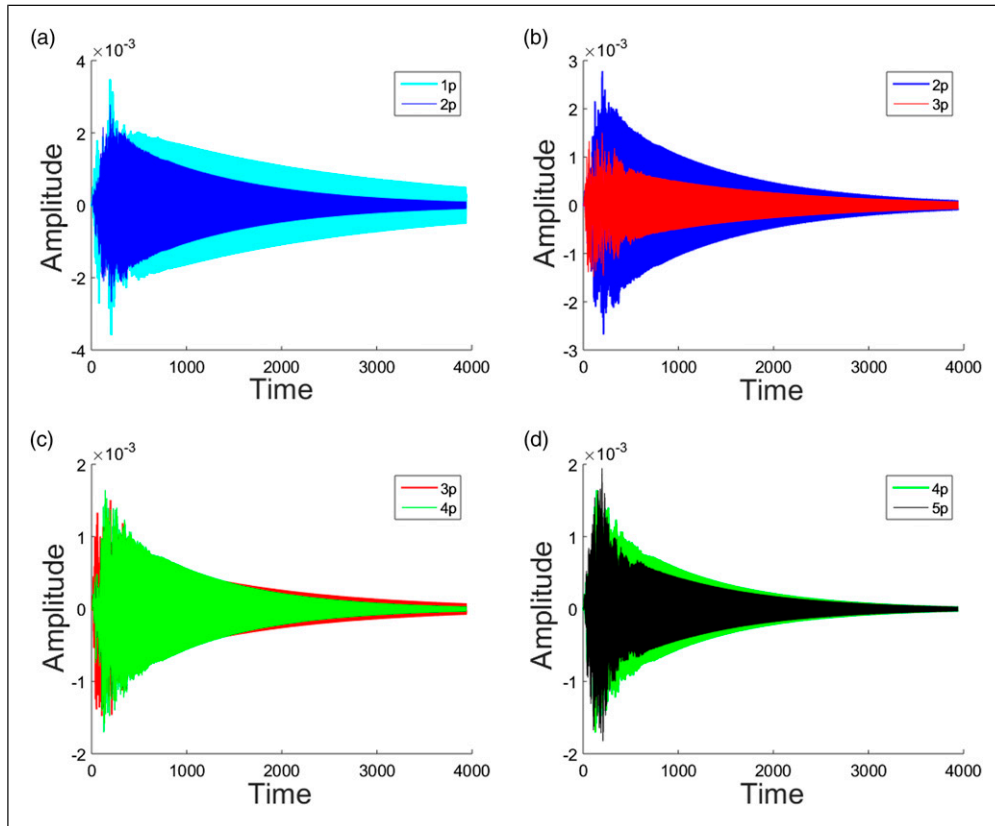


Figure 7. Angular displacement of the central column according to the number of floors (a) 1 and 2, (b) 2 and 3, (c) 3 and 4, and (d) 4 and 5.

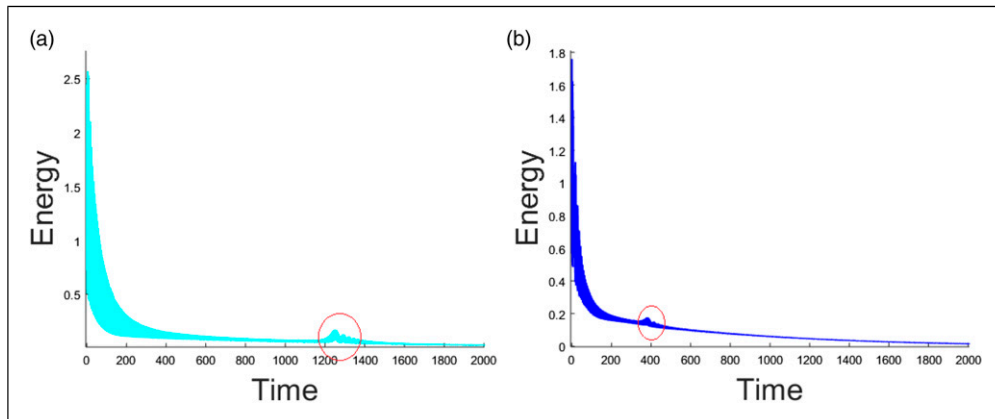


Figure 8. Energy of the system for (a) one and (b) two levels of branches.

two levels, two and three levels, three and four levels, and finally four and five levels are drawn. To return to its initial position, the structure needs to dissipate all the received energy from external excitation; and one can clearly say that the point zero of energy is quickly reached for a larger number of branches.

Figure 10(a) presents the energy of the system during the vibration phenomenon as the function of weight m_1 of the

central column and time. One can bring out one main point: when the central column weight is high, the energy of the system at the beginning at the inverse reduces. It is the same observation on Figure 10(b)–(d), which show the influence of main rod length l_1 , attached mass weight m_2 , and the distance between that attached mass and the central column l_2 . The main results to retain is that for each parameters of the system, up to the plotted taken value, when they increase, the

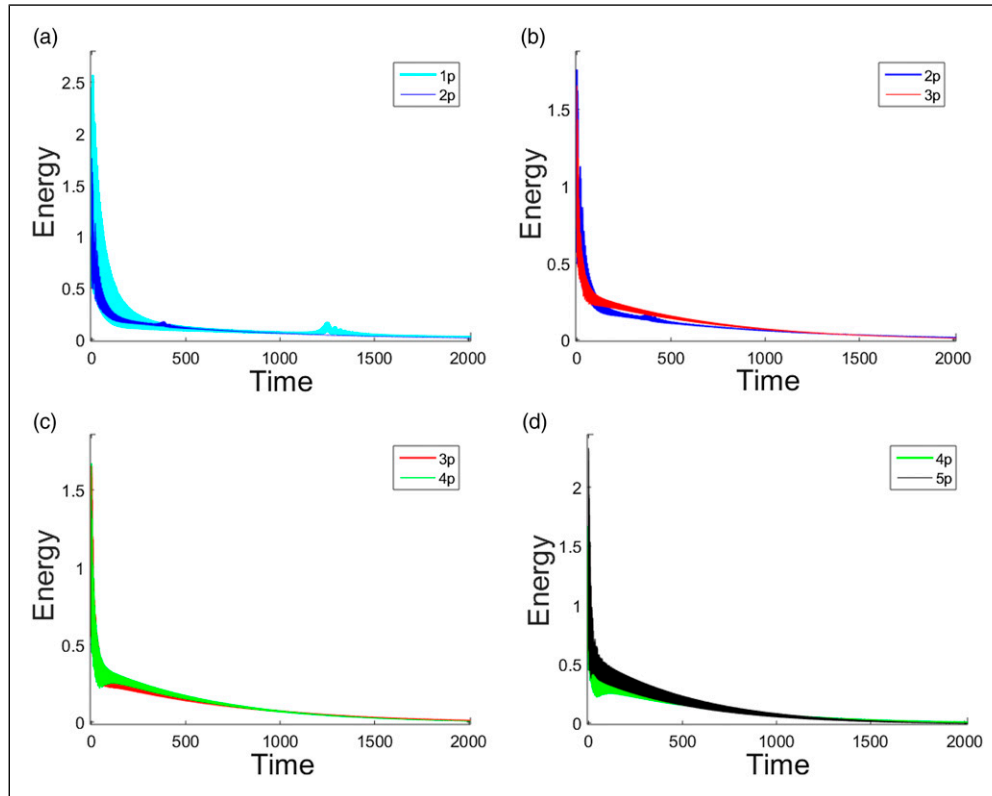


Figure 9. Energy of the system for (a) one–two, (b) two–three, (c) three–four, and (d) four–five levels branches.

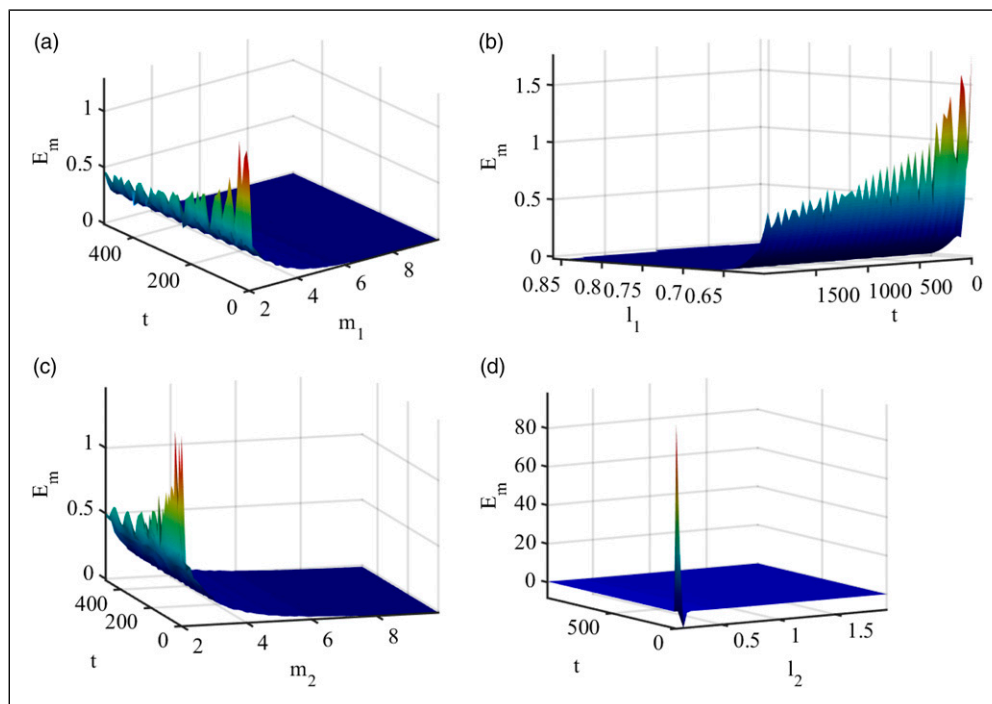


Figure 10. Effects of the design parameters on the energy of the system: (a) mass of the central rod, (b) length of the central rod, (c) level masses, and (d) level length.

total energy of the system decreases, and this has no effect on the time history of energy. Only for length l_2 , when its high value is really helpful for the structure because the most it increases the structure dissipates quickly the energy, and even the time history is quite affected by its value. Nullification of the energy of the system is rapidly denoted

$$\begin{aligned}
& A'(\phi_k)\ddot{\theta} + B'(\dot{\phi}_k, \phi_k)\dot{\theta} + D'(\phi_k)\dot{\theta}^2 + K_1\theta + \left(30m_1 - \frac{5}{2}M\right)gl_1 \sin \theta + \left(\frac{l_1}{l_2} \cos \phi_0 \sin \phi_1 - 1\right)C_2\dot{\phi}_1 \\
& + \left(2\frac{l_1}{l_2} \cos \phi_0 \sin \phi_2 - 1\right)C_2\dot{\phi}_2 + \left(3\frac{l_1}{l_2} \cos \phi_0 \sin \phi_3 - 1\right)C_2\dot{\phi}_3 + \left(4\frac{l_1}{l_2} \cos \phi_0 \sin \phi_4 - 1\right)C_2\dot{\phi}_4 \\
& + \left(5\frac{l_1}{l_2} \cos \phi_0 \sin \phi_5 - 1\right)C_2\dot{\phi}_5 + \left(\frac{l_1}{l_2} \cos \phi_0 \sin \phi_1 - 1\right)2K_2\phi_1 + \left(2\frac{l_1}{l_2} \cos \phi_0 \sin \phi_2 - 1\right)2K_2\phi_2 \\
& + \left(3\frac{l_1}{l_2} \cos \phi_0 \sin \phi_3 - 1\right)2K_2\phi_3 + \left(4\frac{l_1}{l_2} \cos \phi_0 \sin \phi_4 - 1\right)2K_2\phi_4 + \left(5\frac{l_1}{l_2} \cos \phi_0 \sin \phi_5 - 1\right)2K_2\phi_5 \\
& - 2m_1l_1l_2 \cos \phi_0 \left(\dot{\phi}_1^2 \cos \phi_1 + 2\dot{\phi}_2^2 \cos \phi_2 + 3\dot{\phi}_3^2 \cos \phi_3 + 4\dot{\phi}_4^2 \cos \phi_4 + 5\dot{\phi}_5^2 \cos \phi_5\right) \\
& - m_1gl_1 \sin(2\phi_0) [\sin \phi_1 \sin(\theta + \phi_1) + 2 \sin \phi_2 \sin(\theta + \phi_2) + 3 \sin \phi_3 \sin(\theta + \phi_3) + 4 \sin \phi_4 \sin(\theta + \phi_4) \\
& + 5 \sin \phi_5 \sin(\theta + \phi_5)] = 0 \\
& 2m_1l_2^2\ddot{\phi}_k + C_2\dot{\phi}_k + 2K_2\phi_k - \left(\frac{2m_1gl_2}{\sin \phi_0}\right) \sin(\theta + \phi_k) + \left(\frac{2(k)m_1l_1l_2}{\dot{\theta}^2 \cos \phi_0}\right) \cos \phi_k = 2((k)m_1l_1l_2 \cos \phi_0 \sin \phi_k - m_1l_2^2)\ddot{\theta}
\end{aligned} \tag{6}$$

With new coefficients

$$\begin{aligned}
A'(\phi_k) &= \frac{25}{4}Ml_1^2 + 110m_1l_1^2 - 2m_1l_1^2 \cos^2 \phi_0 (\sin^2 \phi_1 \\
& + \sin^2 \phi_2 + \sin^2 \phi_3 + \sin^2 \phi_4 + \sin^2 \phi_5)
\end{aligned}$$

$$\begin{aligned}
B'(\dot{\phi}_k, \phi_k) &= C_1 - 4m_1l_1l_2 \cos \phi_0 (\dot{\phi}_1 \cos \phi_1 + 2\dot{\phi}_2 \cos \phi_2 \\
& + 3\dot{\phi}_3 \cos \phi_3 + 4\dot{\phi}_4 \cos \phi_4 + 5\dot{\phi}_5 \cos \phi_5)
\end{aligned}$$

$$\begin{aligned}
D'(\phi_k) &= 2m_1l_1^2 \cos^2 \phi_0 (\cos \phi_1 \sin \phi_1 + 4 \cos \phi_2 \sin \phi_2 \\
& + 9 \cos \phi_3 \sin \phi_3 + 16 \cos \phi_4 \sin \phi_4 \\
& + 25 \cos \phi_5 \sin \phi_5) - 2m_1l_1l_2 \sin \phi_0 (\sin \phi_1 \\
& + 2 \sin \phi_2 + 3 \sin \phi_3 + 4 \sin \phi_4 + 5 \sin \phi_5)
\end{aligned}$$

Therefore, the system returns quickly to its initial position by dissipating its energy when the length of its branches is considerable. Particularly for the length of the location of the mass (l_2), the highest value is the function of the length of the central column to avoid the fact that masses will touch the ground or touch each other. And to make sure that, this condition will be taken into account; the length should satisfy: $l_2 < l_1/\sin(\phi_0)$.

5. Conclusion

This study has analyzed the energy variation and the vibration control of a set of pendulums. A mathematical modeling of the damping mechanism due to the transfer of

energy between the central column as a pendulum and branches as pendulums too was investigated. The equations of the motion of the structure with all its branches were given by using the Lagrangian of the system. It was shown after dynamics evaluation that when the system is moved from its initial and equilibrium position, the energy received by the central column is distributed to the different branches of the structure, leading to a self-vibration control of the

system; branches have a damping effect on the structure. All that results were confirmed even when the structure faces an external force such as earthquake loads. It was also found that one can increase or decrease the damping ratio according to the length and the weight of the central rod and even those of branches. One can also deduct that to keep that configuration of the structure, the limit value acceptable of l_2 is the function of the length of the central column l_1 and the angle ϕ_0 of its position. A real representation of this structure is shown in Figure 11.

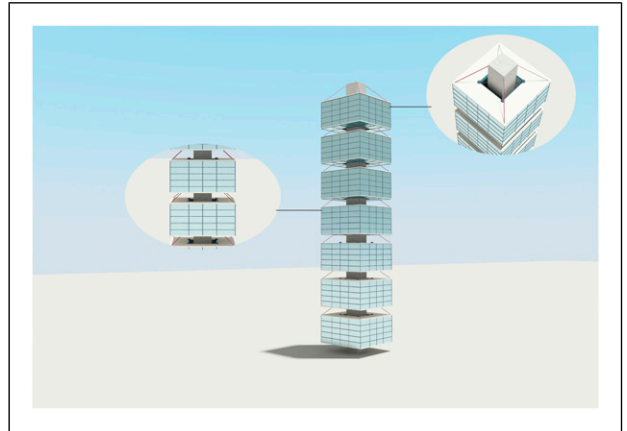


Figure 11. A modern pagoda structure.

Declaration of conflicting interests

The author(s) declared no potential conflicts of interest with respect to the research, authorship, and/or publication of this article.

Funding

The author(s) disclosed receipt of the following financial support for the research, authorship, and/or publication of this article: E. R. Fankem is grateful to the University of Kassel in Germany for invitation for a research visit within the DAAD STIBET scholarship. Prof. Nana Nbandjo is grateful to the Alexander von Humboldt Foundation for financial support.

ORCID iD

Blaise Romeo Nana Nbandjo  <https://orcid.org/0000-0001-7331-1115>

References

- Anh ND, Nguyen NX and Quan NH (2016) Global-local approach to the design of dynamic vibration absorber for damped structures. *Journal of Vibration and Control* 22(14): 3182–3201.
- Avossa AM, Giacinto DD, Malangone P, et al. (2018) Seismic retrofit of a multispan prestressed concrete girder bridge with friction pendulum devices. *Shock and Vibration* 2018: 1–22.
- Bock T, Linner T and Miura S (2011) Robotic high-rise construction of pagoda concept: innovative earthquake-proof design for the Tokyo sky tree. In: 2011 council on tall buildings and urban habitat world conference, Seoul, Korea, 10–12 October 2011.
- Djanan AN, Nbandjo BN and Woafu P (2015) Self-synchronization of two motors on a rectangular plate and reduction of vibration. *Journal of Vibration and Control* 21(11): 2114–2123.
- Dorka UE (2004) Erdbebensicherung durch structural control. *Stahlbau* 73: 661–667.
- Dorka UE (2014) Seismic control for elevated roads. *Building Materials and Structures* 57: 9–20.
- Fujita K, Hanazato T and Sakamoto I (2004) Earthquake response monitoring and seismic performance of five-storied timber pagoda. In: 13th world conference on earthquake engineering, Vancouver, Canada, 1–6 August 2004.
- Hanazato T, Ayaki D, Ogiwara Y, et al. (2012) Seismic design and construction of a traditional timber-made five-storied pagoda by applying coupled vibration control. In: 15th world conference on earthquake engineering, Lisbon, Portugal, 24–28 September 2012.
- Ishida S (1993) *The critical behavior of the wooden pagoda under earthquakes*. Technical Report no. 15, July. AIJ Kinki branch, pp. 71–85.
- Iyengar RN and Shinozuka M (1972) Effect of self-weight and vertical acceleration on the behaviour of tall structures during earthquake. *Earthquake Engineering & Structural Dynamics* 1: 69–78.
- Kim H-S and Kang J-W (2017) Smart outrigger damper system for response reduction of tall buildings subjected to wind and seismic excitations. *International Journal of Steel Structures* 17(4): 1263–1272.
- Kitio Kwuimy CA, Nana Nbandjo BR and Woafu P (2006) Optimization of electromechanical control of beam dynamics: analytical method and finite differences simulation. *Journal of Sound and Vibration* 298: 180–193.
- Kujawski E and Tang Y (2009) *Simultaneous calculation of direct and indirect levelling in investigating deformations of pagoda-type building*. Reports on Geodesy.
- Lin YK, ASCE F and Yong Y (1987) Evolutionary Kanai-Tajimi earthquake models. *Journal of Engineering Mechanics* 113: 1119–1137.
- Metsebo J, Nana Nbandjo BR and Woafu P (2016) Dynamic responses of a hinged-hinged Timoshenko beam with or without a damage subject to blast loading. *Mechanics Research Communications* 71: 38–43.
- Minowa C, Kawai N, Maekawa H, et al. (2010) Observation of wind and earthquake responses of national heritage five story wooden pagoda. In: World conference on timber engineering, Riva del Garda, Italy, 20–24 June 2010.
- Muto K (1949) Five-story pagodas and earthquake resistance. *Journal of the Disaster Prevention* 11.
- Nakahara K, Hisatoku T, Takahashi Y, et al. (2000) Earthquake response of ancient five-story pagoda structure of Horyu-ji temple in Japan. In: 12th world conference on earthquake engineering, Auckland, New Zealand, 30 January–4 February 2000.
- Nana Nbandjo BR (2004). *Dynamics and active control with delay of the dynamics of unbounded monostable mechanical structures with ϕ 6 potential*. PhD Thesis in Non-linear Mechanics, University of Yaoundé I, Yaoundé, Cameroon.
- Nana Nbandjo BR and Dorka UE (2016) Effect of tendon structural control on the appearance of horseshoes chaos on a cantilever beam due to seismic action. *Advances in Mechanical Engineering*.
- Ndemanou BP, Fankem ER and Nana Nbandjo BR (2017) Reduction of vibration on a cantilever Timoshenko beam subjected to repeated sequence of excitation with magneto-rheological outriggers. *Structural Design of Tall and Special Buildings* 26: e1393.
- Ndemanou BP, Nana Nbandjo BR and Dorka U (2016) Quenching of vibration modes on two interconnected buildings subjected to seismic loads using magneto rheological device. *Mechanics Research Communications* 78: 6–12.
- Omori H (1921) About the seismic vibration of five-story pagodas. *Journal of Architecture and Building Science* 415: 219–226.
- Oumarou AS, Nana Nbandjo BR and Woafu P (2011) Appearance of horseshoes chaos on a buckled beam controlled by disseminated couple forces. *Communications in Nonlinear Science and Numerical Simulation* 16: 3212–3218.
- Tanabashi R (1960) *Earthquake Resistance of Traditional Japanese Wooden Structure*. Special lecture of 2WCEE. Japan.
- Theckes B, De Langre E and Boutillon X (2011) Damping by branching: a bioinspiration from trees. *Bioinspiration & Biomimetics* 6 046010 (11pp).
- Ueda A et al. (1996) *Why five story pagodas hardly collapsed*. Shincho-sha.
- Wu Y, Song X, Gu X, et al. (2018) Dynamic performance of a multi-story traditional timber pagoda. *Engineering Structures* 159: 277–285.